Efficient Probabilistic Structural Response Prediction for Aircraft Turbulence and Offshore Wave Loading

A thesis submitted in accordance with the requirements of the University of Liverpool for the degree of Doctor in Philosophy by

Luke Andrew Lambert

April 2015

"Who then is this, that even the wind and the sea obey him?!"

- Mark 4:41

Abstract

This thesis takes an interdisciplinary approach to the problem of the aleatory uncertainty manifest in the design of engineering structures that are subject to random loading, with specific application to continuous gust loading on aircraft and wave loading on offshore structures. The main focus is on aircraft gust loading because this is the area in which more significant progress is made. A review of the literature on gust loading is carried out to evaluate the sufficiency of existing methods and the possibility of a unified certification model is discussed.

In order to obtain reliable probabilistic design loads using conventional stochastic simulation techniques, a large number of simulations are required to derive probability distributions that have adequately low sampling variability in the area of interest. A novel method, called the Efficient Threshold Upcrossing method, is developed that reduces the required number of simulations by at least 2 orders of magnitude. The method is initially developed for the efficient derivation of short-term offshore structural response statistics and is subsequently applied to the modelling of aircraft response to continuous turbulence.

The ETU method was successfully extended to take into account long-term statistics of nonlinear aircraft response and it was shown that reliable design exceedance curves can be obtained by as little as 4% of the computational cost of the conventional method.

The current methods for the computation of design loads for nonlinear aircraft are limited to discrete, '1 - cosine' gust encounters as the continuous turbulence models are only applicable to linear aircraft response. However, the most significant outcome of this thesis is that this is no longer the case, because the ETU method provides a way to calculate nonlinear response statistics in the time domain at a significantly lower computational cost.

Mathematical models of a simple offshore structure, and both linear and nonlinear aircraft, are developed and a more robust technique is introduced for simulating patches of continuous turbulence. These models, which have the ability to generate random inputs, are used to derive response probability distributions for each of the test structures. The results obtained by applying the new approaches to these data sets show that they offer a marked improvement in performance.

Acknowledgements

Firstly, I would like to say a massive thank you to my supervisors, Dr. Gholamhossein Najafian and Prof. Jonathan Cooper, for all the support and expertise that they have given me over the past few years. I would especially like to thank them for their patience and willingness to take time to help me solve the numerous problems I've faced and guide me through each step of the project, for giving me the freedom to be creative and go off on tangents, but more than anything, for believing in me enough to give me this unique opportunity.

I would also like to thank my wife, Meredith, for her continual love and encouragement, and for all the sacrifices that she has gladly made so that I could complete my PhD. She has been more patient and understanding than I could have ever asked.

Finally, this research was financially supported by the Engineering and Physical Sciences Research Council (EPSRC) and the University of Liverpool, for which I am very grateful.

Contents

Nomenclature

General

δ	Random Phase Angle	rad
i	$\sqrt{-1}$	
λ	Average Number of Threshold Upcrossings	
μ_x	Mean Value of Random Process, $\{x(t)\}$	
ω	Angular Frequency	rad/s
σ_x	Standard Deviation of Random Process, $\{x(t)\}$	
τ	Arbitrary Time Difference	s
a	Spectral Amplitude	m or m/s
C	Correlation Coefficient	
G	Number of Groups used in ETS or ETU Analysis	
g	Acceleration Due to Gravity	m/s^2
N	Number of Sample Records	
N_h	Number of Harmonics	
R_x	Autocorrelation Function of Random Process, $\{x(t)\}$	
T	Duration of a Sample Record	s
t	Time	s
T_n	Time period of the n^{th} harmonic	s
U	Number of Threshold Upcrossings	

Aerospace Engineering

γ_e	Mode Shape Describing Wing Bending Deformation
γ_y	Scaled Peak-Response Amplitude

κ_e	Mode Shape Describing Wing Twist Deformation	
μ	Wing Mass per unit Span	kg/m
Ω	Spatial Frequency	rad/m
ϕ	Theodorsen's Function	
Φ_w	Spectral Density of Vertical Gust Velocity	m^2/rad.s or m^2/s
ρ	Density of Air	kg/m^3
θ	Pitch Displacement	rad
A	Altitude	ft
a_{T}	Tailplane Lift Curve Slope	rad^{-1}
a_{W}	Wing Lift Curve Slope	rad^{-1}
b_1	Intensity Scale Parameter for Non-Storm Turbulence	m/s
b_2	Intensity Scale Parameter for Storm Turbulence	m/s
c	Chord Length	m
c_e	Modal Damping	Nm.s/rad
H	Gradient Distance	m
h	Extreme value of a 'low-demand' variable	
I_y	Pitch Moment of Inertia About Aircraft Centre of Mass	$kg.m^2$
k_ε	Downwash Coefficient	
k_e	Modal Stiffness	Nm/rad
L	Characteristic Scale Wavelength	m
l	Distance Between Wing and Tailplane	m
l_{A}	Distance from Centre of Mass to Elastic Axis	m
l_{E}	Distance from Elastic Axis to Mass Axis	m
l_{T}	Distance of Tailplane From Aircraft Centre of Mass	m
l_{WM}	Distance from Centre of Mass to Wing Root	m
l_{W}	Distance from Centre of Mass to Wing Aerodynamic Centre	m
l_{W}	Distance of Wing From Aircraft Centre of Mass	m
L_g	Gust Length	m
l_y	Pitch Radius of Gyration	m
m	Mass of Aircraft	kg

m_{W}	Mass of Wing	kg
m_e	Modal Mass	kg
M_{bw}	Wing Bending Moment	Nm
M_{tw}	Wing Torsion Moment	Nm
n	Load factor	
N_0	Characteristic Frequency	Hz
N_{A}	Number of Altitude Bands	
N_{T}	Number of Turbulence Severity States	
P_1	Probability of Non-Storm Turbulence	
P_2	Probability of Storm Turbulence	
p_i	Complexity Factor for Statistical-Discrete-Gust	
q_e	Displacement of Flexible Mode	
s	Aircraft Semi-Span	m
S_{T}	Tailplane Area	m^2
S_{W}	Wing Planform Area	m^2
u_0	Intensity Parameter for Statistical-Discrete-Gust	
V	Airspeed	m/s
w_g	Gust Velocity	m/s
w_{g0}	Design Gust Velocity	m/s
y	General Aircraft Response Variable	
z	Heave Displacement	m
Z_t	Tailplane Shear Force	N
Z_w	Wing Shear Force	N
$\boldsymbol{A}_y$	Internal Load Transformation Vector Relating to Acceleration	
$\boldsymbol{B}_y$	Internal Load Transformation Vector Relating to Velocity	
$\boldsymbol{C}_y$	Internal Load Transformation Vector Relating to Displacement	
$\boldsymbol{D}_y$	Internal Load Transformation Vector Relating to Gust Input	
$\boldsymbol{R}_T$	Gust Dependent Aerodynamic Vector for the Tailplane	
$\boldsymbol{R}_W$	Gust Dependent Aerodynamic Vector for the Wing	
$\mathbf{C}$	Aerodynamic Damping Matrix	

$\mathbf{K}$	Structural Stiffness Matrix	
$\mathbf{M}$	Mass Matrix	
$\mathbf{T}_{zq}$	Frequency Domain Response Transformation Matrix	
$\mathrm{E}(x)$	Expected Value of a Variable x	
$\mathrm{N}(x)$	Frequency of Exceedance of the Threshold x	Hz

Offshore Engineering

$\dot{u}$	Horizontal Water Particle Acceleration	$\mathrm{m/s^2}$
η	Surface Elevation of the Sea	m
ρ	Density of Sea Water	$\mathrm{kg/m^3}$
A	Response Threshold Value	
C_d	Drag Coefficient	
C_m	Inertia Coefficient	
D	Cylinder Diameter	m
d	Water Depth	m
H_s	Significant Wave Height	m
K	Shape Parameter for Generalised Extreme Value Distribution	
k	Wave Number	rad/m
l_{seg}	Length of One Cylindrical Segment	m
N_{N}	Number of Structural Nodes	
q	Morison Force per unit Length	N/m
r	General Response Value	
S_η	Spectral Density of Surface Elevation	$\mathrm{m^2s/rad}$ or $\mathrm{m^2s}$
T_z	Average Zero-Upcrossing Period of a Sample Record	s
u	Horizontal Water Particle Velocity	m/s
Z	Distance of a Node from the Sea bed	m
z	Vertical Distance from Mean Water Level	m

Abbreviations

BS	Base Shear Force
CDF	Cumulative Distribution Function
DFT	Discrete Fourier Transform

DSA Deterministic Spectral Amplitude

ETS Efficient Time Simulation

ETU Efficient Threshold Upcrossing

LRWT Linear Random Wave Theory

MWL Mean Water Level

NSA Non-Deterministic Spectral Amplitude

OTM Over-turning Moment

PDF Probability Density Function

Chapter 1

Introduction

1.1 Background and Motivation

1.1.1 Uncertainty in Aerospace Engineering

Unsteady loads calculations are an important aspect of the design and development of an aircraft, and have an impact upon the concept and detailed structural design, aerodynamic characteristics, weight, flight control system design, control surface design and performance. They determine the most extreme stress levels and estimate fatigue damage and damage tolerance for a particular design. For this purpose, loads cases due to dynamic gusts and manoeuvres are applied to detailed structural models in order to determine the worst values for a range of different Interesting Quantities (IQs).

The requirements for certified loads are defined in the context of the design envelope shown in figure 1.1 (Wright & Cooper 2007). Certification specifications require that enough points, on or within the boundary of the design envelope, are investigated to ensure that the most extreme loads for each part of the aircraft structure are identified. In this context, the design envelope encompasses the respective ranges of permitted mass / centre of mass envelopes. Currently, the airworthiness regulations require certification in terms of single isolated discrete gusts in the time domain and 'patches' of continuous Gaussian turbulence in the frequency domain; both vertical and lateral gusts and turbulence are considered.

A major issue faced in the design of aircraft, along with virtually all other engineering

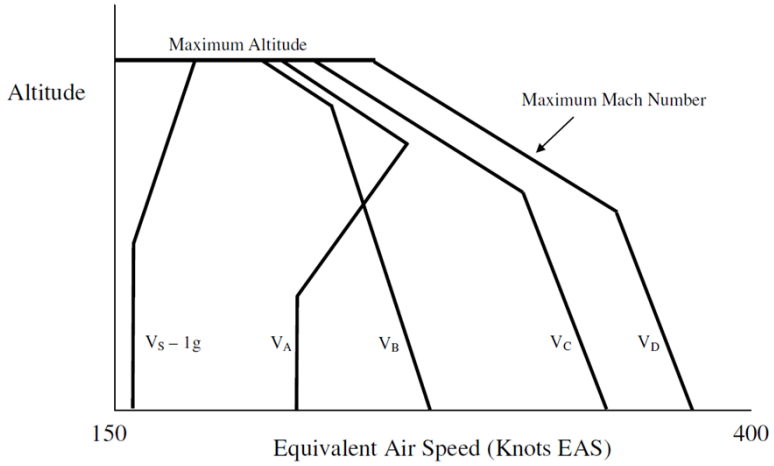

Figure 1.1: Flight Envelope: Design Speed vs Altitude (Wright & Cooper 2007)

structures, is the presence of uncertainty in both the natural processes that influence the loads they are subjected to, and the manufacturing processes used for their production. In engineering design, the problem of uncertainty is a difficult one, so it is important to be clear about the nature of the uncertainty being considered in order to help solve the problem effectively. Engineering uncertainty can be divided into two categories, *epistemic* and *aleatory* uncertainty, both of which play an important role in different parts of the engineering design process. Epistemic uncertainty is the kind that, in theory, could be eliminated by more advanced knowledge or equipment, even though it may not be available in practice. For example, a standard tape measure may measure to the nearest millimetre, introducing an uncertainty in its measuring capability of ± 0.5mm, which could be reduced by using a more accurate device such as a laser distance measurer. Aleatory uncertainty, on the other hand, is caused by processes that are *inherently random*, which means that it cannot be eliminated or reduced, only accounted for. For example, if a person travels to work at a busy time every day, the exact length of time it takes them will vary from day to day even if they take the same route, because of the traffic. This journey time cannot be made quicker by gaining more information about the traffic or by buying a different car, but they may choose to begin their journey earlier to account for the possibility of more traffic. In other words, even if all the available variables could be kept perfectly constant, the result would be different every time. This means that aleatory uncertainty is often a more difficult problem to deal with because

in order to account for it, relatively complex models or high factors of safety are usually required.

This project is concerned with the development and application of modelling techniques that enable the *aleatory* uncertainty associated with aircraft and offshore structures to be taken into account. It is hoped that this will contribute to the bringing about of designs that are more economical and to a greater understanding of the random processes involved.

One of the main sources of aleatory uncertainty in aircraft design is the occurrence of loading due to the aforementioned atmospheric turbulence encounters, which is known as gust loading. In order to account for this uncertainty, aerospace loads engineers require information about the velocity of the gusts that aircraft are likely to encounter, for which is it necessary to make idealisations about the structure of atmospheric turbulence. As will be discussed in detail in Chapter 2, the mathematical description of this turbulence is a highly controversial subject and there are two, allegedly conflicting, overall approaches that are currently in use. Although controversial, the issue is an important one because reducing the weight of an aircraft while maintaining its safety has a hugely positive effect on the manufacturing costs, fuel costs, and ultimately flight costs, not mention the positive impact it has on the environment. In addition, saving time in the design process by developing convenient and practical methods to account for gust loading uncertainty would be highly beneficial for loads engineers. A general picture of the accepted structure of atmospheric turbulence is shown in figure 1.2, but will be further explained in Chapter 2.

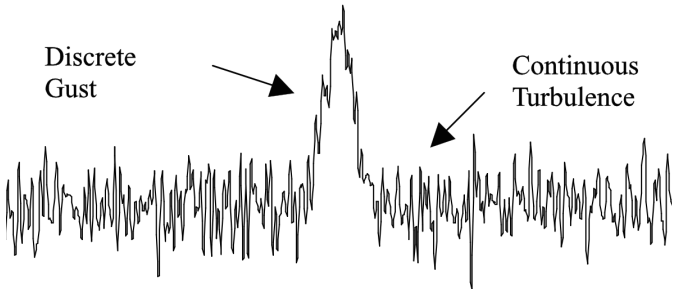

Figure 1.2: The General Structure of Atmospheric Turbulence (Wright & Cooper 2007)

Alternative gust loading prediction methods have been presented to the gust loads community but there have not been any dramatic changes to the requirements for a long time and the current methods are highly deterministic, leaving room for improvements using a probabilistic approach.

1.1.2 Uncertainty in Offshore Engineering

There are many different types of offshore structure, such as jacket structures (see figure 1.3) or floating structures that are tethered to the sea bed, all of which are affected in different ways by random loads produced by water waves. This introduces aleatory uncertainty into their design, which is accounted for by assuming a mathematical description of the surface elevation (the displacement of the water from the mean water level) of the waves. This description varies depending on the specific conditions that a structure is designed for, but the most common description is based on Linear Random Wave Theory (LRWT), the main mathematical principles of which are outlined in section 3.2 of this thesis.

The main problem faced by engineers in this area is that although good probabilistic methods are available, they require an extremely large number of calculations to obtain accurate results, which is incredibly time consuming, even for the simplest structures because of the inherent nonlinearity involved in the determination of Morison loads. As structures become more complex, usually in deeper water, their dynamic response becomes a more important part of the design, resulting in even more time consuming methods. This issue is consequently addressed by the implementation of more deterministic methods for the sake of convenience, resulting in designs that are more conservative, which of course increases the cost. One of the primary aims of this project, therefore, is to research and develop techniques that reduce simulation time by using less data, whilst maintaining the accuracy and reliability of the design.

Another issue is the demand for offshore structural models to take into account other factors such as current, load intermittency in the splash zone (the area of the structure that is exposed to water and air at different times), and the aforementioned dynamic

effects, which will all inevitably require increasingly complex modelling.

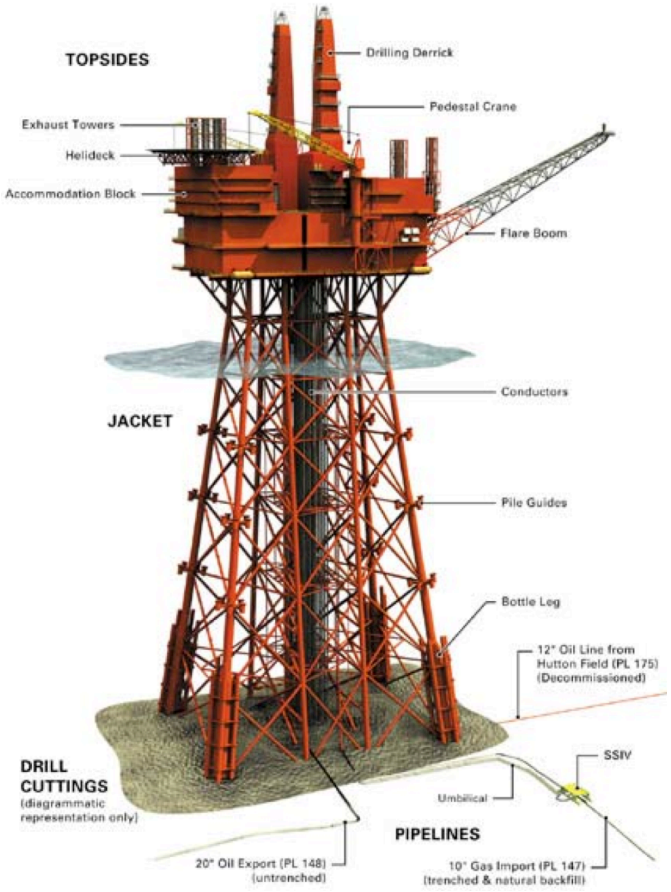

Figure 1.3: Example of a Typical Jacket Structure (Courtesy of BP)

1.1.3 Interdisciplinary Approach

One of the great advantages of this project is that it provides an opportunity to integrate two separate engineering disciplines in order to discover new applications of leading edge techniques for dealing with uncertainty. The reason these two disciplines are a good combination is that the random processes that cause much of their aleatory uncertainty are very similar in nature, especially since water waves are primarily caused by wind.

Therefore, the benefit that this project offers by combining knowledge of uncertainty in offshore and aerospace engineering is that it explores the different ways that are currently used to describe what are essentially very similar processes. For example, the probabilistic methods used for offshore structures can be used to great advantage in the

search for aircraft designs that are more economical, provided they are properly applied and could be complemented by the development of methods for reducing simulation times.

Although original contribution has been made to both disciplines, the focus of this thesis is inclined towards aerospace engineering because that is the area in which more significant progress has been made.

1.1.4 Research Objectives

In summary, the main objectives of the research carried out in this project are:

(1) To explore techniques that speed up the derivation of offshore structural response statistics and find ways to improve existing techniques as well as develop new ones, so that offshore structures can be designed more efficiently.

(2) To investigate the aspects of the probabilistic modelling of offshore structural response that can be applied to the field of aircraft gust loading and produce a stochastic model for probabilistic aircraft response.

(3) To apply new techniques for speeding up probabilistic response calculations to the aircraft stochastic gust model, so that the response of *nonlinear* aircraft to continuous turbulence can be determined probabilistically, instead of limiting it to deterministic, discrete gusts. There are many different types of aircraft nonlinearity, however, and it is beyond the scope of this thesis to investigate all of them, so this work will only include structural nonlinearity in the form of cubic stiffening of the wing.

(4) To critically evaluate any new techniques that are developed by comparing them to conventional methods, reviewing their limitations and considering the effect of the key assumptions that are made.

1.2 Overview of Thesis Content

As well as presenting the foregoing background and motivation for the project, this chapter specifically outlines original contribution that the author has made to the fields of offshore and aerospace engineering and also includes a list of the author's publications.

Chapter 2 contains a review of the literature on aircraft gust loading, which serves to more fully set out the problems involved in the determination of reliable gust design loads, and explore the ways in which the field of aerospace engineering may benefit from the research in this thesis.

Chapter 3 presents some of the relevant mathematical background that is required to understand the analysis presented in this thesis, but is limited to only the background that is common to both offshore and aerospace engineering, in order to avoid repetition in their respective chapters.

Chapter 4 is focussed on the development of the probabilistic offshore structural response model that is used for the wave loading analysis in this thesis, along with a description of the conventional method for the derivation of extreme response probability distributions. It also explains and demonstrates the difference between short-term and long-term response statistics, concepts which play an important role in probabilistic design.

Chapter 5 presents an existing method for speeding up the derivation of offshore structure response probability distributions, known as the Efficient Time Simulation (ETS) technique, and looks at ways that the ETS method might be enhanced to produce more accurate distributions. The chapter also develops a new method, called the Efficient Threshold Upcrossing (ETU) method, which is based on the same fundamental principles as the ETS method, but seeks to produce more reliable distributions by including more information about the statistical properties of the structural response.

Chapter 6 is focussed on the development of separate linear and nonlinear probabilistic aircraft response models that are used for the gust loading analysis presented in this thesis. The current techniques for simulating patches of continuous turbulence are improved for additional robustness and the conventional method for

deriving aircraft response statistics is described. Furthermore, the effect of accounting for long-term statistics is included by introducing the concept of a 'turbulence severity state.'

Chapter 7 applies the newly developed ETU method to enable the statistics of aircraft gust response to be calculated efficiently. A preliminary study is first presented where the methodology is demonstrated using only the linear aircraft response model. The method is then applied to the derivation of nonlinear aircraft response statistics, and is also extended to account for the long-term statistics.

Chapter 8 summarises the conclusions that are made throughout the thesis, evaluates the achievement of the research objectives set out in the previous section and outlines areas where further research might be beneficial.

1.3 Outline of Original Contribution

The original contributions of the author to the fields of offshore wave loading and aircraft loading are primarily concentrated in chapters 5 and 7, respectively, and are centred around the development of the Efficient Threshold Upcrossing (ETU) method. There is also some original contribution in chapter 6 regarding the methods for simulating patches of continuous turbulence and the development of the nonlinear gust response model.

The original contributions to the field of offshore wave loading are:

- The investigation into the enhancement of the ETS technique by fitting the results to analytical generalised extreme value distributions before apply total probability theorem.
  (Chapter 5)

- The development of the ETU method to speed up the derivation of reliable short-term response probability distributions for quasi-static structures that are exposed to random wave loading.
  (Chapter 5)

The original contributions to the field of aircraft gust loading are:

- The inclusion of non-deterministic spectral amplitudes in the simulation of continuous gust patches, which is a more robust approach.
  (Chapter 6)

- The development of a MATLAB-based stochastic gust response model that enables the derivation of short-term and long-term exceedance curves for quasi-steady nonlinear aircraft, which enables probabilistic design loads to be determined.
  (Chapter 6)

- The application of the ETU method to the efficient derivation of reliable short-term response exceedance curves for quasi-steady nonlinear aircraft that are subjected to continuous turbulence.
  (Chapter 7)

- The extension of the ETU method to account for long-term response statistics for the efficient determination of probabilistic design loads for nonlinear aircraft. (Chapter 7)

1.4 List of Publications

1.4.1 Conference Proceedings (Peer-Reviewed)

Lambert, L. A., Najafian, G., Cooper, J. E. (2013), **Probabilistic Modelling of Aircraft Response to Non-Gaussian Continuous Turbulence.** *in* '54th AIAA Structures, Structural Dynamics, and Materials Conference,' Boston, Massachusetts.

Lambert, L. A., Najafian, G., Cooper, J. E., Abu Husain, M. K., and Mohd Zaki, N. I. (2013), **Efficient Estimation of Offshore Structural Response Based on Threshold Upcrossing Rates.** *in* 'ASME 32nd Int. Conference on Ocean, Offshore and Arctic Engineering,' Nantes, France.

Abu Husain, M. K., Mohd Zaki, N. I., Lambert, L. A., Wang, Y., Najafian, G. (2013), **Long-Term Probability Distribution of Extreme Offshore Structural Response Via an Efficient Time Simulation Method.** *in* 'ASME 32nd Int. Conference on Ocean, Offshore and Arctic Engineering,' Nantes, France.

Dale, A. S., Lambert, L. A., Cooper, J. E., Mosquera, A. (2013), **Aerodynamic Study Of Adaptive Camber-Morphing Wing Using 0-ν Honeycomb.** *in* 'Int. Forum on Aeroelasticity and Structural Dynamics,' Bristol, UK.

Chapter 2

Review of the Literature on Gust Loading

This chapter contains a review of the literature on aircraft gust loading, which seeks to more fully set out the problems involved in the determination of reliable gust design loads. The sufficiency of existing methods is evaluated, forming the basis for the motivation behind most of the original research carried out in this project.

2.1 The Key Approaches

One of the main sources of uncertainty in aircraft load prediction is the occurrence of random gust loading from atmospheric turbulence. In order to account for this in the design of an aircraft, it is necessary to describe the expected gust velocities mathematically so that the corresponding structural responses can be determined. To do this, there are two key approaches and there has been much debate over which is the most appropriate method, within these approaches, to account for the range of applications. Hoblit (1988) covers both approaches in detail, with particular attention to the determination of aircraft structural loads. *Introduction to Aircraft Aeroelasticity and Loads* (Wright & Cooper 2007) is a more recent text that contains a very useful chapter covering these two approaches.

The first approach is the *discrete gust*, where gust velocity is represented by an

isolated idealised event that is described deterministically. The earliest description of discrete gusts (Rhode & Lundquist 1931) took the form of a simple step input of a field of uniform velocity, but shortly after, Rhode (1937) adapted it to take the form of the linear ramp gust in order to take into account differences in aircraft motion. Since then, it has been modified (Pratt 1953) to become what is now known as the '1 - cosine' gust, which meant that the structural dynamic response could be considered. In this approach, the gust velocity w_g experienced by the aircraft is described in the time domain as

$$w_g(t) = \frac{w_{g0}}{2}\left(1 - \cos\frac{2\pi V}{L_g}t\right) \tag{2.1}$$

where w_{g0} is the design gust velocity, L_g is the length of the gust and V is the true airspeed.

This type of gust profile has a fixed shape as shown in figure 2.1 in its general form, in which the gust velocity varies in space but is easily computed as a function of time t using equation 2.1.

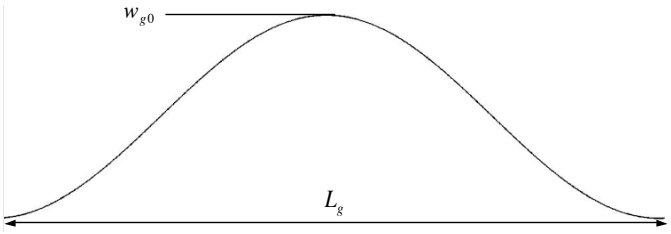

Figure 2.1: General Form of the '1 - cosine' Gust

The second approach is *continuous turbulence*, where the gust velocity is represented by a random signal varying over a potentially infinite length of time. As one might expect, this has been idealised for design purposes so that the random signal, also known as a stochastic gust patch, is considered to occur over a finite length of time. Other idealisations vary, dependent on individual methods, and will be considered later in this chapter. This approach arose from work by Rice (1944) on the mathematical description of random signals, which was later applied specifically to gust loading problems in the

early 50s (Liepmann 1952, Press & Mazelsky 1954). It works by using information about the Power Spectral Density (PSD) of the atmosphere to solve for the gust velocity in the frequency domain by Fourier analysis, enabling the expected RMS value and the frequency of exceedance to be calculated deterministically, although the method is based on probability. The first frequency spectrum used for this method was the Dryden spectrum (Liepmann 1952) but since then, the Von Karman spectrum (von Karman 1948), shown in figure 2.2, has become the standard for design use because it is a more accurate fit with observed data and is better supported by theory at the high frequencies (Hoblit 1988). Figure 2.3 shows a typical gust patch, but a significant distinction between the two approaches should be highlighted at this point: there are an infinite number of possible shapes for a continuous turbulence profile, which is reflective of reality, but the '1 - cosine' gust is limited to a fixed shape.

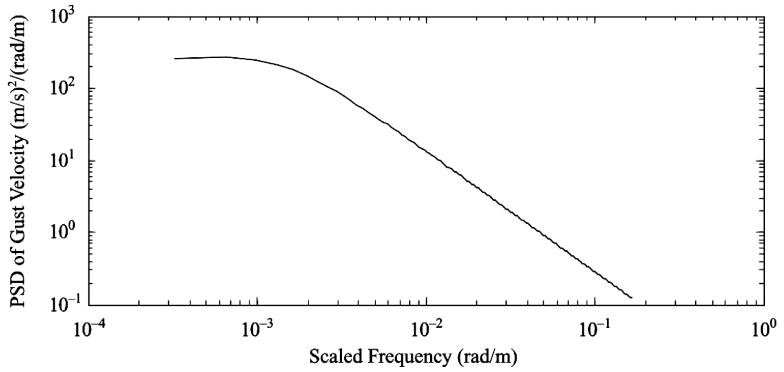

Figure 2.2: Von Karman Spectrum Taken from Wright & Cooper (2007)

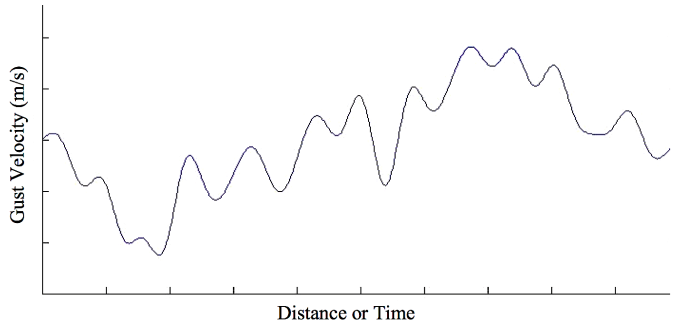

Figure 2.3: Example of a Continuous Gust Patch

The current design regulations (Federal Aviation Regulations (FAR), 1996 and Joint Airworthiness Requirements (JAR), 2007) require both of the above approaches to be

carried out; a '1 - cosine' analysis for the determination of the limit gust load and a PSD analysis for the dynamic response. There is more flexibility in the continuous turbulence requirements, for example FAR 25 states that the prescribed design criteria may be overlooked if *"more rational criteria can be shown."* No such freedom exists for the discrete gust requirements and it has been suggested (Noback 1986) that the reason for this is that there is a higher appreciation of the '1 - cosine' method within both FAR and JAR. Clearly there have been amendments to FAR and JAR since these suggestions were made, but the sections of the regulations on which the argument is based remain unchanged. The main point that Noback (1986) makes is that the PSD method is used as a supplementary requirement to make sure that the response characteristics do not substantially deviate from those of the discrete gust. He points out that the possible difference in the nature of the two methods may result in a conflict situation. For this reason it is important to have a good understanding of these methods and the underlying assumptions when considering the most appropriate methods to use. As new methods have been developed, some of which will be outlined in the next section, this conflict has been a central factor in the reception of these methods.

2.2 Latest Advancements

Since the earliest description of gust profiles, there has been a lot of progress in aircraft development, resulting in more complex designs that require lighter and more flexible aircraft. This has resulted in a number of advancements in the methods used to design for gust loading in the search for quicker and more accurate structural loads determination. The biggest advancement in this area was the discovery of a relationship between gust velocity and gust length, which was not taken into account in the design regulations until more recent amendments. It was recommended by Noback (1986) that the regulations be amended to take into account this relationship by making the design gust velocity, $w_{g0} \propto H^{1/3}$, where H is known as the 'gradient distance' and is half the gust length. Since then, it has been shown (Jones 1989) that a more suitable relationship is $w_{g0} \propto H^{1/6}$, which has been adopted by both FAR and JAR. The comparison of these power laws is shown in figure 2.4.

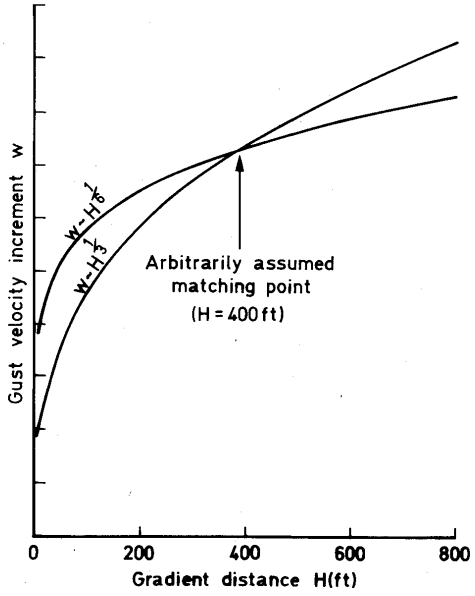

Figure 2.4: Comparison of the Two Power Laws by Jones (1989)

In addition, entirely new methods have been developed, some of which propose a different description of gust velocity, and some of which offer different ways of finding the best design gust velocity. The rest of this section focuses on some of these methods and a discussion of their potential benefits or limitations will follow.

2.2.1 Statistical-Discrete-Gust Method

The Statistical-Discrete-Gust (SDG) method was developed by Jones (1968) and has been by far the most significant development of the earlier work on gust loading. In 2004, Jones et al. (2004) produced a full report for the Federal Aviation Administration (FAA) to consider Jones' method as a replacement for both the Discrete Tuned Gust and Power Spectral Density methods in the design requirements.

Jones et al. (1988) claims that the SDG method *"resolves the dilemma, faced by the designer, in choosing between random-process and deterministic models for input disturbances."* His method is based on modelling the gust velocity as an ensemble of individual discrete ramp components related to an intensity parameter u_0, that is

$$p_i u_0 = \frac{w_{g1}}{H_1^{1/6}} = \frac{w_{g2}}{H_2^{1/6}} = \dots \tag{2.2}$$

where i increases to the number of individual ramp components and p_i is a 'complexity factor' dependent on i. In its simplest form, the ensemble consists of a single ramp component where $p_1 = 1$, resulting in equation 2.3:

$$u_0 = \frac{w_{g0}}{H^{1/6}} \tag{2.3}$$

The innovation of the SDG method is that it enables the maximum response of nonlinear systems to be predicted (Jones 1980, 1989, 2009*a*) by introducing the scaled peak-response amplitude γ_y for a specific response variable y so that

$$\gamma_y\left(H, u_0\right) = \frac{y\left(H, u_0\right)}{u_0} \tag{2.4}$$

for a nonlinear system.

Jones (1980, 2007) has also extended his method to an explicit statistical interpretation for use in a 'mission analysis' design requirement. It produces the number of expected response peaks $\mathrm{N}\left(y\right)$ per unit distance flown, that are greater than

magnitude y using the relationship

$$\mathrm{N}(y) = \frac{\alpha}{\lambda \bar{\bar{H}}(u_0)} \mathrm{e}^{-u_0/\beta} \tag{2.5}$$

where λ in this instance is known as the pattern sensitivity factor, $\bar{\bar{H}}$ is the value of H associated with the intensity parameter u_0 and α and β are related to so-called intermittency parameters.

A more detailed explanation of equation 2.5 can be found in Jones (1980) but it should be pointed out that it is based on the same mathematical description of turbulence outlined above.

In summary, the basis for the SDG theory is that there is a certain range of turbulence, known as the inertial range, in which the stationary-Gaussian assumption breaks down and that in order to account for the non-Gaussian characteristics of turbulence in this range, the phases of the Fourier components cannot be considered statistically independent of one another (Jones 1989). Jones' solution to this is to model atmospheric turbulence as a process of scale-dependent intermittency (Jones et al. 1988), rather than a continuous one, which is based on classical theory of self-similarity (Kolmogorov 1941) and fractal geometry (Mandelbrot 1982).

2.2.2 Matched-Filter Theory

Matched Filter Theory (MFT) was first developed by North (1943), where it was originally applied to determination of signal discrimination in radar, but later Papoulis (1970) showed that the theory could be extended to find maximum responses, obtaining results in 'simple algebraic terms' rather than by using integral equations and the calculus of variations. It was not until 1991, following an investigation by NASA into the SDG method (Perry et al. 1990), that MFT was applied to aeroelastic systems, specifically the computation of time-correlated gust loads (Pototzky et al. 1991).

The basic principle of MFT, as applied to gust loading, is that it allows direct determination of the input signal that produces the maximum response of a system. This means that it enables calculation of the maximum load response and the 'critical'

gust profile. Initially, the MFT method was only able to account for linear systems (Pototzky et al. 1991) but since then, it has been adapted to take into account system nonlinearity to some extent using one-dimensional and multidimensional search procedures (Scott et al. 1993). The main difference between the linear and the nonlinear MFT-based methods is that the linear method guarantees that there is no other normalized signal that will produce a response value greater than the calculated maximum response. However, when the system is taken as nonlinear, there is no guarantee that the value calculated from the optimization procedure is a global maximum. A clear explanation and comparison of both these methods and their relation to stochastic-simulation-based methods is given by Scott et al. (1995).

2.2.3 Stochastic Simulation

Stochastic simulation techniques are closely linked to Matched-Filter Theory methods because they have been used as part of the validation for MFT results. They are characterised by having some random aspect to their description of turbulence that is not typically found in the alternative methods. Stochastic simulation in general is not confined to a single method, but there are of course common themes throughout the variety of available stochastic methods, namely the use of the description of gust velocity as continuous turbulence rather than a discrete gust, introducing a probabilistic aspect. However, the balance of deterministic and probabilistic analysis within an individual method seems to vary between different methods.

For example, one recent stochastic-simulation-based method presented by Scott et al. (1995) is referred to as an 'extracting and averaging procedure,' in which what is known as a stochastic gust patch of total duration, T is generated from the Von Karman spectrum using a Fourier analysis.[1] The 'time history' of the response of an aircraft model to this gust patch is generated using a transfer function, the points where the peak loads occur are identified, and the largest of these peaks is selected. This enables a sample of time span $\pm\tau_0$ to be extracted, centred around the point where the peak load occurred, which in turn enables the corresponding gust velocity profile, the one that

[1] This is the usual practice for stochastic methods; see Chapter 6.

caused this particular response record, to be extracted. The rest of the gust patches and response records are discarded and the extracted records of duration $2\tau_0$ are averaged and used for determining the aircraft design loads. Evidently, this process does introduce a deterministic aspect into the method in the arbitrary selection of values of T and τ_0, which have been shown to affect the results, and the averaging procedure clearly moves away from a probabilistic analysis.

Another gust model, produced by Vink & de Jonge (1997), has the option of a stochastic simulation method if the user desires to employ a continuous turbulence approach. It works in a similar way to the previous model (without the extracting and averaging procedure); by generating a single 10-second sample of the gust velocity profile and the corresponding response values based on aircraft properties that can be defined by the user. The model also enables the response to a '1 - cosine' gust to be determined and for both types of analysis there are options to consider the aircraft model as 'plunge only', 'plunge & pitch', or 'plunge, pitch & 3 flexible modes'. This entire gust model is limited to use for a linear system and its purpose is *"to study various aspects of aircraft response to turbulence."* Figure 2.6 shows response time histories that correspond to the continuous gust patch shown in figure 2.5. The interesting quantities for which time histories are shown in Figure 2.6 are load factor, wing root shear force, wing root bending moment, wing root torsion moment and tail root shear force.

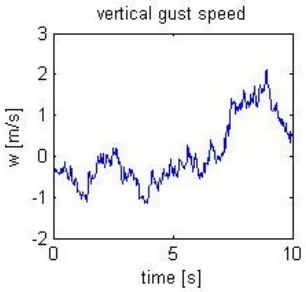

Figure 2.5: Stochastic Gust Input from the NLR Model

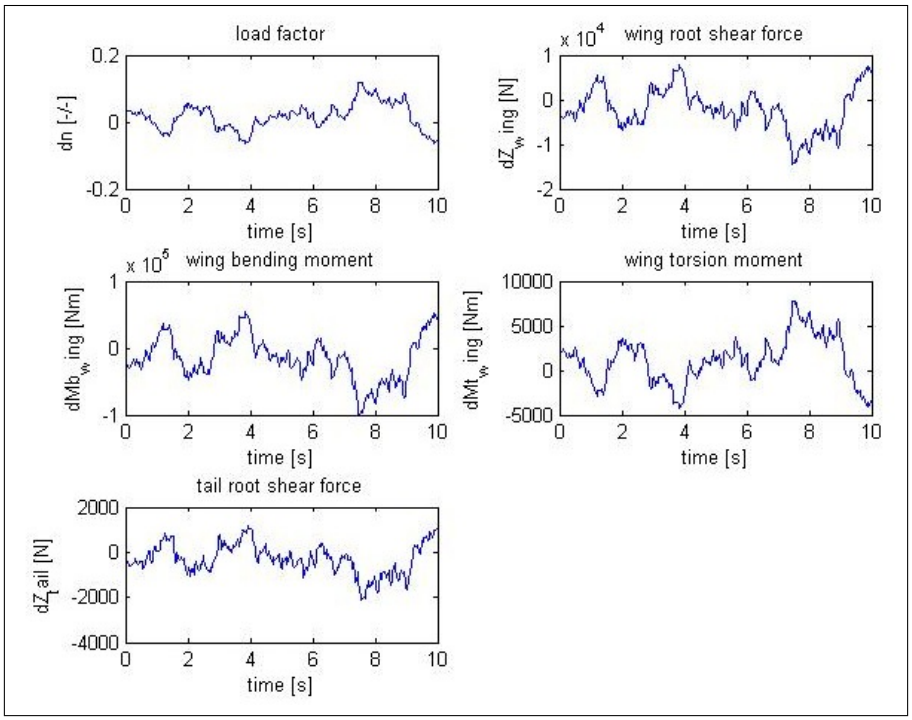

Figure 2.6: Loads Time Responses to Stochastic Gust Patch from the NLR model

2.3 The Sufficiency of Existing Methods

Noback (1986) states that *"the problem of the determination of airplane loads due to atmospheric gusts is an old one; but it has certainly not yet been solved."* Although this statement was made in 1986, there has been very little in the way of changes to the design requirements since then, which would explain why there is still so much controversy surrounding the subject today. The main areas of discussion are regarding the best overall approach to use for the description of gust velocity (discrete gust or continuous turbulence), and between which should be considered the decisive individual method ('1 - cosine,' Classic PSD, SDG, MFT or Stochastic Simulation techniques) when predicting the limiting structural loads of an aircraft.

One main argument in favour of continuous turbulence over discrete gust methods is that it is a much more realistic representation of the atmosphere (Abdulwahab & Hongquan 2008, Hoblit 1988, Steiner & Pratt 1967). Of course, this is undisputed because gust loading does in fact occur continuously, not in isolation (Flomenhoft 1994). Disagreements arise, however, when the idealisation of continuous turbulence as a stationary-Gaussian process, is brought into question. Jones (1989) explains that it is generally accepted that more extreme fluctuations of gust velocity are not adequately represented by the Gaussian model, which is backed up by Etkin (1981) and Chen (1972). It is apparent that in the inertial range of turbulence, there are instances of higher peak gust velocities than would be predicted by the stationary-Gaussian model (Jones et al. 1988). Even Hoblit (1988) grants that *"there is accumulating evidence that actual turbulence is not really stationary and Gaussian"* and outlines numerous examples where this has been the case. Nevertheless, he still maintains that although much severe turbulence may not be strictly stationary-Gaussian, it does have the appearance of continuous turbulence, and he outlines two studies of measured turbulence encounters that strongly support this claim (Jones 1964, Strom & Weatherman 1963).

Another very important objection to J. G. Jones' criticism of PSD methods that Hoblit (1988) makes is that there is a difference between non-Gaussian turbulence and non-stationary turbulence; a topic that is thoroughly discussed in AFFDL-TR-68-127

(Crooks et al. 1968). Jones immediately attributes the departure from self-similarity of continuous turbulence to the conclusion that *"turbulence velocity in the inertial subrange is strongly non-Gaussian"* (Jones et al. 1988). Hoblit points out that there is a tendency to assume implicitly that a sample is stationary and then to evaluate whether it is Gaussian, and suggests that this inclination comes from the absence of any definite way to evaluate stationarity, where it is a simple matter to compute the probability density and compare it with a Gaussian curve. He then goes on to explain that it is entirely possible for a given sample to be *locally* Gaussian, but non-stationary overall, which would produce a non-Gaussian sample if, say, two locally Gaussian samples with different RMS values were combined. This means that the departures from self-similarity in the extreme values that Jones refers to also have the possibility of being explained by a low probability occurrence of the combination of a number of differing high-RMS-value, locally Gaussian patches.

Having said this, so far there has not been a practical way of modelling turbulence in this way, which means that there does need to be a design method that accounts for the undeniable deviations from the stationary-Gaussian model. This explains why the '1 - cosine' gust is still included in the design requirements (Federal Aviation Regulations 1996, Joint Airworthiness Requirements 2007), given that the design gust velocities are deterministically selected based on older aeroplanes that are assumed to have a satisfactory safety record (Noback 1986). In view of the above discussion, the apparent conflict between these two approaches would appear to be unnecessary. The justification for this conclusion is best conveyed by the following quote from Bernard Etkin (1981):

> "In the application of gust information to structural design, there will no doubt continue to be controversy on the relative merits of power-spectral-density methods and discrete gust methods, and on how well each represents the real physics of the atmosphere. This controversy will not be resolved in favour of one or the other - both techniques have their place in the spectrum of design and analytical tools and *both represent aspects of reality.*"

It is, therefore, a fair assessment to say that the only way to reduce the number of design requirements and improve them is to come up with a single, feasible method

that is able to adequately represent all the aspects of reality encompassed by *both* of the above approaches.

This is the claim that Jones makes of his Statistical-Discrete-Gust model in putting it forward as an alternative to the current design requirements (Jones et al. 2004). In this documentation, he states:

> "This method claims to have the potential to replace the Power Spectral Density Model and the Tuned Isolated Discrete Gust, which jointly ensures that an airplane has sufficient structural strength for encounters with continuous turbulence and discrete gusts of design-level intensity."

The main reasons, given in the above reference, that Jones deems the SDG method as superior to existing methods are as follows. Firstly, he points out that the PSD method assumes that the phases of the Fourier components that make up the gust profile are purely random, when in fact, they are strongly correlated. He explains that the SDG method, on the other hand, offers the capability of modelling localized discrete fluctuations explicitly in terms of ramp-shaped gust components, which takes into account the effects of the phase correlations that are present in severe turbulence and result in the supposedly non-Gaussian effects. Secondly, he calls attention to the fact that the Tuned Isolated Discrete Gust is limited to a single-shape gust profile, which is a significant disadvantage when it comes to aircraft with widely differing dynamic response characteristics because in reality they can tune to gust patterns of different shapes. In solution to this, Jones explains that his method can be interpreted as a generalization of the existing discrete gust model to take into account tuning to gust patterns of different shapes. Finally, as mentioned previously, the main advantage that the SDG method has is the ability to solve for both a linear and a nonlinear response using a search procedure.

Despite the apparent benefits of the SDG method, it has been met with a considerable amount of opposition and was not accepted as a replacement for the current design requirements by the FAA, following their investigation for which the full documentation mentioned above (Jones et al. 2004) was produced.

One common objection to the SDG method is that it is based on theory that is largely unfamiliar within the engineering environment, in contrast with both PSD and '1 - cosine' methods. This objection is brought up by T. A. Zeiler (Jones et al. 2004) as one of the reviewers of the SDG method selected by the FAA. It is also backed up by Hoblit (1988), who summarises his view by stating that the method is *"hopelessly cumbersome to use, is far from straightforward in its derivation, provides a good deal less information than current PSD methods, and is probably no more realistic."* The arduous nature of the method, another common objection, was confirmed later by NASA's investigation into the SDG method (Perry et al. 1990). It was found that, depending on which of the two SDG analysis methods is used, linear or nonlinear, an SDG analysis results in a computational cost of between 20 and 60 times that of a PSD analysis. In his comment on this investigation, Etkin (1992) agrees that the SDG method is simply an approximate representation of the PSD method and goes on to ask the question, *"Why use an approximation when the real thing is available?"* He then goes on to point out that, although it is clearly not to save computing time, the methods ability to use non-Gaussian turbulence inputs is one advantage, but that it makes no provision for the variation of vertical gust across the span, *"raising serious concerns about its utility for finding asymmetric loads associated with lateral response modes."*

More recently, R. P. Chen (1995) writes that *"the present SDG method is inadequate as a gust loads design tool"* even though his paper proves that there is an equivalence between the results of PSD and SDG methods within the linear 'overlap.' The main reason that he gives for this rejection, among others, is that *"it is inconceivable that any airframe manufacturer, large or small, will invest 20 times longer CPU time to obtain mere consistent values."* However, he does conclude his paper by commending the SDG method for its usefulness in raising consciousness of the relatively unfamiliar subject of fractal geometry.

The consensus seems to be that the main source of value found in the SDG method is its ability to take into account nonlinear inputs and nonlinear systems, even though other methods are still favourable due to their relative simplicity and practicality. The FAA summarise the current state of the SDG method following their investigation with

the following extract included at the end of their report (Jones et al. 2004):

> "The FAA is comfortable with the current turbulence design criteria and structural level of safety.
>
> Although a single SDG method may offer some simplification for the applicant, and some useful ability with respect to nonlinear systems, it does not appear to offer substantial advantages over-and-above the current combination of PSD and TDG.
>
> However, the SDG method continues to be a candidate as a viable criteria alternative to current practice, and the FAA would be receptive to future representations on the matter from industry or individuals, provided resolution of at least the following:
>
> (1) Traditional levels of safety: the acceptability of reductions in severity of lateral design loads is presently uncertain, and an issue which must be addressed.
>
> (2) Industry acceptance: there should be the prospect of widespread willingness to substitute existing methodologies, not currently in evidence.
>
> (3) Maturity: sufficient additional investigation and analysis to firmly establish the proposed design standard and associated numerical constants, including consideration of altitude effects."

As for Matched Filter Theory based methods, it has been shown (Scott et al. 1995, Zeiler 1997) that they yield *"strikingly similar"* results to those produced using the stochastic simulation based method described earlier, with a slightly lower computational cost for the one-dimensional search analysis and a much higher cost for the multidimensional search. As yet, the method does not appear to have been considered as a replacement for the current design requirements. This is probably because the stochastic method it is compared to is a more deterministic idealisation of the classic PSD method and the nonlinear aspect is still far too computationally costly to replace the more convenient '1 - cosine' gust, given that they are both entirely deterministic and able to take into account nonlinearity.

The above discussion shows that the sufficiency of a gust loading prediction method does not depend solely on its ability to describe turbulence accurately, but also on its practicability within the context of the aircraft design process and its ease of understanding in relation to the loads engineers who are likely to use it. It has also been highlighted that, when it comes to the practicability of a given method, the issue of computational cost is of particular interest to aircraft designers, who require accurate limit loads for range of mass cases at a large number of points on the flight envelope. It is a reasonable conclusion that, despite some weaknesses, the current requirements remain the most sufficient for designing aircraft to withstand loading from atmospheric turbulence, but there is scope for improvements in future research.

2.4 Opportunities for Further Development

2.4.1 A Unified Model for Gust Response

Etkin (1981) suggests that a cause for satisfaction is the virtual absence, in recent years, of primary structure failures in transport aeroplanes attributable to inadequate design loads. Evidently, this trend has continued since his paper was written, which is a source of great confidence in the safety provided by the current requirements. However, when it comes to the search for more economical designs, it should also be pointed out that this absence of failure may also be evidence that there is room for further weight saving without reducing safety (Etkin 1981). Of course, whether this room for increased economy exists or not can only be proven when a new method, deemed to be equally or more reliable than the current methods, produces design loads that are lower than the current ones.

It was shown in the previous section that the methods currently used for determining the limiting structural loads due to gusts are largely deterministic, which is one reason for the potential room for improvement. This is because the '1 - cosine' gust is considered a 'worst case' analysis, which means that the majority of aircraft will probably never experience gust velocities anywhere near those predicted. The problem with this is that it does not allow the designer to select information based on the likelihood of a particular gust occurring. In other words, it provides no information on how often the proposed 'worst case' gust should be expected to occur, because in reality there is no such thing as a 'worst case' gust. There is only an arbitrary gust velocity chosen based on the strength of older aeroplanes assumed to have a satisfactory safety record (Noback 1986). A probabilistic method, on the other hand, would allow selection of design loads based on their probability of occurrence, which in one sense is still just as arbitrary in its choice, but has the added advantage of providing the designer with more information. This potential for more information is one of the major advantages that PSD methods have over the Discrete Tuned Gust, along with the infinite variation of gust profile shapes. However, currently they are still partially deterministic and their inability to take into account the non-stationary or non-Gaussian nature of extreme gusts means

that '1 - cosine' gusts are still the best option.

In light of this discussion, the opportunities for further development are evident. In order to test whether there is room for further improvement in gust prediction, it would be highly beneficial to develop a new method, extended from the PSD method, that makes it possible to account for both non-Gaussian turbulence and nonlinear systems, that is entirely probabilistic, and that is based on real information about the atmosphere. It seems that the best way to develop a truly probabilistic model is by the use of stochastic simulation techniques, which for the above purpose would likely become very long-winded. Therefore, further research into analytical techniques that dramatically reduce computation with a minimal impact on the accuracy of the results would be highly beneficial in the development of a new gust load prediction method. If computational cost could be reduced, it may be possible to extend the capability of PSD methods to *nonlinear* response because calculating time domain responses to stochastic inputs is not impossible, but is so time consuming that it has never been a viable option. A probabilistic model with the ability to account for nonlinear response characteristics would be a significant contribution to the field of aircraft loads analysis.

2.4.2 Wider Applications

The need to determine accurate response statistics for systems that are exposed to random inputs is certainly not unique to the field of aerospace engineering. One of the fundamental problems that will be explored in this thesis, is that the accuracy of the statistics is dependent upon the number of samples that are simulated, i.e. low sampling variability, and therefore the response of any system must be simulated a very large number of times if the probabilities of rare events are to be calculated reliably. This problem occurs in any discipline that involves the statistical modelling of systems with aleatory uncertainty. Hence, there are many fields that might benefit from the method developed later in this thesis, which aims to reduce the number of simulations required to derive response statistics with acceptably low sampling variability, thereby reducing the sizeable computational cost usually incurred. The scope of this work is to apply the method to the areas of offshore and aerospace engineering, but there are some

other examples of areas for which the method may be relevant.

For instance, Monte-Carlo simulation techniques have recently gained enormous popularity in the field of radiotherapy (Seco & Verhaegen 2013), in which random particle interactions on a microscopic level can be simulated in order to provide solutions for macroscopic systems. A specific example of where such methods have been used is in the theoretical testing of improved instrumentation for measuring the levels of in-flight ionizing radiation that aircrews are subjected to (Benson et al. 2002). Much of the radiation levels to which they are exposed vary strongly with solar activity, which is inherently random, and analytical estimates of the response of the instruments can only be made based on measured data that does not account for variations in flight path and altitude (Scraube et al. 1999, Benson et al. 2002). This leads to the need for complex numerical models, which sometimes include nonlinear particle interactions that must be solved in the time domain (Seco & Verhaegen 2013), incurring a significant computational cost.

Another area in which Monte-Carlo simulation techniques play a huge part is finance. For example, quantitative analysts use complex numerical models to estimate fair prices for derivative securities, which are affected by a large number of random variables that can be included in the models, such as stock prices, exchange rates and interest rates (McLeish 2005). Boyle (1977) developed a stochastic-simulation-based method for estimating the value of stock options but identified that

> "One potential drawback of the method arises from the fact that the standard error of the estimate is inversely proportional to the square root of the number of simulation trials. Although any desired degree of accuracy can be obtained by performing enough simulation trials there are usually more efficient ways of reducing the error."

This demonstrates that it is not just in engineering that analysts are seeking to benefit from techniques that improve the efficiency of Monte-Carlo methods. It is true that advancements in computer technology are enabling increasingly more calculations to be carried out at greater speed, but any further increases in efficiency that can be made using mathematical techniques, such as the ones developed in this thesis, will

still serve to facilitate the modelling of more complex systems until such a time as the available computational power renders their benefits negligible.

Chapter 3

General Mathematical Background

This chapter only covers the mathematical background that is relevent to *both* offshore and aerospace aspects of the project, whereas background that is limited to each individual discipline will be covered in their respective chapters. Although the equations in this chapter apply to both disciplines, they have been written as though applied to offshore engineering for the sake of simplicity. For example, the mathematical descriptions that form the basis of Linear Random Wave Theory (LRWT) in section 3.2 can also be used to describe atmospheric turbulence, the only difference being the notation.

3.1 Random Processes

The characteristic property of a random physical process is that it cannot be described by an explicit mathematical relationship. It is therefore always necessary to make assumptions about the nature of a particular random process in order to create an adequate model to represent it. To begin to make an idealised mathematical definition of a random process, a judgement must be made as to whether it is stationary or non-stationary, and as to which probability distribution most realistically represents it. The importance of the concept of stationarity in this project was highlighted in

Chapter 2, along with the Gaussian vs. non-Gaussian issue.

3.1.1 Stationary and Non-stationary Processes

A time history of a random process $\{x(t)\}$ that is observed over a finite time interval is known as a *sample record*. A process is truly stationary if its mean value μ_x and autocorrelation function R_x remain constant over time and over the infinite ensemble of possible sample records, denoted by $\{\}$. The mean values and autocorrelation functions are found by taking average values of $x(t)$ at t_1, or t_1 and τ, respectively, for the number of sample records N. This is demonstrated in equations 3.1 and 3.2 (Bendat & Piersol 1971).

$$\mu_x(t_1) = \lim_{N\to\infty} \frac{1}{N} \sum_{k=1}^{N} x_k(t_1) \tag{3.1}$$

$$R_x(t_1, t_1+\tau) = \lim_{N\to\infty} \frac{1}{N} \sum_{k=1}^{N} x_k(t_1)\, x_k(t_1+\tau) \tag{3.2}$$

Hence, the process $\{x(t)\}$ is truly stationary when the following conditions are satisfied:

(i) $\mu_x(t_1) = \mu_x$ and $R_x(t_1, t_1+\tau) = R_x(\tau)$

(ii) $\mu_x(k) = \mu_x$ and $R_x(\tau, k) = R_x(\tau)$

If only condition (i) is satisfied then $\{x(t)\}$ is said to be weakly stationary, but for many practical applications, verification of weak stationarity justifies an assumption of strong stationarity (Bendat & Piersol 1971). The surface elevation η of the sea is modelled as an stationary random process for a single sea state, but is *non-stationary* when more than one sea state is considered, hence the 3-hour-interval approximation. Non-stationarity is simply a failure to meet the requirements for stationarity outlined above.

3.1.2 Gaussian and Non-Gaussian Processes

A random process $\{x(t)\}$ is considered Gaussian if the probability density function of the x values, as $T \to \infty$, can be described by equation 3.3 (Montgomery & Runger 2002), along with its subsequent derivatives ($\dot{x}, \ddot{x}$, etc.)

$$\mathrm{p}(x) = \frac{1}{\sqrt{2\pi}\sigma_x} \exp\left[\frac{(x-\mu_x)^2}{2{\sigma_x}^2}\right], \qquad -\infty \leq x \leq \infty \tag{3.3}$$

There are some processes than are inherently Gaussian, but many processes are assumed to be Gaussian when the values are closely described by equation 3.3, even if it is not a perfect fit. Furthermore, the Gaussian distribution probability distribution of the process itself, and there may be aspects of the process for which another distribution is more suitable. For example, surface elevation η is represented by the Gaussian distribution, but the wave heights of η, that is, the difference in height between corresponding crests and troughs, are often defined by the Rayleigh distribution, an assumption which is discussed in section 4.3.

The cumulative probability distribution of $\eta_{\max}$ (Abu Husain & Najafian 2011) that can be used to validate simulated extreme surface elevation values is

$$\mathrm{P}(\eta_{\max} \leq \eta_{\max *}) = \exp\left[-\frac{T}{T_z}\exp\left(-\frac{{\eta_{\max *}}^2}{2{\sigma_\eta}^2}\right)\right] \tag{3.4}$$

where $*$ denotes a given value of the variable that precedes it.

This shows that even if some aspects of a physical process are non-Gaussian (i.e. not adequately described by equation 3.3), they may be described by alternative distributions, which can be determined by stochastic simulation techniques.

3.2 Linear Random Wave Theory

Linear Wave Theory (Airy 1841), which was developed by George Biddell Airy in the 19$^{\text{th}}$ Century, is still today the most commonly used description of ocean waves. However, there are a number of assumptions that from the basis for their mathematical description:

(i) The water is homogeneous and incompressible, thus the density is uniform;

(ii) Water viscosity and surface tension can be ignored;

(iii) The waves are long-crested, which means that they are represented by a two-dimensional analysis;

(iv) The waves do not change shape as they travel across the surface of the water;

(v) The sea bed is horizontal and impermeable;

(vi) There is no motion of the water apart from that induced by the waves.

The mathematical description of linear random waves given in sections 3.2 and 3.3 is taken from Dean & Dalrymple (1991), unless otherwise stated. Linear Random Wave Theory (LRWT) defines a unidirectional sea as the summation of a large number of harmonics or linear regular waves having equally-spaced discrete frequencies. At a point x or at time t a linear regular wave with amplitude a and angular frequency ω has surface elevation $\eta(x,t)$ above the mean water level (MWL), and takes the form

$$\eta(x,t) = a\cos(kx - \omega t) \tag{3.5}$$

So the surface elevation of a sample of random waves consisted of N_h superimposed harmonics is defined as

$$\eta(x,t) = \sum_{n=1}^{N_h} a_n \cos(k_n x - \omega_n t + \delta_n) \tag{3.6}$$

where a_n is the amplitude of the n^{th} harmonic, which is known as the spectral amplitude. k_n is the wave number, which, in the absence of current and for water depth d, is defined by the following relationship:

$$\omega_n{}^2 = gk_n \tanh k_n d \tag{3.7}$$

The phase angles δ_n of the components are considered to be random and independent from each other. They are uniformly distributed in the range $0 \leq \delta_n \leq 2\pi$ their probability density function is

$$\mathrm{p}\left(\delta\right) = \frac{1}{2\pi} \tag{3.8}$$

The mean square value of η, for the n^{th} harmonic, $\bar{\eta_n}^2$, for fixed values of δ_n and x, is calculated by

$$\bar{\eta_n}^2 = \frac{1}{T_n}\int_0^{T_n} a_n{}^2 \cos^2\left(-\omega_n t\right) \mathrm{d}t = \frac{a_n{}^2}{2} \tag{3.9}$$

where T_n is the period of the n^{th} harmonic; and because the phase angles are assumed to be uncorrelated, the variance of η is

$$\sigma_\eta{}^2 = \sum_{n=1}^{N_h} \frac{a_n{}^2}{2} \tag{3.10}$$

This information, with the assumptions that precede it, is essential for performing a spectral analysis, as shown in the following section.

3.3 Spectral Analysis

By definition, a frequency spectrum gives the spectral density $S_\eta(\omega)$ a continuum of frequencies, but assume that for a discrete number, N_h of harmonics, the frequencies are equally spaced at $\Delta\omega$. Each frequency ω_n is at the centre of a band of width $\Delta\omega$, and the variance associated with the n^{th} band is $S_\eta(\omega)\Delta\omega$. Therefore

$$S_\eta(\omega_n)\Delta\omega = \frac{{a_n}^2}{2} \tag{3.11}$$

Combining equations 3.10 and 3.11 for the infinite number of harmonics found in the reality gives

$${\sigma_\eta}^2 = \int_0^\infty S_\eta(\omega)\,\mathrm{d}\omega \tag{3.12}$$

and from equations 3.6 and 3.11

$$\eta(x,t) = \sum_{n=1}^{N_h} \sqrt{2S_\eta(\omega_n)\Delta\omega}\cos(k_n x - \omega_n t + \delta_n) \tag{3.13}$$

which means that if the frequency spectrum is defined for a given location, it is possible to simulate a (random) surface elevation sample record using the following approach.

First, it is necessary to generate a set of random independent phases, along with corresponding *deterministic* amplitudes $a_{n_{\text{DSA}}}$ for each harmonic from equations 3.8 and 3.14, respectively.

$$a_{n_{\text{DSA}}} = \sqrt{2S_\eta(\omega_n)\Delta\omega} \tag{3.14}$$

However, an alternative method suggested by Rice (1944), in which the amplitudes are treated as random variables instead of just the phase angles, has been shown (Morooka & Yokoo 1997, Tucker et al. 1984) to produce sample records that more accurately represent their frequency spectrum. Using *non-deterministic* spectral amplitudes, the sea surface is represented as the discrete Fourier series:

$$\eta(t) = \sum_{n=1}^{N_h} (A_n \cos \omega_n t + B_n \sin \omega_n t) \tag{3.15}$$

where A_n and B_n are random variables with standard deviation $\sigma_n = \sqrt{S_\eta(\omega_n)\,\Delta\omega}$.

Morooka & Yokoo (1997) showed that, by applying the following trigonometric identities:

$$R_n = \left({A_n}^2 + {B_n}^2\right)^{1/2} \tag{3.16}$$

$$\delta_n = \arctan\left(\frac{B_n}{A_n}\right) \tag{3.17}$$

equation 3.15 can be rewritten as

$$\eta(t) = \sum_{n=1}^{N_h} R_n \cos(\omega_n t + \delta_n) \tag{3.18}$$

in which R_n is the *random* amplitude of the n^{th} harmonic and δ_n is its phase angle.

Morooka & Yokoo (1997) also stated that A_n and B_n can be expressed as

$$A_n = \alpha_n \left[S_\eta(\omega_n)\,\Delta\omega\right]^{1/2} \tag{3.19}$$

$$B_n = \beta_n \left[S_\eta(\omega_n)\,\Delta\omega\right]^{1/2} \tag{3.20}$$

where α_n and β_n are independent random numbers, of Gaussian distribution and zero mean.

Substituting the random components A_n and B_n into equation 3.16 gives

$$R_n = \left[{\alpha_n}^2 S_\eta(\omega_n)\,\Delta\omega + {\beta_n}^2 S_\eta(\omega_n)\,\Delta\omega\right]^{1/2} \tag{3.21}$$

which can be written as

$$R_n = \sqrt{2S_\eta(\omega_n)\,\Delta\omega}\sqrt{\frac{{\alpha_n}^2 + {\beta_n}^2}{2}} \tag{3.22}$$

This gives the relationship between the non-deterministic spectral amplitudes $a_{n_{\mathrm{NSA}}}$ $(= R_n)$ to the original deterministic amplitudes $a_{n_{\mathrm{DSA}}}$:

$$a_{n_{\mathrm{NSA}}} = a_{n_{\mathrm{DSA}}} \sqrt{\frac{{\alpha_n}^2 + {\beta_n}^2}{2}} \tag{3.23}$$

Due to the robustness of this alternative method, it is the *non-deterministic* spectral amplitudes that will be used for all the simulations in this work.

Once the amplitudes have been determined, the Discrete Fourier Transform (DFT) of the surface elevation can be constructed by describing the contribution of each harmonic in the form

$$\eta_n(x,t) = \frac{a_{n_{\mathrm{NSA}}}}{2} \mathrm{e}^{\mathrm{i}(\delta_n - k_n x)} \mathrm{e}^{\mathrm{i}\omega_n t} + \frac{a_{n_{\mathrm{NSA}}}}{2} \mathrm{e}^{-\mathrm{i}(\delta_n - k_n x)} \mathrm{e}^{-\mathrm{i}\omega_n t} \tag{3.24}$$

which for a fixed point, $x = 0$, can be expressed as the sum of two complex exponential terms with frequencies, ω_n and $-\omega_n$:

$$\eta_n(t) = X_n \mathrm{e}^{\mathrm{i}\omega_n t} + Y_n \mathrm{e}^{-\mathrm{i}\omega_n t} \tag{3.25a}$$

$$X_n = \frac{a_{n_{\mathrm{NSA}}}}{2} \mathrm{e}^{\mathrm{i}\delta_n} \tag{3.25b}$$

$$Y_n = \frac{a_{n_{\mathrm{NSA}}}}{2} \mathrm{e}^{-\mathrm{i}\delta_n} \tag{3.25c}$$

Making use of the fact that Y_n is the complex conjugate of X_n means that a sample record of $\eta(t)$ can be generated very quickly by calculating the inverse Fast Fourier Transform of its DFT.

3.4 Probability Theory

Some of the basic principles of probability theory that have played an important role in being applied to the uncertainty in this project are outlined in this section. The equations in this section are taken from Montgomery & Runger (2002), with the exception of equation 3.30.

3.4.1 Total Probability Theory

The addition rule states that the probability of the union of two mutually exclusive events, X and Y, is calculated by

$$\mathrm{P}(X \cup Y) = \mathrm{P}(X) + \mathrm{P}(Y) \tag{3.26}$$

The multiplication rule states that the conditional probability of an event X, given Y has occurred, is calculated by

$$\mathrm{P}(X \mid Y) = \frac{\mathrm{P}(X \cap Y)}{\mathrm{P}(Y)} \tag{3.27}$$

Consider j mutually exclusive and collectively exhaustive events that are denoted by $E_1, E_2 \ldots E_j$, and an event A in the same sample space. It follows that the joint events $A \cap E_1, A \cap E_2 \ldots A \cap E_j$, are mutually exclusive, and since A can be defined as $(A \cap E_1) \cup (A \cap E_2) \cup \cdots \cup (A \cap E_j)$, equation 3.26 means that the probability of A can be found by

$$\mathrm{P}(A) = \sum_{j=1} \mathrm{P}(A \cap E_j) \tag{3.28}$$

Combining equation 3.27 with equation 3.28 results in the *Total Probability Theorem*, that gives the total probability of event A based on its conditional probabilities:

$$\mathrm{P}(A) = \sum_{j=1} \mathrm{P}(A \mid E_j)\,\mathrm{P}(E_j) \tag{3.29}$$

As shown in chapter 4, these concepts become very useful when it comes to modelling a random process that is governed by other random factors, such as the probability of

a specific sea state occurring, which affects the total probability of the surface elevation values.

3.4.2 Empirical Probability Distributions

An empirical cumulative probability distribution can be determined based on the number of points in the distribution N after the values are ranked in ascending order. The probability that the random variable x will not exceed a given value h, can be approximated using the following equation (Gringorten 1963), in which n is the rank of the corresponding point from 1 to N:

$$\mathrm{P}\left(x \leq h_n\right) = \frac{n-a}{N+b} \tag{3.30}$$

where, for extreme value distributions, a and b are assumed to be 0.44 and 0.12, respectively.

Chapter 4

Mathematical Modelling of Wave Loading

4.1 Simulation of Random Sea Waves

This section describes the method for simulating ocean waves that can be described by Linear Random Wave Theory and thus, are under the assumptions given in 3.2.

4.1.1 Water Particle Kinematics

The surface elevation of sea waves can be used to determine more useful information that is more directly related to the loading on an offshore structure, namely the velocities and accelerations of the water particles at the coordinates (x_1, z) and at time t. These are also modelled as a random process described by the summation of a large number of harmonics. The horizontal water particle velocity u and acceleration $\dot{u}$ caused by the n^{th} harmonic are defined by equations 4.1 and 4.2, respectively (Stokes 1847).

$$u_n(x_1, z, t) = a_n \omega_n \frac{\cosh[k_n(z+d)]}{\sinh(k_n d)} \cos(\omega_n t - k_n x_1 + \delta_n) \tag{4.1}$$

$$\dot{u}_n(x_1, z, t) = a_n {\omega_n}^2 \frac{\cosh[k_n(z+d)]}{\sinh(k_n d)} \sin(\omega_n t - k_n x_1 + \delta_n) \tag{4.2}$$

where d is the water depth and z is the vertical distance from the mean water level (upwards positive).

For a given surface elevation frequency spectrum, the corresponding horizontal water particle velocity and acceleration frequency spectra can be obtained using the transfer functions that are based on equations 4.1 and 4.2, respectively, by employing the following relationships:

$$S_u(\omega) = S_\eta(\omega) |H_u(\omega)|^2 \tag{4.3}$$

$$S_{\dot{u}}(\omega) = S_\eta(\omega) |H_{\dot{u}}(\omega)|^2 \tag{4.4}$$

for which the transfer functions are calculated by

$$H_u(\omega_n) = \omega_n \frac{\cosh[k_n(z+d)]}{\sinh(k_n d)} \mathrm{e}^{-\mathrm{i}k_n x_1} \tag{4.5}$$

$$H_{\dot{u}}(\omega_n) = \mathrm{i}{\omega_n}^2 \frac{\cosh[k_n(z+d)]}{\sinh(k_n d)} \mathrm{e}^{-\mathrm{i}k_n x_1} \tag{4.6}$$

This means that a previously calculated DFT of the surface elevation can be directly multiplied by the transfer functions $H_u(\omega)$ and $H_{\dot{u}}(\omega)$ to obtain the respective DFTs of u and $\dot{u}$. This enables time histories of both these 'response' parameters to be calculated quickly by computing the inverse Fast Fourier Transform of their DFTs. This technique can be applied to any system parameter that is a *linear* response to the original random input and is not limited to random waves only.

4.1.2 Sea States

A important concept in this project is the use of sea states to describe the intensity of the conditions for a particular duration, usually 3 hours or so, where they are considered constant. A sea state is defined by the average values of information about the wave heights and time-periods of the surface elevation during the chosen duration.

Information about the conditions of the sea during one of these 3-hour periods is given in the form of a corresponding frequency spectrum. The magnitude of the frequency spectrum is determined by the sea state, whereas the particular shape of the frequency spectrum depends on the geographical location of the waves being considered. The relationship between a frequency spectrum and the actual surface elevation of the sea at a particular point was outlined in section 3.3.

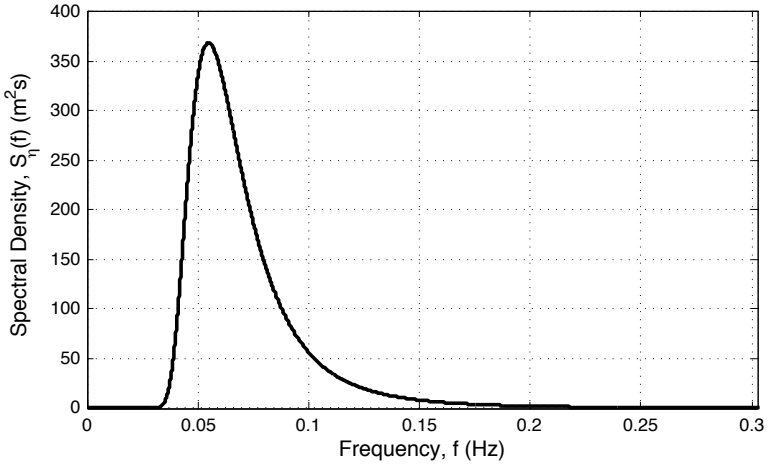

Figure 4.1: Pierson-Moskowitz Wave Spectrum

Figure 4.1 shows the well-known Pierson-Moskowitz Spectrum (Pierson & Moskowitz 1964), which is used to describe waves in the North Atlantic and is defined as

$$S_\eta(f) = \frac{{H_s}^2}{4\pi {T_z}^4 f^5} \exp\left(-\frac{1}{\pi {T_z}^4 f^4}\right) \tag{4.7}$$

where H_s is the significant wave height, which is defined as the average value of the highest third of all wave heights (distance from trough to crest) that occur in a given duration. T_z is the average zero-upcrossing period, which is essentially the given duration divided by the number of waves that occur in that duration, where a wave is defined as the surface elevation having crossed the mean water level twice (once upwards and once downwards). A sea state, therefore, can be considered as a period of time for which the values of H_s and T_z can realistically be assumed to be constant.

To reiterate, the specific values shown on the y-axis would vary with sea state (i.e.

every 3-hours or so) but the shape of the spectrum is characteristic of the North Atlantic at all times.

4.2 Simulation of Extreme Quasi-Static Response Statistics

4.2.1 A Simple Model

In order to keep computational cost to a minimum when simulating a large number of sample records, a very simple offshore structure, shown in figure 4.2, is used in this study. In fact, the model would be more accurately described as a loads model, since it is only the geometry, not the actual structure, that is modelled. In other words: it is assumed to be a rigid structure. The test 'structure' is a cylindrical monopod divided into five segments and the distributed loading is represented by a nodal load at the midpoint of each segment. Clearly, only five segments would not be sufficient for an accurate calculation of design response, but for the purpose of comparing methods it makes no difference whether there are five segments or five-hundred. Also, the model does not take into account the effect of current or load intermittency in the splash zone. The structure has drag and inertia coefficients of $C_d = 0.8$ and $C_m = 1.7$, respectively. Unless stated otherwise, the water depth is taken to be 50 m, the leg has a constant diameter of 3.0 m and the sea state for the short-term cases is defined by $H_s = 15$ m and $T_z = 13$ s.

It should be noted that the goal of the research at this point is not to analyse highly complex structures, but to develop mathematical techniques that can work on any structure. Therefore, the very simple structure shown in figure 4.2 is sufficient because, without prolonged simulation time, it allows the techniques to be tested, which verifies them for use on more complex models.

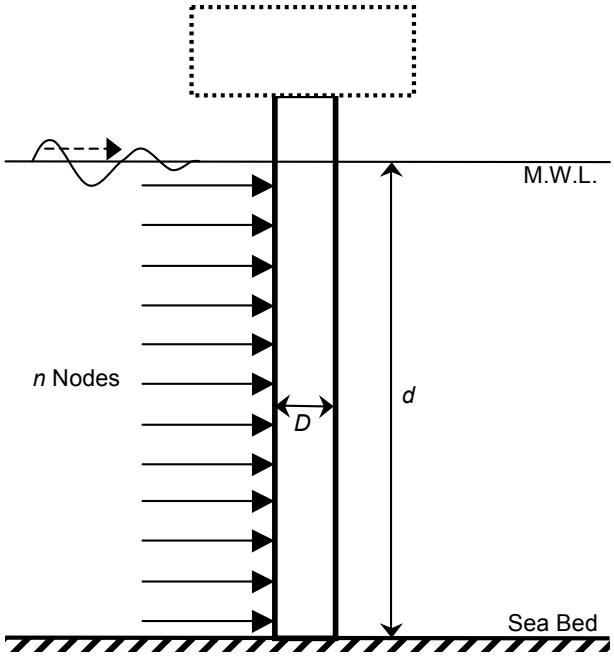

Figure 4.2: Simple Offshore Structural Model: $d = 50$ m, $D = 3$ m, $n = 5$ nodes

4.2.2 Offshore Structural Response

Morison Loading on Cylindrical Members

Morison's equation (Morison et al. 1950) states that the wave-induced horizontal force per unit length q on a vertical submerged cylinder (cylinder diameter / wavelength $< 1/5$) is the sum of a *nonlinear* drag component q_d and a linear inertial component q_i. This is shown in the following equation:

$$q = q_d + q_i = k_d|u|u + k_i\dot{u} \tag{4.8a}$$

$$k_d = \frac{1}{2}C_d\rho D \tag{4.8b}$$

$$k_i = \frac{1}{4}C_m\rho\pi D^2 \tag{4.8c}$$

The drag and inertia coefficients, C_d and C_m, are dependent on Reynold's number, Kuelegan-Carpenter number and cylinder roughness. In using Morison's equation to calculate the nodal forces, it is assumes that vortex-induced transverse forces have a negligible effect (Sarpkaya & Isaacson 1981).

Effect of Load Nonlinearity

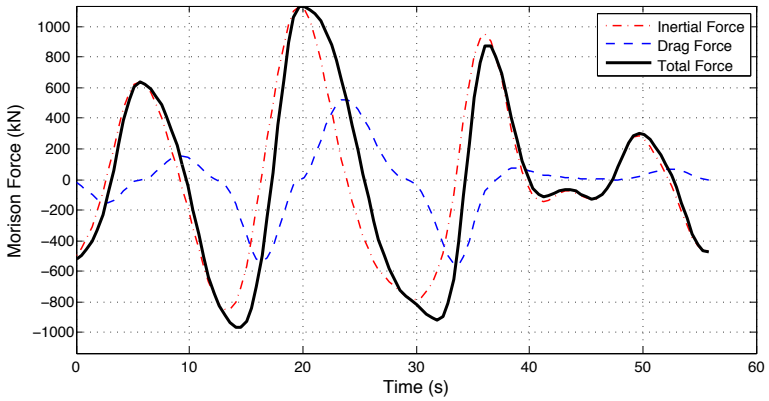

(a) Inertia-dominated Structure, $D = 3.0$ m

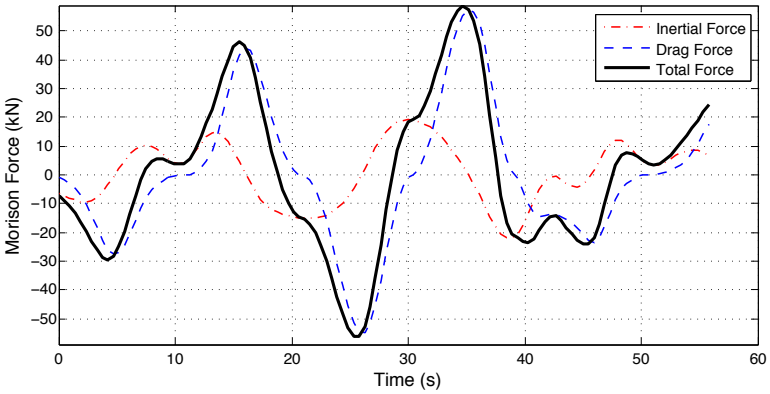

(b) Drag-dominated Structure, $D = 0.5$ m

Figure 4.3: Components of Morison Load on Drag- and Inertia-dominated Structures

Evidently, the calculation of the Morison force at each node on the structure, first requires the evaluation of the water particle kinematics at the corresponding nodes. As previously mentioned, the water particle kinematics are linearly related to the surface elevation and hence can be calculated using simple transfer functions. The loads however, cannot be calculated using transfer functions due to the nonlinearity of the drag component, which can be seen in equation 4.8a. The difference between the loads on drag- and inertia-dominated structures can be demonstrated by varying the diameter of the cylindrical elements and examples of short sample records of Morison load including drag and inertia components are given in figure 4.3.

Figures 4.4a and 4.4b are cumulative probablity distributions from a much longer

sample records of total morison load and correspond to the same diameters used in the previous figures. It is clear that the drag-dominated structure results in a highly non-Gaussian response probability distribution, which indicates strong nonlinear behaviour because a linear system would have produced a Gaussian response to the Gaussian input. In comparison, linear behaviour is exhibited by the inertia-dominated structure in figure 4.4a.

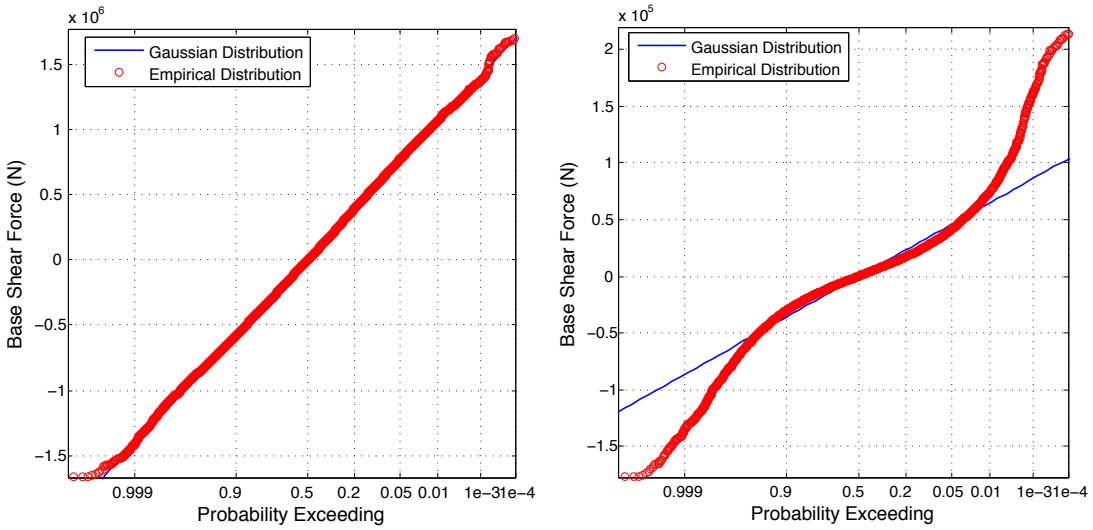

(a) Inertia-dominated Structure, $D = 3.0$ m **(b)** Drag-dominated Structure, $D = 0.5$ m

Figure 4.4: CDFs of Base Shear Force; derived from a Single Sample Record in each case

As one would expect, these figures are in agreement with equation 4.8, but more importantly, they reinforce the point that a frequency domain analysis, which relies upon a linear relationship between input (surface elevation) and response (Morison load dependent), is not sufficient for calculating the statistical properties of offshore structural response (Tickell 1977). Thus, the rest of the analysis must be carried out in the time domain, unless a linearised approximation for the drag component is used, which would of course sacrifice some of the accuracy and reliability of the results. But for structures that exhibit strong nonlinearities, i.e. drag-dominated structures, this type of analysis would be completely unreliable. Here lies the heart of the problem that is being tackled in this project: to calculate the loads in the time domain at every node is extremely time consuming compared to the alternative frequency domain

approximations, but it is absolutely necessary if one is to conduct a reliable structural analysis. This problem is magnified when considering the sheer number of sample records that need to be simulated in order to generate even short-term response statistics, but this will be discussed a little later in this chapter.

Interesting Quantities

Once the Morison loads on the structure have been calculated for a given sample record, they can be used to establish a time history of whichever structural response parameter that is of particular interest for the design, often called an *interesting quantity*. The interesting quantities considered in this project are limited to base shear (BS) and over-turning moment (OTM), but of course there are a vast number of responses that an engineer might want to calculate in reality (e.g deck deflection, stresses in critical members, etc.). In this case, assuming a linear system in which dynamic effects are negligible, the quasi-static base shear force and over-turning moment at the sea bed is calculated using equations 4.9 and 4.10, respectively.

$$BS = \sum_{k=1}^{N_{\mathrm{N}}} q_k l_{\mathrm{seg}} \tag{4.9}$$

$$OTM = \sum_{k=1}^{N_{\mathrm{N}}} q_k Z_k l_{\mathrm{seg}} \tag{4.10}$$

where Z_k is the distance of the k^{th} node from the sea bed and l_{seg} is the length of one cylindrical segment, which is equal to d/N_{N}.

4.2.3 Short-Term Response Statistics

In order to compute an empirical distribution for an interesting quantity, it is necessary to simulate a large number of sample records. Figure 4.4 gave examples of CDFs using all the load values from a single sample record, but for design purposes, it is more useful to calculate an *extreme* value distribution, which is the probability distribution of the

single maximum value from each of a range of response sample records. This distribution gives the proportion of sample records that can be expected to have extreme values that exceed a certain value.

This distribution is considered to be *short-term* if only a single sea state is considered. In other words, all of the surface elevation sample records are generated using the exact same frequency spectrum, i.e. the exact same values of H_s and T_z. The conventional procedure for calculating a short-term extreme response distribution is as follows:

(1) The frequency spectrum, defined by equation 4.7, is used along with equation 3.23 to generate random amplitudes and phases for a range of harmonics. Thus, the discrete fourier transform of a surface elevation sample record can be defined using equation 3.25.

(2) The DFTs of the horizontal water particle velocity and acceleration at each node are calculated using equations 4.5 - 4.6. Then sample records of u and $\dot{u}|$ are calculated by taken the inverse Fourier Transform of their respective DFTs.

(3) The water particle kinematics sample records are used to calculate the Morison forces at the respective nodes using equation 4.8.

(4) Equations 4.9 and 4.10 can then be used to determine the structural response in term of base shear and over-turning moment. If required, time histories of other interesting quantities can be established.

(5) The maximum (extreme) value of an interesting quantity for this sample record is extracted.

(6) For the exact same input parameters, steps (1) to (5) are repeated for a very large number of sample records, say 100,000, and the extreme values of the interesting quantities are ranked in ascending order.

(7) The empirical cumulative probability distribution of each interesting quantity is given by equation 3.30.

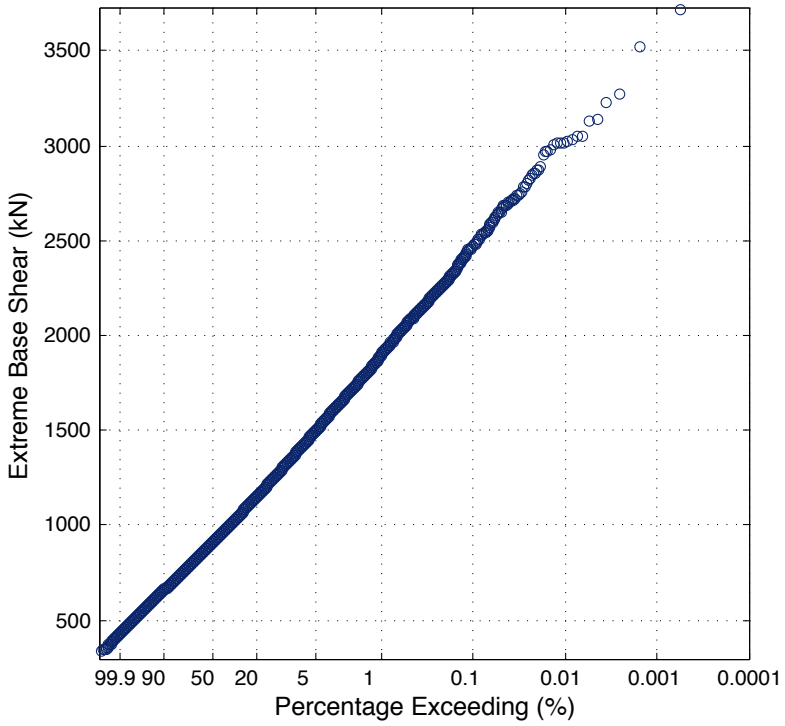

Figure 4.5: Short-Term Probability Distribution of Base Shear using the Conventional Method

Figure 4.5 shows an example of an extreme response distribution, plotted to the Gumbel scale, that was obtained using the method outlined above.[1] It can be clearly observed that, although the distribution consists of 100,000 data points (one extreme value from each simulated response sample record), the vast majority of them are nowhere near the tail of the distribution, which is the area of greatest value when it comes to estimating design response values. However, reducing the number of simulations using the conventional method would simply increase the sampling variability, and hence the reliability, at the high extreme values (the 'tail' of the distribution). Thus, the reason that the Conventional method takes so long is that it requires a very large number of simulations to produce a distribution with a tail that is adequately reliable for obtaining design response values.

[1] In this case, two-minute sample records were used to reduce computational cost, but three-hour sample records would be more realistic.

4.2.4 Long-Term Response Statistics

'Short-term' probability distributions describe the probability of exceedance of the interesting quantities for a single sea state, which is defined by specific values of H_s and T_z. A 'long-term' probability distribution is one that enables the *total probability* of exceedance to be determined on the basis of all possible sea states. In other words, it takes into account the fact that random waves are actually non-stationary by applying the probability of occurrence of a large number of stationary processes (individual sea states).

For example, the probability distribution in figure 4.5 shows the probability that the structure response will exceed a value $r_{\max}$ based on the *condition* that the sea state, $H_s = 15$ m, $T_z = 13$ s, has already occurred. This probability can be written in general terms as $\mathrm{P}\left(r_{\max} \mid H_s \cap T_z\right)$, which means that, from equation 3.29, the total probability of $r_{\max}$ for the range of j sea states can be written as

$$\mathrm{P}\left(r_{\max}\right) = \sum_{j=1} \mathrm{P}\left[r_{\max} \mid \left(H_s \cap T_z\right)_j\right] \mathrm{P}\left[\left(H_s \cap T_z\right)_j\right] \tag{4.11}$$

In order to illustrate the application of this to the design of offshore structures, the following example has been provided, using extreme surface elevation $\eta_{\max}$ instead of extreme response $r_{\max}$ so that the analytical distribution could be used and thus, no simulations were necessary.

Suppose there are three sea states that could possibly occur, denoted by SS1, SS2 and SS3. Evidently, they are collectively exhaustive and mutually exclusive so the sum of their probabilities of occurrence must be equal to one. The properties of the sea states are:

SS1: $H_s = 5$ m, $T_z = 7.9$ s, $\mathrm{P(SS1)} = 0.2$

SS2: $H_s = 10$ m, $T_z = 11.2$ s, $\mathrm{P(SS2)} = 0.7$

SS3: $H_s = 15$ m, $T_z = 13.7$ s, $\mathrm{P(SS3)} = 0.1$

With these properties, equation 4.12 can be used to find the total probability of the extreme values of surface elevation for all three sea states:

$$\begin{aligned} \mathrm{P}\left(\eta_{\max}\right) = \quad & \mathrm{P}\left(\eta_{\max} \mid \mathrm{SS1}\right) \mathrm{P}\left(\mathrm{SS1}\right) + \\ & \mathrm{P}\left(\eta_{\max} \mid \mathrm{SS2}\right) \mathrm{P}\left(\mathrm{SS2}\right) + \mathrm{P}\left(\eta_{\max} \mid \mathrm{SS3}\right) \mathrm{P}\left(\mathrm{SS3}\right) \end{aligned} \tag{4.12}$$

Figure 4.6 shows the theoretical solution for $\mathrm{P}\left(\eta_{\max}\right)$ and compares it to the individual probability distributions $\mathrm{P}\left(\eta_{\max} \mid \mathrm{SS1}\right)$, $\mathrm{P}\left(\eta_{\max} \mid \mathrm{SS2}\right)$ and $\mathrm{P}\left(\eta_{\max} \mid \mathrm{SS3}\right)$.

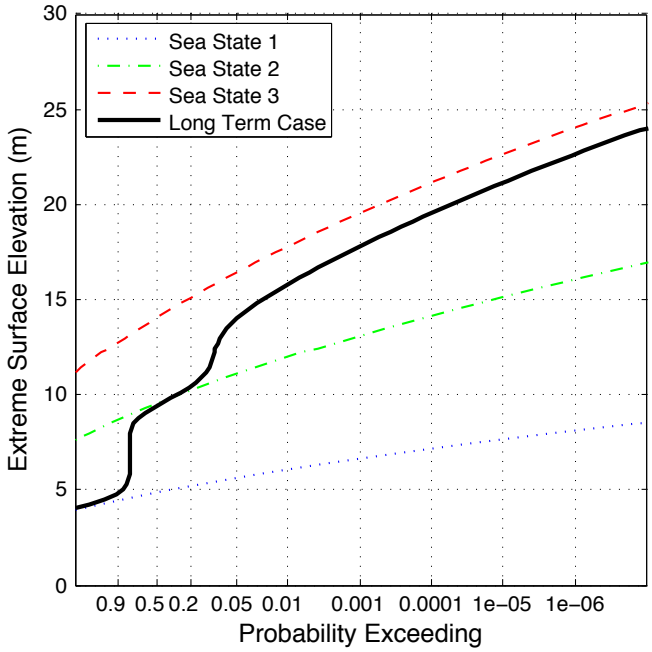

Figure 4.6: Example of Long-term CDF of Extreme Surface Elevation using only 3 Sea States

For design purposes, one might assume that taking the worst conditions that could

occur and simulating sample records for that sea state would be a sensible solution. However, in this case it is clear that the use of the long-term case predicts lower extreme values for a given design probability of exceedance than if the worst-case sea state, SS3, is used. This demonstrates that to achieve the most efficient designs, *all* of the possible conditions that could occur must be taken into account. This magnifies the problem of the high computational cost when it comes to simulating long-term structural response distributions, for which *no analytical solution is available* due to the nonlinearity of the drag component of the Morison load.

As one would expect, in reality there is a much larger number of possible sea states that could occur. Also, H_s and T_z are not statistically independent, so $\mathrm{P}(\eta_{\max})$ must be calculated for each joint event $H_s \cap T_z$. This means that in order to find the total probability of $\eta_{\max}$, the joint probability distribution of H_s and T_z must be determined. Fortunately, real data is available that makes this possible as shown in figure 4.7, which is known as a sea state scatter diagram. This particular data was taken from the Forties region of the North Sea, the conditions of which have been assumed for all the simulations in this project.

From figure 4.7 the probability of the joint event $H_s \cap T_z$ can be calculated by dividing the number of times that the sea state $H_s \cap T_z$ occurred by the total number of recorded sea states (88053 in this case). Therefore, the sea state scatter diagram is essentially a joint probability mass function of H_s and T_z. Given this information, the long-term distribution of extreme surface elevation can be established, which can later be used to validate the offshore structural response model used in this project.

It is important to note, however, that since the sea state scatter diagram is comprised of data that was measured over a finite period of time that is relatively short (approximately 27 years), there are extreme sea states that could theoretically occur at that site, that are not accounted for in the data in table 4.7 because they did not occur during the time the data was being recorded. This leads to unreliable long-term surface elevation probability distributions because sea state conditions of greater intensity (and of greater return period) than those measured are not accounted for (Goda 2010). Trial calculations have shown that scatter diagrams should cover the

average occurrence of sea states over a duration which is at least 10 times as long as the service life of the structure (Inglis et al. 1985). Clearly, this amount of measured data is not available given that offshore structures are typically designed for loads that occur once every hundred years. Therefore, in order to calculate reliable long-term probability distributions for offshore structural response, the sea state scatter diagram must be extrapolated to account for the more extreme sea states. This extrapolation has not been carried out for the work in this project, because it is not necessary for simply demonstrating the method for simulating long-term statistics, but it would need to be if one were calculating actual design loads.

Significant Wave Height (Measured) in metres																			
	Σ Cum.	88053	88051	88051	87531	79593	57544	29719	11362	3327	784	159	32	8	0	0	0		
	Σ	2	0	520	7938	22049	27825	18357	8035	2543	625	127	24	8	0	0	0		
From >=	To <																	Σ	Σ Cum.
16	16.5	0	0	0	0	0	0	0	0	0	0	0	0	0	0	0	0	0	0
15.5	16	0	0	0	0	0	0	0	0	0	0	0	0	0	0	0	0	0	0
15	15.5	0	0	0	0	0	0	0	0	0	0	0	0	0	0	0	0	0	0
14.5	15	0	0	0	0	0	0	0	0	0	0	0	0	0	0	0	0	0	0
14	14.5	0	0	0	0	0	0	0	0	0	0	0	0	0	0	0	0	0	0
13.5	14	0	0	0	0	0	0	0	0	0	0	0	0	0	0	0	0	0	0
13	13.5	0	0	0	0	0	0	0	0	0	0	0	0	0	0	0	0	0	0
12.5	13	0	0	0	0	0	0	0	0	0	0	0	0	0	0	0	0	0	0
12	12.5	0	0	0	0	0	0	0	0	0	0	0	0	0	0	0	0	0	0
11.5	12	0	0	0	0	0	0	0	0	0	0	0	0	0	0	0	0	0	0
11	11.5	0	0	0	0	0	0	0	0	0	0	1	0	0	0	0	0	1	1
10.5	11	0	0	0	0	0	0	0	0	0	0	3	1	0	0	0	0	4	5
10	10.5	0	0	0	0	0	0	0	0	1	2	4	4	0	0	0	0	11	16
9.5	10	0	0	0	0	0	0	0	0	1	6	6	4	0	0	0	0	17	33
9	9.5	0	0	0	0	0	0	0	0	4	13	5	4	0	0	0	0	26	59
8.5	9	0	0	0	0	0	0	0	0	16	26	9	3	0	0	0	0	54	113
8	8.5	0	0	0	0	0	0	0	2	21	47	6	2	0	0	0	0	78	191
7.5	8	0	0	0	0	0	0	0	2	67	58	3	0	1	0	0	0	131	322
7	7.5	0	0	0	0	0	0	0	6	128	50	5	2	1	0	0	0	192	514
6.5	7	0	0	0	0	0	0	1	51	219	60	5	0	0	0	0	0	336	850
6	6.5	0	0	0	0	0	0	3	165	270	42	5	1	0	0	0	0	486	1336
5.5	6	0	0	0	0	0	1	9	462	309	44	1	0	0	0	0	0	826	2162
5	5.5	0	0	0	0	0	3	92	887	299	29	5	0	0	0	0	0	1315	3477
4.5	5	0	0	0	0	0	3	477	1273	203	19	2	0	0	0	0	0	1977	5454
4	4.5	0	0	0	0	2	24	1613	1255	201	26	3	0	1	0	0	0	3125	8579
3.5	4	0	0	0	0	2	318	3029	996	148	23	4	0	0	0	0	0	4520	13099
3	3.5	0	0	0	0	10	1889	3546	776	133	30	4	0	0	0	0	0	6388	19487
2.5	3	0	0	0	2	205	4940	3151	675	153	22	1	0	0	0	0	0	9149	28636
2	2.5	0	0	0	17	2102	7079	2624	612	131	28	10	0	0	0	0	0	12603	41239
1.5	2	0	0	0	302	6717	6545	1808	394	79	22	11	0	2	0	0	0	15880	57119
1	1.5	0	0	11	2592	8091	4765	1334	247	66	31	12	2	3	0	0	0	17154	74273
0.5	1	0	0	356	4390	4470	2031	565	178	70	30	10	1	0	0	0	0	12101	86374
0	0.5	2	0	153	635	450	227	105	54	24	17	12	0	0	0	0	0	1679	88053
0	0	0	1	2	3	4	5	6	7	8	9	10	11	12	13	14	15	PhysE	
0	0	1	2	3	4	5	6	7	8	9	10	11	12	13	14	15	16		
		Mean Zero-crossing Period (Seconds)																	

Figure 4.7: Data Taken from the Forties Region of the North Sea from June 1974 to August 2001 (Provided by the Health and Safety Executive, UK)

4.3 Model Validation

Before techniques for speeding up the derivation of structural response distributions can be tested, it is necessary to ensure that the model that will be used is reliable. Of course, structural response distributions can not be compared to analytical equations, because they do not exist; otherwise the distributions would not need to be simulated at all. The properties of simulated surface elevation sample records, however, can be compared with analytical equations that describe linear random waves and Gaussian processes. Due to the linear relationship with surface elevation, the water particle kinematics of the model can also be validated using analytical probability distributions. It must be assumed that if the model behaves in a way that is consistent with these analytical descriptions, the properties of the simulated structural response are also realistic. Figure 4.8 defines some of the properties of random sea waves that will be examined in order to validate the capability of the model.

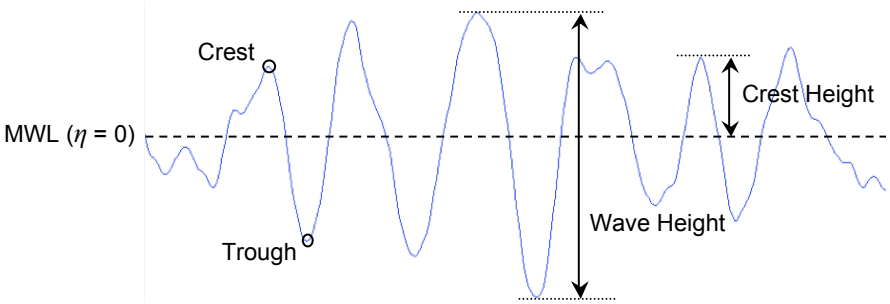

Figure 4.8: Properties of Sea Waves

Figures 4.9 - 4.13 show comparisons of simulated data from the model in section 4.2 with analytical descriptions of the CDFs of each wave property. Figure 4.9, plotted on a Gaussian scale, compares the simulated values of η from a single sample record to the theoretical CDF of a zero-mean Gaussian process,

$$\mathrm{P}\left(\eta \leq \eta_*\right) = \frac{1}{2}\left[1 + \mathrm{erf}\left(\frac{\eta_*}{\sqrt{2{\sigma_\eta}^2}}\right)\right] \tag{4.13}$$

where, because the sea is modelled as a narrow-banded process, the standard deviation of the surface elevation σ_η is directly related to the significant wave height in the following way (Hoffman & Karst 1975):

$$H_s \approx 4\sigma_\eta \tag{4.14}$$

Figure 4.10 compares simulated values of $\eta_{\max}$ from a large number of sample records to the theoretical distribution given in equation 3.4, and is plotted to the Gumbel scale. Both figures 4.9 and 4.10 show that the model behaves as expected; any deviation from the theoretical distribution in either case is clearly due to sampling variability, which is a product of the aleatory uncertainty within the process. Figures 4.12 and 4.13, on the other hand, display systematic deviation from the theoretical distributions, which must be justified if the model is to be deemed sufficiently realistic.

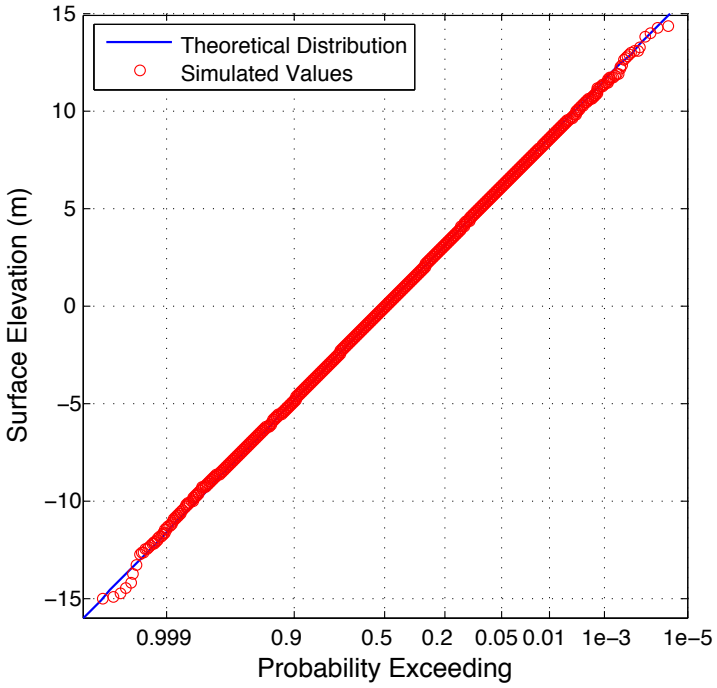

Figure 4.9: CDF of Surface Elevation Values from a Single 3-hour Sample Record

Assuming that the crest height is equal to $H/2$, figure 4.12 compares simulated crest heights from a single sample record to an analytical distribution for wave heights that is based on the Rayleigh distribution (Tayfun 1980) which, combined with equation 4.14, gives

$$\mathrm{P}\left(H \leq H_*\right) = 1 - \exp\left(-\frac{2{H_*}^2}{{H_s}^2}\right) \tag{4.15}$$

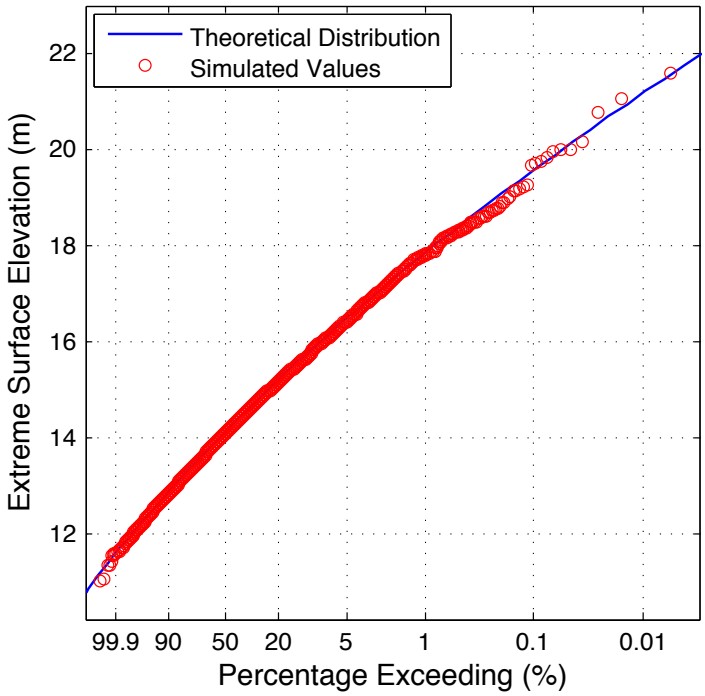

Figure 4.10: CDF of Extreme Surface Elevation from 10,000 Sample Records

Figure 4.12 shows that the empirical distribution of wave crests deviates from equation 4.15 for lower crest heights. This is most likely due to the way that crest heights have been extracted from the sample records. In the program used to calculate crest heights, a wave is considered to be between two points of zero-upcrossing, which means that some smaller waves that occur will be missed because they occur entirely above or below the mean water level. Figure 4.11 demonstrates this, and it is clear that it is these smaller waves that are less likely to cross the MWL and thus are undetected by the program, which accounts for the apparent scarcity of smaller wave crests in the distribution from figure 4.12.

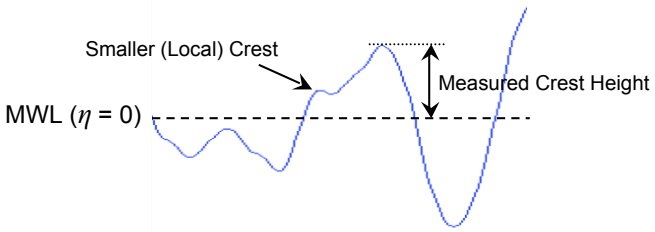

Figure 4.11: Limitation in the Measurement of Crest Height from Simulated Data

The deviation of the empirical data in figure 4.13 from the theoretical distribution is in fact consistent with reality because the Rayleigh distribution has been shown to be overly conservative at predicting large (crest-to-trough) wave heights (Tayfun 1981). This is due to the fact that the crest and the trough of a wave do not occur at the same time, and so for high crests, associated troughs are likely to have a smaller amplitude (Forristall 1984). Thus, the assumption that the wave height is twice the crest height becomes invalid for higher crest heights, especially for spectra that are not quite as narrow, such as the Pierson-Moskowitz spectrum used in this study.

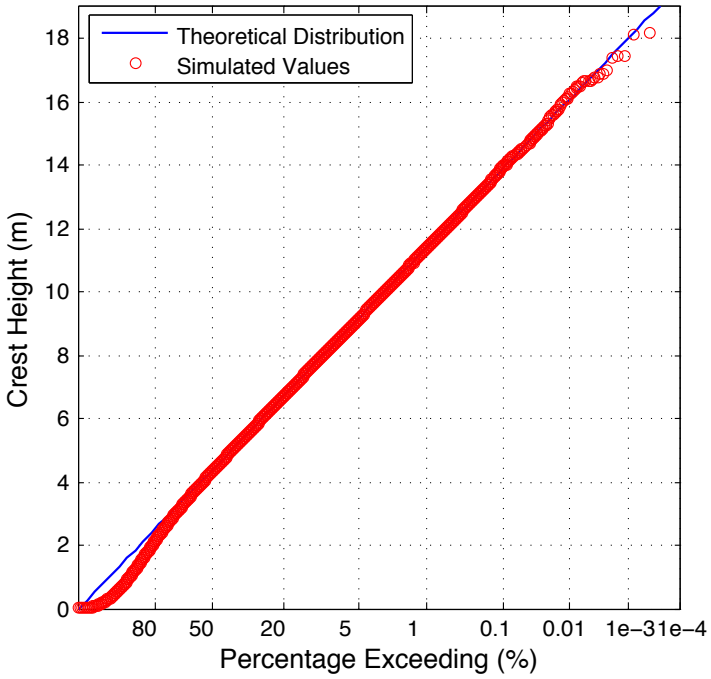

Figure 4.12: CDF of Crest Heights from a Single 40-day Sample Record Plotted to the Rayleigh Scale

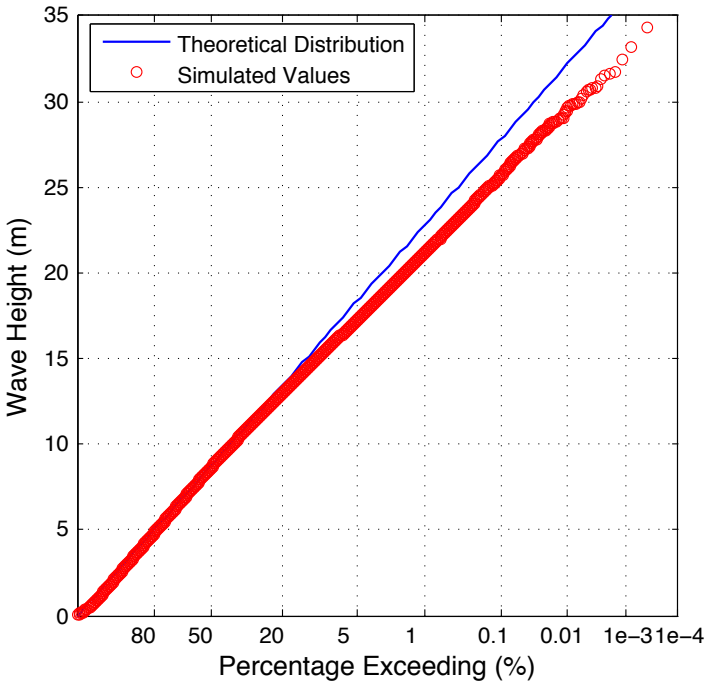

Figure 4.13: CDF of Wave Heights from a Single 40-day Sample Record Plotted to the Rayleigh Scale

Figures 4.14 and 4.15, show that the empirical distributions of water particle kinematics and their extreme values are also consistent with reality. The slight deviation in figure 4.15b is most likely due to some small error in the calculation of $\sigma_{\dot{u}}$ for defining the theoretical distribution, rather than the simulated data.

Up until now, the distributions in this section have been short-term, assuming the sea state ($H_s = 15\text{m} \cap T_z = 13\text{s}$) has occurred, but it is necessary to confirm that the model performs realistically for the full range of sea states that could possibly occur. In this case, simulated extreme values are compared to a theoretical long-term CDF of $\eta_{\max}$ based on the sea state scatter diagram shown in figure 4.7. As observed in figure 4.16, the model gives an excellent fit between the empirical and theoretical curves and it should be noted that the number of simulations is extremely high (10 million in total) in order to produce a tail with sufficiently low sampling variability. This again highlights the importance of developing techniques to reduce the number of simulations required to achieve an accurate distribution when it comes to calculating time-domain response statistics.

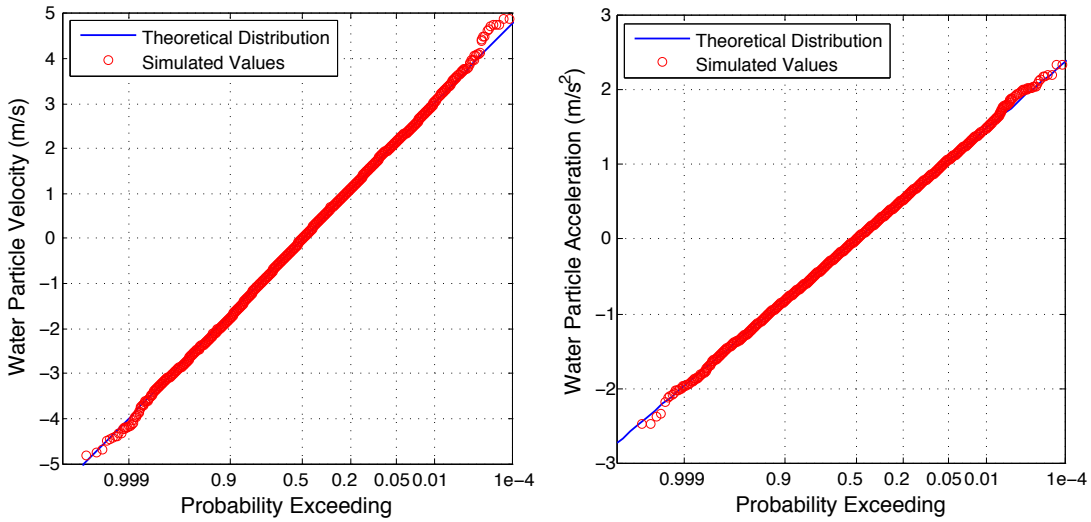

(a) Horizontal Water Particle Velocity **(b)** Horizontal Water Particle Acceleration

Figure 4.14: CDFs of Water Particle Kinematics Values from a Single 90-minute Sample Record

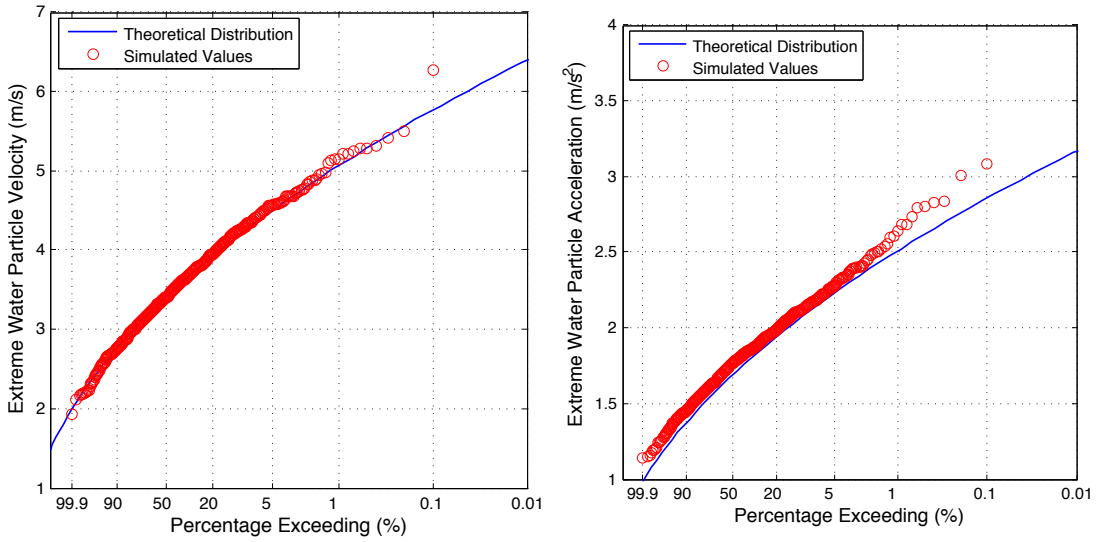

(a) Horizontal Water Particle Velocity **(b)** Horizontal Water Particle Acceleration

Figure 4.15: CDFs of Extreme Water Particle Kinematics from 10,000 Sample Records

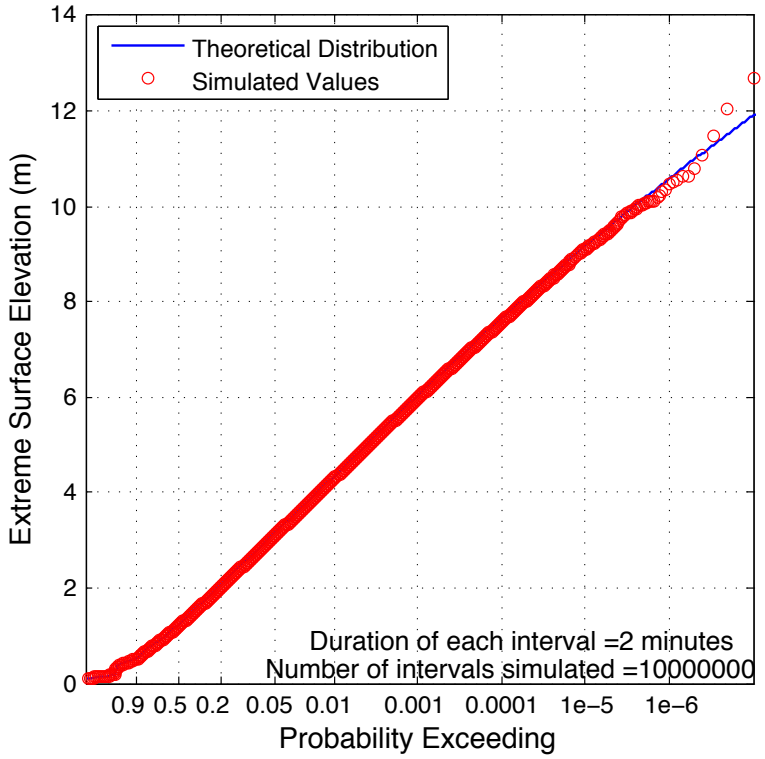

Figure 4.16: Long-Term CDF of Extreme Surface Elevation

Chapter 5

Speeding Up the Derivation of Response Probability Distributions

5.1 Improving the Reliability of the Efficient Time Simulation Technique

5.1.1 The Original ETS Technique

The main problem faced when calculating probability distributions of extreme structural response is that in order to obtain a few data points in the most unlikely region of extreme response values, a very large number of response sample records must be simulated. However, for design purposes, one is primarily interested in the tail of the probability distribution (the rarest occurrences), and even though hundreds of thousands of sample records have been simulated, the vast majority of the data points lie in the region that is of little interest. This means that only a very small amount of the simulation time is taken up by calculating the useful information of the response extreme values at the tail of the distribution. The challenge, if reducing the number of simulations, is to maintain the accuracy of the results. Fortunately the accuracy of any new technique can be confirmed by comparing the response probability distributions to

those of the conventional method outlined in section 4.2.

One way that the number of simulations can be reduced whilst maintaining a sufficient number of points in the tail of the distribution is using the Efficient Time Simulation (ETS) Technique (Abu Husain & Najafian 2010). This spreads out the sampling variability, transferring it to the parts of the distribution that are of little or no interest to the designer. The underlying approach employed by this method takes advantage of the fact that there is a strong correlation between extreme response values and extreme surface elevation values. This is a very useful correlation because it indicates that surface elevation sample records with high extreme values are likely to produce response sample records with high extreme values. Conversely, low surface elevation extreme values can be expected to bring about low response extreme values. Abu Husain & Najafian (2010) show correlation coefficients as high as 0.939 and 0.955, for the relationship of extreme surface elevation with extreme base shear and over-turning moment, respectively.

The correlation is exploited by dividing the theoretical probability distribution for extreme surface elevation (equation 3.4) into several groups such that the probability that a given surface elevation extreme value $\eta_{\max*}$ will fall into a certain group can be easily calculated. The fact that the response is calculated in the time domain means that converting surface elevation sample records to response sample records constitutes the vast majority of the simulation time. Dividing the surface elevation sample records into groups according to their extreme values allows a limit to be placed upon the number of response sample records that are calculated within each group. This means that it is no longer necessary to calculate a large number of response records in order to obtain the relatively small number of extreme values that form the tail of the response distribution. Once the chosen number of response sample records within a particular group have been calculated, all the subsequent surface elevation sample records that fall into that group can be discarded, potentially saving a great deal of simulation time.

Surface elevation sample records are calculated until the chosen number of response sample records for each group have been generated, at which point the desired data can be extracted from each sample record in order to determine the statistical properties of

the structural response. In the offshore engineering aspect of this project, seven groups were used ($G = 7$), separated by six boundaries for which the chosen probability values used in this study are presented in figure 5.1.

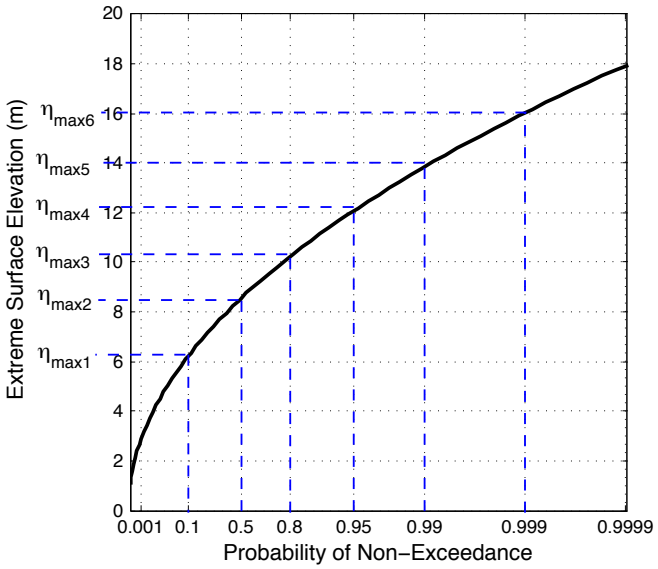

Figure 5.1: Theoretical Extreme Value Distribution for Surface Elevation Divided into 7 Groups

Let S be the set of all the simulated response extreme values such that $S = \{S_1, S_2, \ldots, S_G\}$ where $S_i \subset S$. The values in S are divided into these subsets based on the extreme values of their corresponding surface elevation sample records, using the boundaries specified in figure 5.1.

In order to calculate a response probability distribution from the limited number of sample records in each group, it is first necessary to determine the probability P_i that a sample record belongs to the i^{th} subset of S. This is calculated for each group such that

$$P_1 = \mathrm{P}\left(\eta_{\max 1}\right) \tag{5.1a}$$

$$P_i = \mathrm{P}\left(\eta_{\max i}\right) - \mathrm{P}\left(\eta_{\max i-1}\right), \quad i = 2, 3, \ldots, G-1. \tag{5.1b}$$

$$P_G = 1 - \mathrm{P}\left(\eta_{\max G}\right) \tag{5.1c}$$

In the ETS method, the extreme values are extracted from the response sample records,

and their probability distributions for each group are calculated using equation 3.30. The distribution $\mathrm{P}\left(r_{\max} \leq R\right)$ gives the probability that the extreme response $r_{\max}$ will not exceed a given response value R, and will be denoted as $\mathrm{P}_{r_{\max}}\left(R\right)$. Thus, the cumulative probability distribution of extreme response values within the i^{th} group is denoted as $\mathrm{P}^{(i)}_{r_{\max}}\left(R\right)$. Once $\mathrm{P}^{(i)}_{r_{\max}}\left(R\right)$ has been determined for each group, total probability theorem is applied in the following way to determine the overall probability distribution of $r_{\max}$:

$$\mathrm{P}_{r_{\max}}\left(R\right) = \sum_{i=1}^{G} \mathrm{P}^{(i)}_{r_{\max}}\left(R\right) P_i \tag{5.2}$$

Equation 5.2 makes clear the importance of having a strong correlation between the extreme values of surface elevation and response. The underlying assumption in the method is that the probability P_i that $\eta_{\max}$ will belong to the i^{th} subset is the same as the probability that the corresponding response extreme value $r_{\max}$ will also belong to that subset. Hence, P_i is used in equation 5.2 with regards to the *response*, whereas it was originally calculated from then theoretical extreme value distribution of the *input*.

Although Abu Husain & Najafian (2010) showed high correlation coefficients for both base shear and over-turning moment, they used a different structure to the one in section 4.2. This means the correlations must be calculated again for the structure used in this project in order to verify the aforementioned assumption is valid.

Figure 5.2 demonstrates that there is a very strong correlation between extreme surface elevation and the response extreme values. The correlation coefficients for base shear and over-turning moment of 0.965 and 0.954, respectively, which are very close to those found by Abu Husain & Najafian (2010) with a slightly different structure. The fact that the correlations are not linear does not affect the validity of the ETS method, it only matters that the correlation is strong and positive.

As figures 5.3a and 5.3b show, the original ETS method gives a good approximation of the extreme response distributions compared to those generated using the conventional method. Of course, the number of surface elevation sample records that are converted to response time-histories within each group has large effect on the accuracy of the distributions. In the example in figures 5.3a and 5.3b, there were 100 sample records in each group, making a total of only 700 response

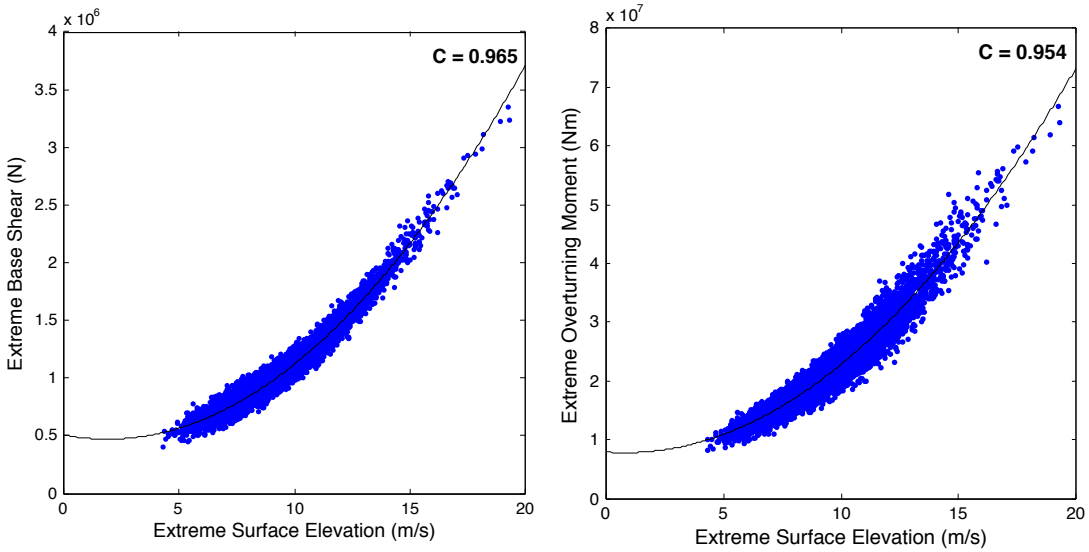

(a) Extreme Base Shear

(b) Extreme Over-turning Moment

Figure 5.2: Correlations Between Extreme Surface Elevation and Corresponding Extreme Response Values Based on 20,000 Simulations

simulations. This is significantly small compared to the 100,000 sample records that were required to generate the conventional distributions. This doesn't tell the whole story though, because the number of response sample records in each group does not have to be equal to that of the other groups, but the effect of changing these values will be investigated later in section 5.2.

It is evident that the need for a strong correlation between input and output parameters leads to the need to verify that such a correlation exists for every new structure. For example, it may be that the correlation only exists for the very simple models that are presented in this thesis, which means that *it is not guaranteed* that the method can automatically be applied to more complex, realistic models. Instead, if the efficient method is to be used, it is necessary to run a number of simulations to establish the correlation between the input and the output. One problem with this is that this process is potentially time-consuming in itself and may negate the effect of using the efficient method in the first place. However, it could be argued that the number of simulations required to assess the correlation, combined with the number of simulations required by the efficient method, may still be smaller than the number of

simulations required by the conventional method. This leads to the obvious question: how many simulations are required in order to give confidence that a strong correlation exists?

No investigation has been undertaken into precisely answering the above question, which is why the correlations in this thesis were calculated using an extremely large number of simulations, as in figure 5.2. However, it might be argued that, because it is a *strong* correlation that is required, such a correlation should become apparent after only a small number of simulations.[1] This means that there is an initial test that can be carried out relatively quickly on any new structure to verify whether or not the efficient method can be used, and if no evidence of a correlation is found using a small number of points, then it may be assumed that the correlation would not be strong enough to justify the use of the method. In such cases, the engineer would be limited to using other methods that may be more time consuming or make further assumptions to simplify the structure so that it can be analysed in the frequency domain.

In order to more precisely define the number of simulations that would be required for such an initial test, it is recommended that future work is carried out in which the correlation coefficients derived from a small number of simulations could be compared to those derived from an extremely large number of simulations, and the smaller number of simulations could be gradually increased until the correlation coefficients converged. This could be carried out upon a range of different structures to see whether the convergence consistently occurs around the same number of simulations.

[1] Around 20 - 50 in the author's experience, which is significantly lower than the hundreds of thousands typically required by the conventional method.

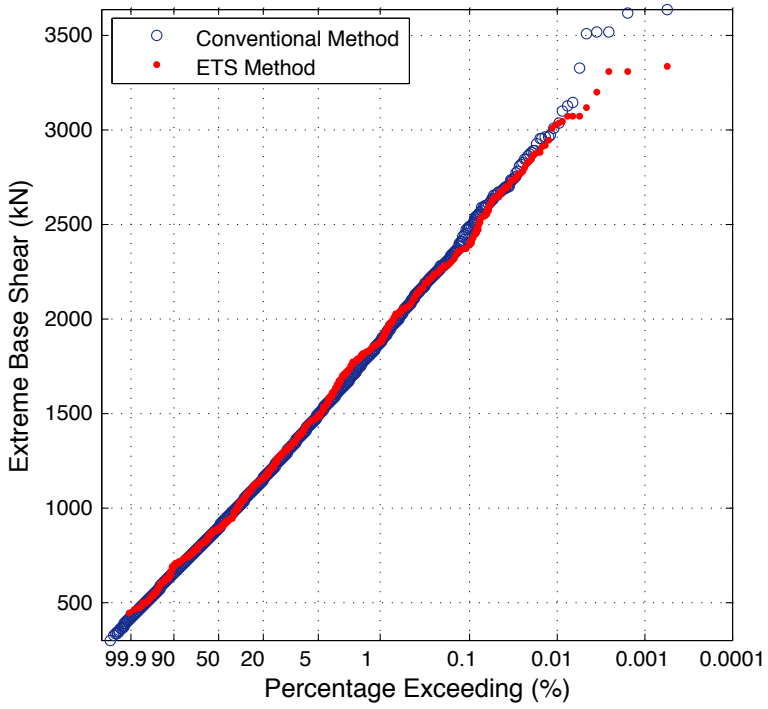

(a) Base Shear

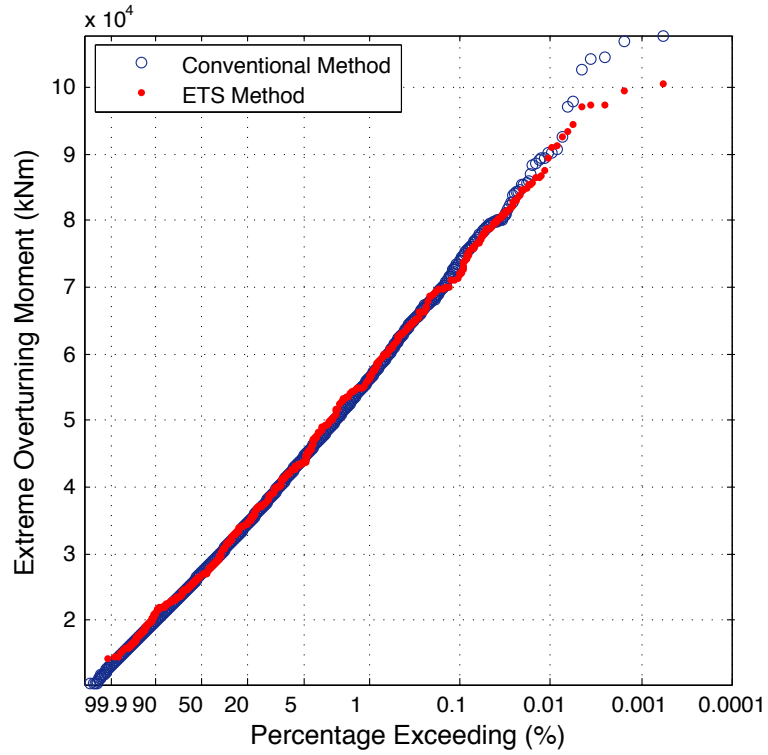

(b) Over-turning Moment

Figure 5.3: CDFs of Extreme Response Using the ETS Technique

5.1.2 The Enhanced ETS Technique

Although the ETS provides a good estimate of response distributions, it does not typically produces a very smooth curve because it introduces sampling variability at the extremes of each group, instead of just the tail of the entire distribution. This results in a curve with a shape that slightly resembles that of an umbrella, which can be observed in figure 5.3. In attempt to minimise this 'umbrella' effect, a enhanced version of the ETS method was developed, which will be presented in this section.

The enhanced version follows the same procedure as the original ETS method, except that the generalised extreme value distribution is fitted to each subset's distribution using MATLAB before total probability theorem is applied. The generalised extreme value distribution essentially 'lets the data decide' on the best extreme value distribution (Gumbel, Frechet or Weibull) to describe it, due to the inclusion of a shape parameter K. The probability density function of $r_{\max}$ in its generalised form is defined as

$$\mathrm{p}\left(r_{\max} \mid K, \mu, \sigma\right) = \left(\frac{1}{\sigma}\right) \exp\left\{-\left[1 + K\frac{(r_{\max} - \mu)}{\sigma}\right]^{-\frac{1}{K}}\right\}\left[1 + K\frac{(r_{\max} - \mu)}{\sigma}\right]^{-1-\frac{1}{K}} \tag{5.3}$$

This parameters K, μ and σ are determined for each group so that the overall distribution can be determined by

$$\mathrm{p}\left(r_{\max}\right) = \sum_{i=1}^{G} \mathrm{p}_i\left(r_{\max} \mid K_i, \mu_i, \sigma_i\right) P_i \tag{5.4}$$

The CDFs in figure 5.4 are based on the same number of simulations as figure 5.3, but were calculated using the enhanced ETS technique. The distributions are somewhat smoother than those from the original method and there is the added advantage of being able to choose the precise range of response values that are plotted, rather than being limited by the random nature of the model. There is of course a limit to this, because extrapolation outside the range of simulated results may make false assumptions about the behaviour of the structure in extreme cases. This is especially the case for structures that exhibit a high degree of nonlinearity.

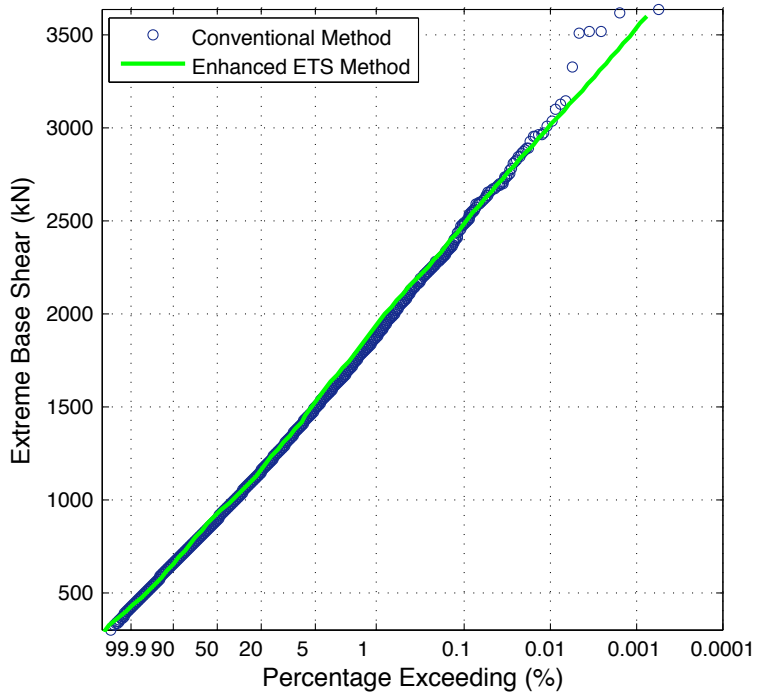

(a) Base Shear

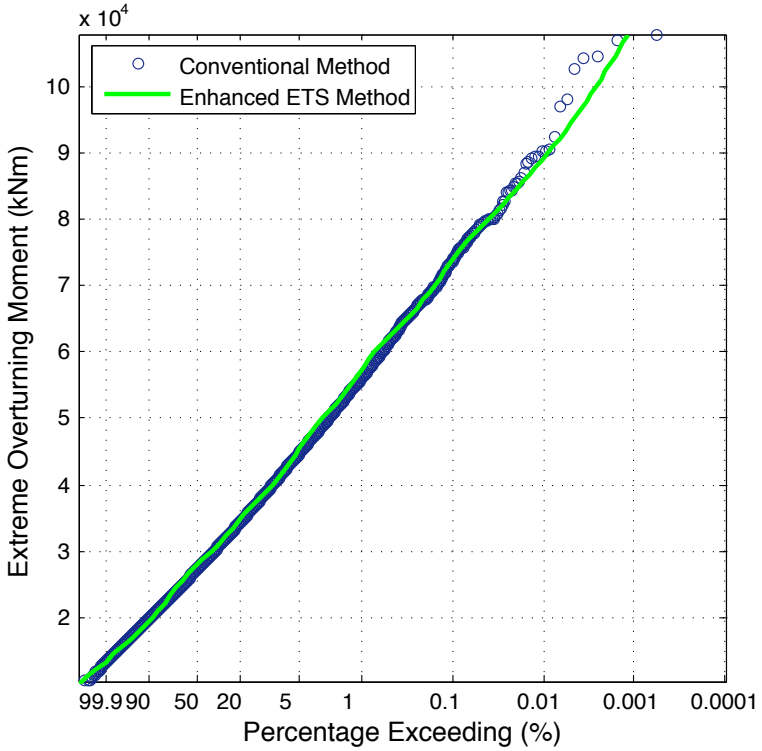

(b) Over-turning Moment

Figure 5.4: CDF of Extreme Response Using the Enhanced ETS Technique

5.1.3 Sampling Variability

Although the CDFs that were generated using the enhanced ETS method appear to be 'smoother' than those generated using the original ETS method, the so-called 'umbrella' effect has not been eliminated. Also, it is very difficult to say, based on a single comparison curve, whether one method is better than the other, given that the computational costs are virtually identical. For two methods with the same computational cost, the most effective method is the one that provides the greatest reduction in sampling variability. Thus, although figures 5.3 and 5.4 serve to validate the respective methods, a better way to compare them is to plot a large number of CDF curves on top of one another. Each method should provide a different 'envelope' of sampling variability, which, if the same number of curves is generated for each method, will allow their accuracy to be compared. This analysis can also include the conventional method in order to visualise the improvement that the ETS techniques provide. For this type of comparison, the number of permitted response simulations in each group has been reduced in order to save time. Because the curves from each ETS technique will allow 20 response simulations in each group, the curves from the conventional method should contain 140 extreme values (20×7) so that the computational cost is the same for all the methods.

The 'envelopes' in figure 5.5 were created by generating 500 curves, from identical input values, for each method and plotting them on top of each other. The comparison clearly shows that there is a reduction in sampling variability when using either ETS method or the enhanced version. Unexpectedly, however, the so-called enhanced ETS method increases the sampling variability in comparison to the original ETS method, especially for the over-turning moment distribution. This means that, although the method is 'enhanced' in terms of the smoothness of the distribution curve, it is actually a little less reliable than the original ETS method. The reason for this reduction in reliability may be that each group's empirical distribution is forced to conform to the analytical generalised extreme value distribution described in equation 5.3, instead of using only the simulated data from the model. If a more reliable distribution is to be obtained from a given number of simulated response sample records, it is necessary

to use more information from each sample record, an option that is explored in the following section.

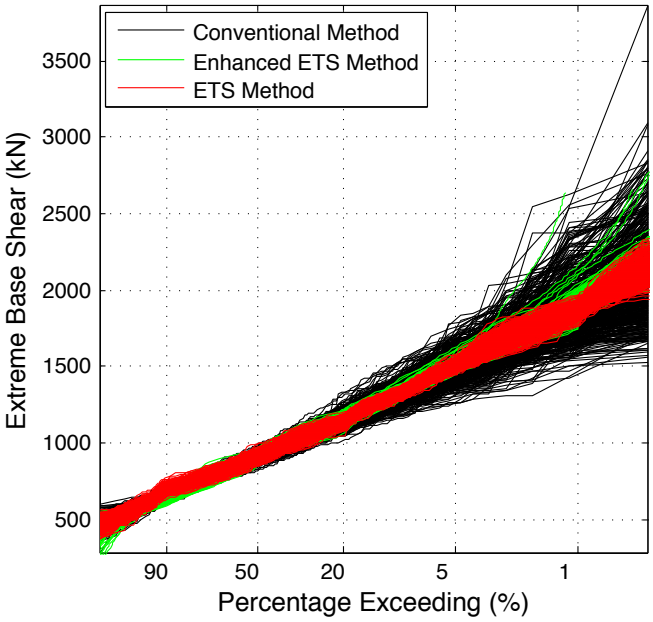

(a) Base Shear

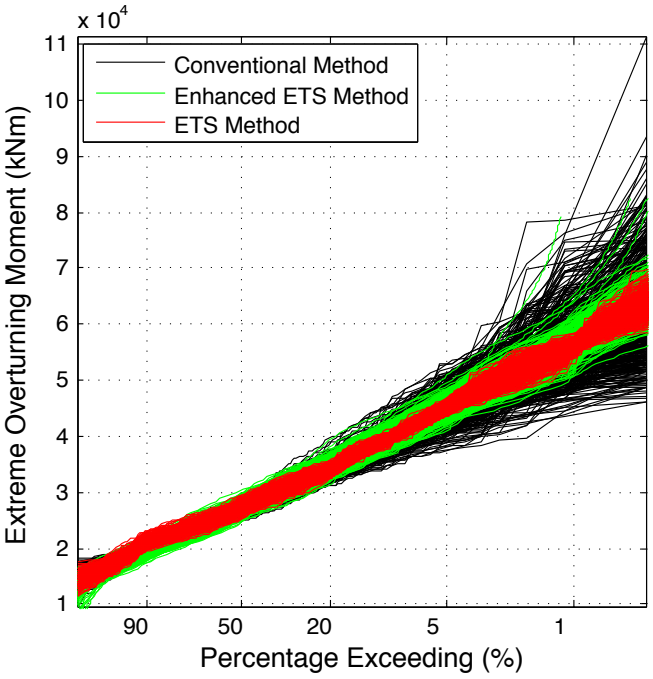

(b) Over-turning Moment

Figure 5.5: Comparison of Sampling Variability 'Envelopes' for Each Method; 140 Simulations for Each

5.2 The Efficient Threshold Upcrossing Method

5.2.1 Method Development and Procedure

The ETS method, outlined in the previous section, was shown to be effective, but there is evidently still room for improvement when it comes to deriving accurate response probability distributions. Even the enhanced version suffers from the so-called 'umbrella' effect around the boundaries of the groups that are used in the analysis. If this problem could be reduced even further, then distributions with acceptably low sampling variability could be derived at an even lower computational cost. This would have an enormous impact on increasingly complex nonlinear structures such as dynamic structures that are exposed to current and load intermittency in the splash zone, which although they are not covered in this project, are important considerations that effect the statistical properties of structural response Tung (1995), Liaw & Zheng (2003).

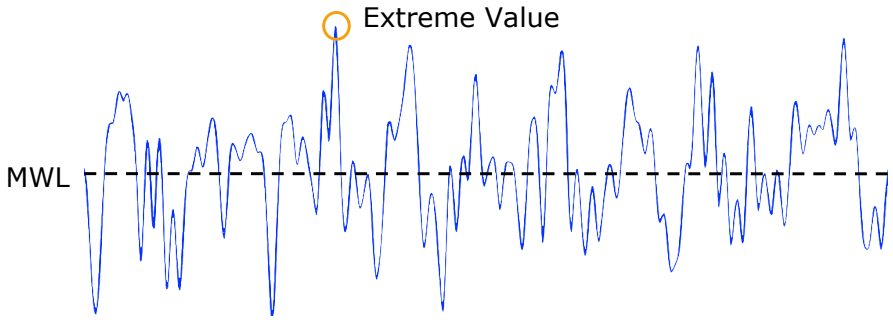

(a) ETS Method

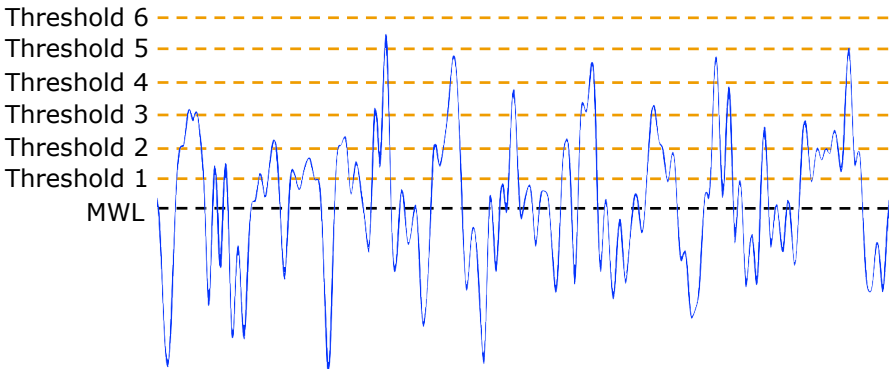

(b) ETU Method

Figure 5.6: Data Extracted for Response Statistics in ETS and ETU Methods

This section presents the newly developed Efficient Threshold Upcrossing (ETU) method, which combines the speed of the ETS method with the superior accuracy of a technique based on threshold upcrossings (Naess et al. 2007). The advantage of the ETU method is that it uses a great deal more information from each response sample record than the ETS method with negligible additional computation cost, meaning that it should require fewer simulations to achieve the same level of sampling variability as the ETS method.

The difference between the ETU and ETS methods is the data that is extracted from the response sample records. In the ETS method, it is only the extreme values that are recorded, and that form the basis for the empirical distribution based on equation 3.30. In the ETU method, however, a larger amount of data is extracted from each sample record so that a more accurate response distribution can be obtained. Instead of using only the extreme values, the number of upcrossings U of a predefined range of response thresholds is counted[2]. This means the response is now being modelled as Poisson process because the probability of the discrete event of a threshold being exceeded is of interest, as opposed to a continuous range of possible extreme values. The average number of upcrossings λ of a response threshold A directly relates to the extreme value distribution (Naess et al. 2007) such that

$$\mathrm{P}\left(r_{\max} \leq A\right) = \exp\left[-\lambda\left(A\right)\right] \tag{5.5}$$

This relationship enables the upcrossing rates for each threshold in each sample record to be used to calculate response probability distributions. The method by which one arrives at the response probability distribution having response sample records that belong to G groups is subsequently outlined.

The range of thresholds is linearly distributed and is defined as the vector $\boldsymbol{A} = [A_1, A_2, \ldots, A_{N_\mathrm{T}}]$, where N_T is the number of thresholds. The average number of threshold upcrossings corresponding to each threshold is therefore defined as the vector $\boldsymbol{\lambda} = [\lambda_1, \lambda_2, \ldots, \lambda_{N_\mathrm{T}}]$. For each group, $\boldsymbol{\lambda}$ must be calculated separately because

[2]Figure 5.6b is for the purpose of representation only. In reality, there are great deal more than 6 thresholds used in the ETU analysis.

the number of simulations in each group $N_{\text{sim}}^{(i)}$ are not necessarily the same. This calculation is carried out using equation 5.6, in which U_i denotes the *total* number of upcrossings of the thresholds in $\boldsymbol{A}$ from all the response sample records in group i.

$$(\boldsymbol{\lambda} \mid \eta_{\max} \in S_i) = \frac{U_i(\boldsymbol{A})}{N_{\text{sim}}^{(i)}} \tag{5.6}$$

Once the vector $(\boldsymbol{\lambda} \mid \eta_{\max} \in S_i)$ has been calculated for each group, total probability theorem is applied to determine the expected values of λ for the range of thresholds $\boldsymbol{A}$. The expected values are denoted by $\mathrm{E}[\boldsymbol{\lambda}]$ and are calculated as

$$\mathrm{E}[\boldsymbol{\lambda}] = \sum_{i=1}^{G} (\boldsymbol{\lambda} \mid \eta_{\max} \in S_i) P_i \tag{5.7}$$

This takes into account the fact that the response sample records belong to separate groups with their own probability of occurrence so that the overall extreme response probability distribution can be obtained by

$$\mathrm{P}(r_{\max} \leq \boldsymbol{A}) = \exp(-\mathrm{E}[\boldsymbol{\lambda}]) \tag{5.8}$$

In order to demonstrate more clearly how it works, a flow diagram of the procedure for deriving an extreme response distribution using the ETU method is shown in figure 5.7. The subset with the highest range of response values, and hence the least likely to occur, will be known as the 'extreme' group, which is the 7^{th} group in this case. All of the other subsets will be known as the 'interim' groups (groups 1-6 in this case). The procedure assumes that the occurrence of sample records belonging to the 'extreme' group is sufficiently rare that the interim groups will already have fulfilled their quota by the time the extreme group has.[3] This means the simulation can be stopped when enough response sample records have been calculated in the extreme group.

One advantage of making the aforementioned assumption is that it is no longer necessary to predetermine the total number of *surface elevation* sample records that need to be generated to obtain enough *response* sample records in the extreme group,

[3]This assumption would only cause a problem if the extreme group only required a very small number of sample records, which would defeat the point of using the method anyway.

which is the approach used in the original ETS method (Abu Husain & Najafian 2010). This saves a small amount of computational cost because it prevents unnecessary surface elevation sample records from being generated that would have been discarded anyway.

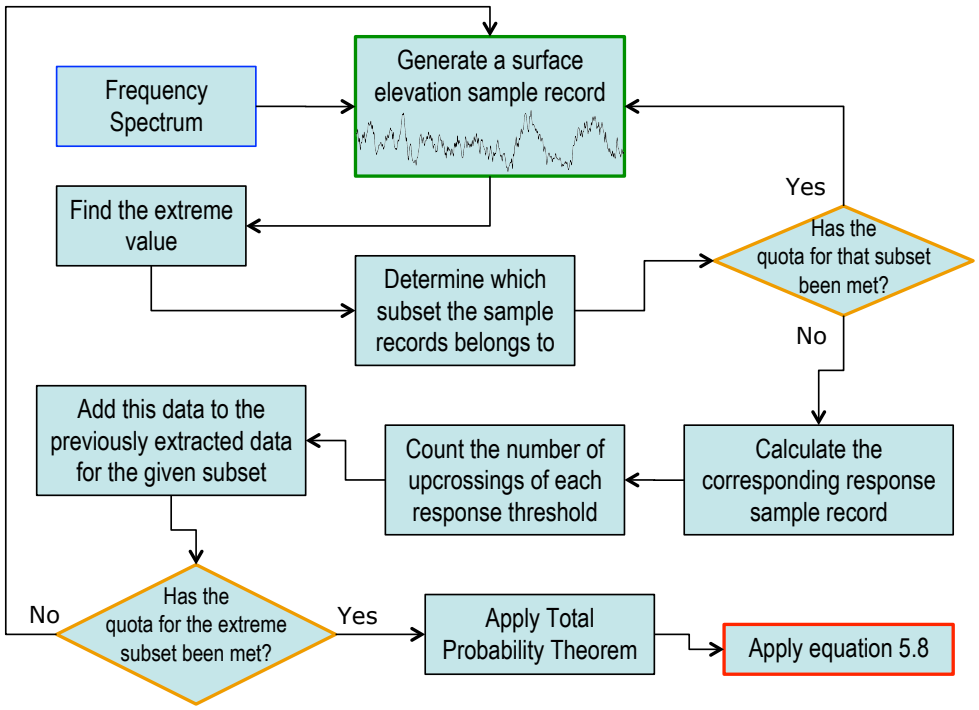

Figure 5.7: Procedure for the Derivation of Extreme Response Probability Distributions using the ETU Method

5.2.2 Validation and Distribution Tailoring

It was previously mentioned that an advantage of the ETS and ETU methods is that each group does not need to contain the same number of response sample records. For example, the area of greatest interest when it comes to design loads is the 'tail' of the extreme value distribution. The tail of the curve is formed using data extracted largely from the sample records in the 'extreme' group (group 7) and not from the 'interim' groups (groups 1-6). Therefore, a more accurate tail can be obtained from the same number of simulations by allowing more simulations in the extreme group and fewer in the interim groups. 'Distribution tailoring' means that, instead of spreading the sampling variability out evenly across the distribution (as in section 5.1), it can be moved away from the parts of the distribution that are most important.

The cases established in table 5.1 are varied in such a way that particular features of the ETU method can be observed. In each case, the number of simulations in the groups has been altered so that it either speeds up the derivation of the probability distribution, or transfers the sampling variability to the areas that are relatively insignificant for practical purposes. These are the cases that will be used to validate the ETU method as well comparing it to the original ETS method. The 'enhanced' version of the ETS method will not be considered because it was deemed to be less reliable than the original version in section 5.1.

For the sake of simplicity, the extreme value distributions in each case are based on short-term statistics (i.e. $r_{\max} \mid H_s \cap T_z$) and the probability that a given sea state will occur has not been taken into account. However, the method can easily be extended to account for the long-term statistics (Abu Husain et al. 2013) outlined in section 4.2, but this will only be exploited in its application to aircraft gust loading in chapter 7.

For ease of reference, the input data for generating all of the following figures are as follows: $C_d = 0.8$, $C_m = 1.7$, $H_s = 15$ m, $T_z = 13$ s, $T = 120$ s, $d = 50$ m, $D = 3.0$ m. Also, the Conventional method response probability distribution is derived from 100,000 response simulations in each case.

Table 5.1: Details of the Analysis for Each Case

	Total No. of Simulations	**No. of Simulations** Interim Groups (1-6)	Extreme Group (7)	**Computational Cost Reduction**
Case 1	700	100	100	99.3 %
Case 2	210	30	30	99.8 %
Case 3	210	10	150	99.8 %
Case 4	100	5	70	99.9 %

Firstly, it can be observed from figure 5.8 that the ETU method agrees extremely well with the Conventional method, even though in this case the probability distribution is derived from approximately 150 times fewer simulations. It is also evident that the ETU method produces a smoother distribution than the ETS method, which is presumably due to the additional information that is extracted from the response sample records in

the ETU procedure.

Case 2 implements a reduction in the total number of simulations, while the proportion of simulations in each group is kept constant. Figure 5.9 demonstrates that, now with 500 times fewer simulations than the Conventional method, the ETU method manifests a slight instability around the tail of the distribution due to the increase in sampling variability. Despite this, it still agrees very well with the Conventional method, especially in the lower part of the distribution.

It is the tail of the distribution, however, that is of greatest value when it comes to acquiring design values, so Case 3 is arranged such that the sampling variability in the tail of the distribution is reduced. While keeping the total number of simulations the same as in Case 2, this is accomplished by transferring it to the lower part of the distribution by reducing the number of simulations in the interim groups and increasing that of the extreme group. The advantage of this can clearly be seen in figure 5.10. It is clear that Case 3, although it is the same speed as Case 2, marks a significant improvement in the accuracy of the tail of the distribution. This demonstrates that the ETU method can be tailored to suit design requirements by rebalancing the number of points in each group so that the most important part of the distribution is sufficiently accurate. As shown, this can be achieved without any extra computational cost.

So far, both the ETU and ETS methods have exhibited similar agreement with the conventional distribution, with the ETU method apparently producing a more reliable curve in the lower part of the distribution. However, because the ETU method extracts more data from the response sample records with no extra computational cost, it should be expected that if the total number of simulations is sufficiently reduced, a noticeable difference in accuracy will appear between the two methods.

Figure 5.11 presents distributions that are derived from 1000 times fewer simulations than the Conventional method, as defined in Case 4. It shows that, even with such a small number of simulations, the ETU method displays a good agreement with the Conventional method, especially in the tail of the distribution. Also, when a very small number of simulations is used, it appears to produce slightly more stable response probability distributions than the ETS method because the number of points

in the distribution is dependent upon the number of thresholds instead of the number of simulations.

Overall, the ETU method appears to produce a more reliable curve in the lower part of the distribution compared to the ETS method, yet performs similarly in the tail. This is consistent with the way that the data is extracted in each method. In the ETS method, each point on the distribution comes from a single sample record, so if there are only a few sample records in the lower groups, then there will only be a few data points in the lower part of the distribution. Likewise, the accuracy of the tail of the distribution depends upon the number of sample records in the extreme group. However, the ETU method is not as straightforward because a single sample record, regardless of what group it belongs to, provides statistical data for all the thresholds that are crossed in its duration. This means that the lower part of the distribution is affected by the sample records in the extreme group *as well as* the ones in the interim groups. The inverse is not true, however, because sample records from the lower groups are very unlikely to cross the thresholds that are crossed in the extreme group, and therefore provide no additional information about the tail of the distribution. This means that the ETU method should be favourable over the ETS method because it allows for fewer simulations in the lower groups, so that more computation time can be focussed on the extreme group, without sacrificing as much accuracy as the ETS method does.

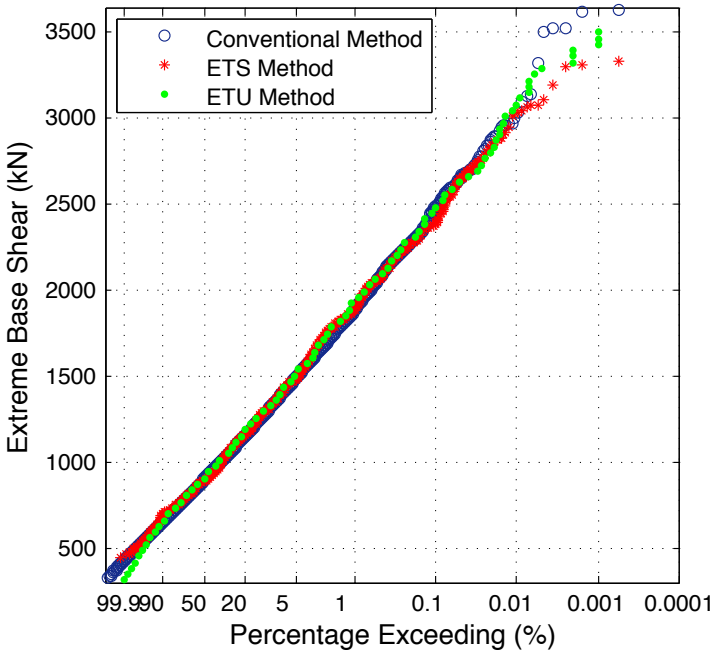

(a) Base Shear

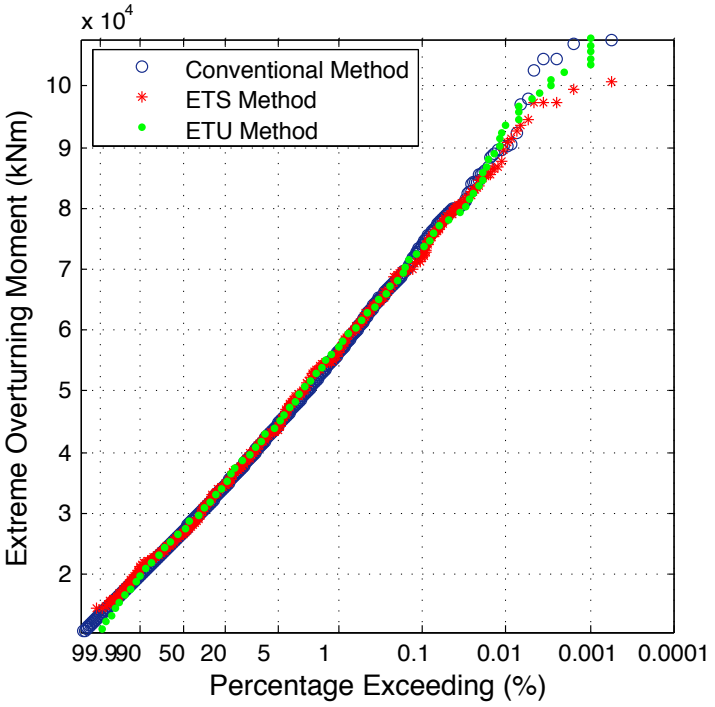

(b) Over-turning Moment

Figure 5.8: CDFs of Extreme Response for Case 1: ∼150 Times Faster

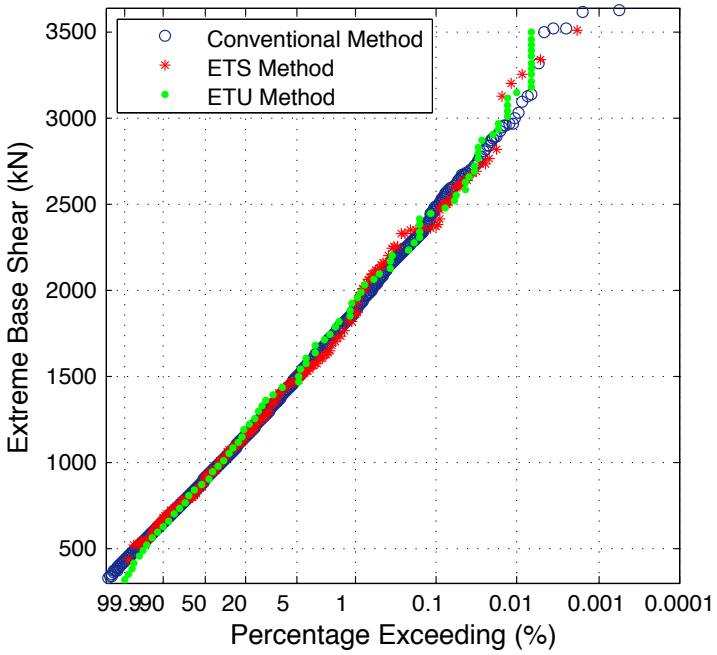

(a) Base Shear

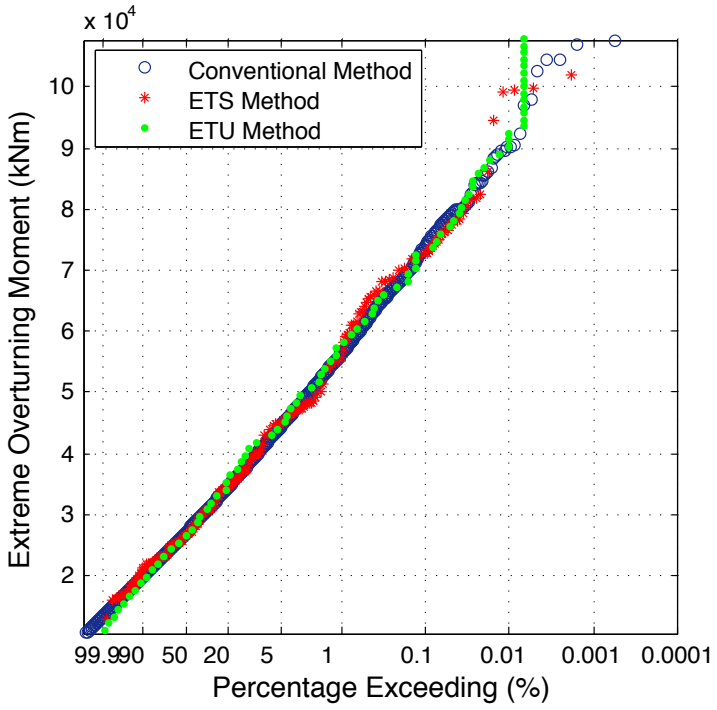

(b) Over-turning Moment

Figure 5.9: CDFs of Extreme Response for Case 2: ∼500 Times Faster

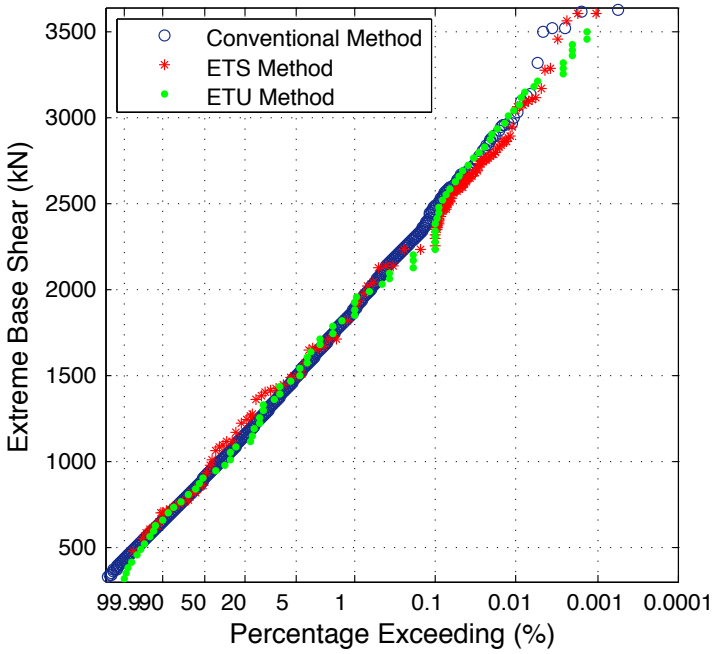

(a) Base Shear

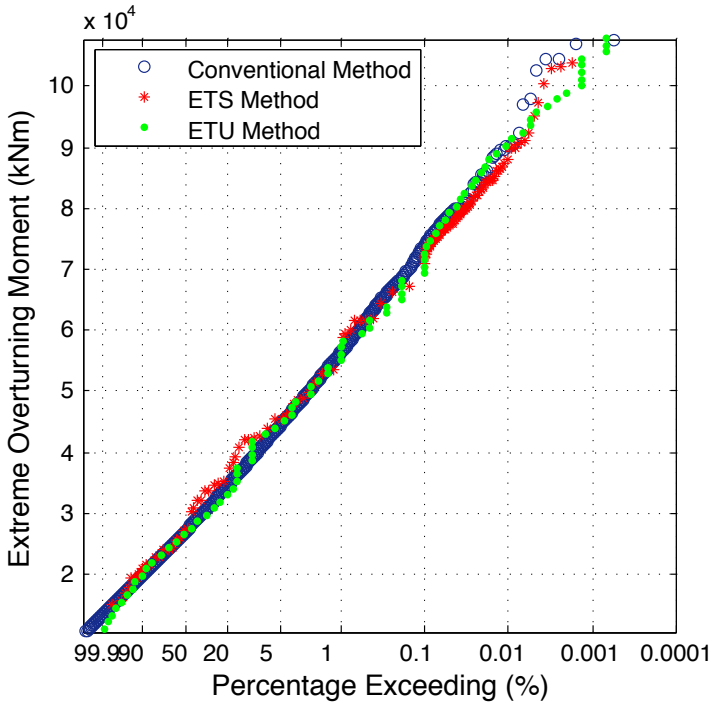

(b) Over-turning Moment

Figure 5.10: CDFs of Extreme Response for Case 3: ∼500 Times Faster

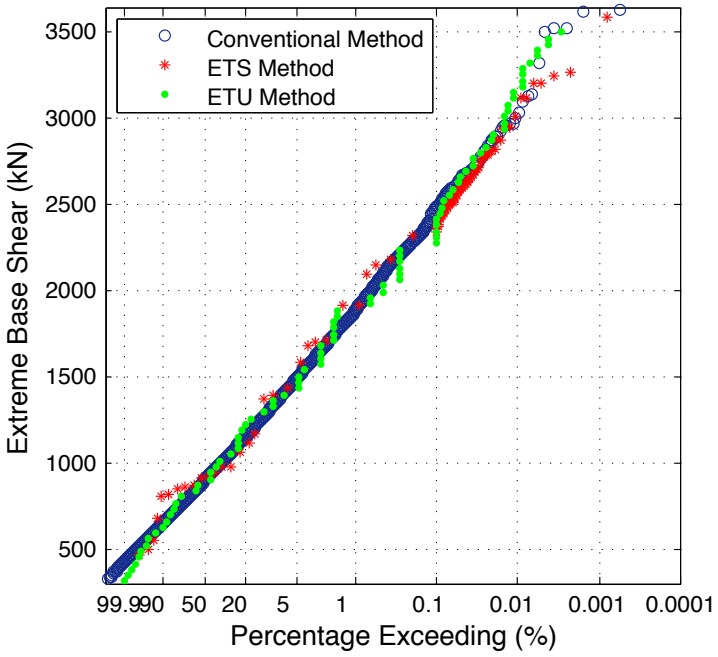

(a) Base Shear

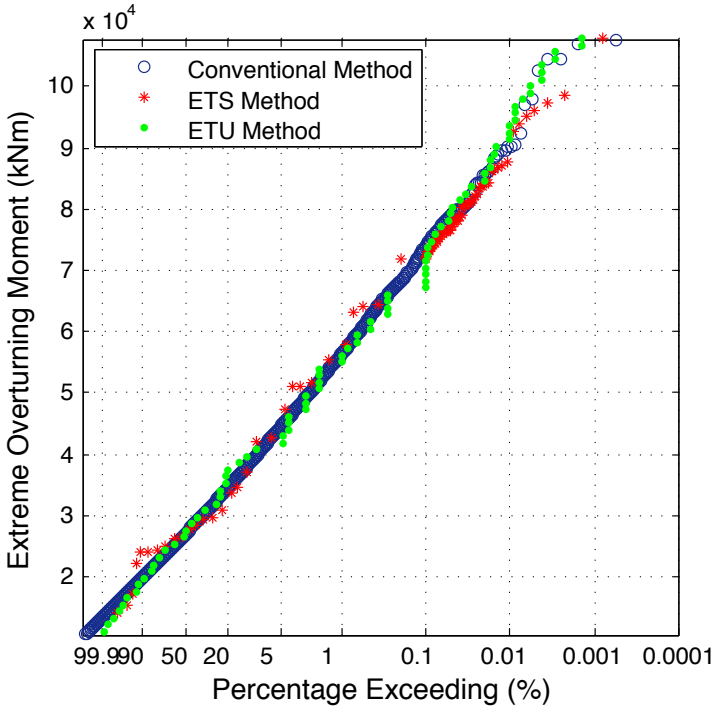

(b) Over-turning Moment

Figure 5.11: CDFs of Extreme Response for Case 4: ∼1000 Times Faster

Selection of the Number of Thresholds

The number of thresholds used in each analysis was 100. The selection of the number of thresholds is somewhat arbitrary, but this is because it does not have a major impact on the effectiveness of the method. It does, however, effect the presentation of the response distribution in that if number of the thresholds is too low, it may not be possible to accurately read the required data from the curve. Figure 5.12 demonstrates (using Case 1 as an example) that distributions with fewer thresholds, still accurately follow the distributions obtained by the conventional method, but would make it increasingly difficult to obtain reliable data, especially if the distribution does not follow a straight line. For example, one would have a problem determining the extreme base shear force that was exceeded in only 0.01% of sample records using the distribution with 10 thresholds in figure 5.12 because there aren't enough points in that region. Therefore, the thresholds need to be sufficiently close together that a simple linear interpolation would give reliable values. Since there is a relatively low-computational cost associated with increasing the number of thresholds, it is preferable to provide more data points than to employ more complex interpolation techniques. The issue of selecting the 'best' number of thresholds to use is more about precision than accuracy and, thus, it is one that must be address on a case-by-case basis. Accordingly, in the work presented in this thesis, 100 thresholds were deemed adequate for the primary purpose of comparing probability distributions that are derived using different techniques.

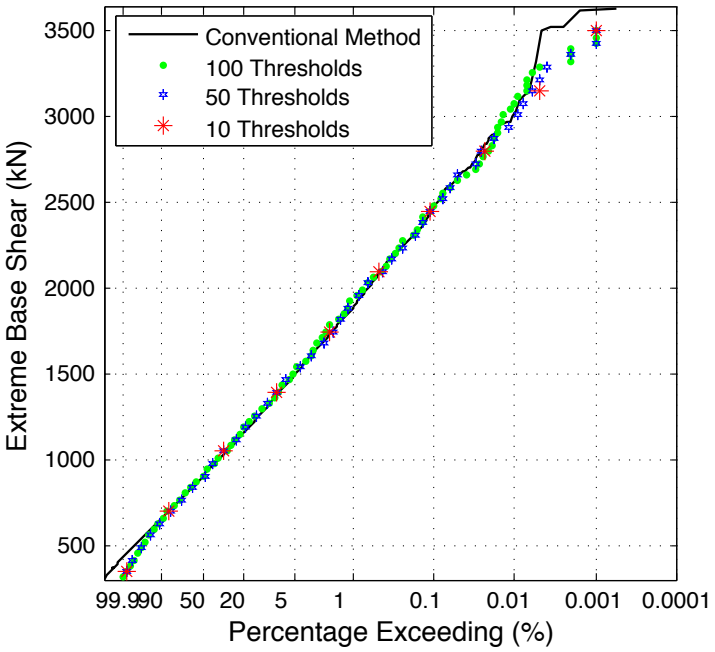

Figure 5.12: Effect of the Number of Thresholds on Response Distribution

Manifestation of Sampling Variability

It can be observed in figures 5.8 - 5.11 that there is a clustering of points towards the extreme values of the response probability distributions for the ETU method. This is a manifestation of the sampling variability, which is very different from that of the conventional and ETS methods because the ETU method models the response statistics as a Poisson process. This means that the data points are not the actual simulated values (as in the conventional and ETS methods), but are instead determined based on the number of exceedances of a predefined threshold value, which is a discrete event. Therefore, the clustering of points occurs when a peak crosses multiple thresholds that are not exceeded by any other peaks, resulting in a number of thresholds that apparently have the same probability of exceedance. Similarly, this phenomenon, can still occur when a threshold is exceeded by more than one peak, but where at least one consecutive threshold is only exceeded by the same peaks. To illustrate this, examples of these occurrences are shown in figure5.13, in which it can be assumed that no other peaks cross any of thresholds in the figure. In this case, thresholds 94 and 95 would have equal probabilities of exceedance because they are only exceeded by the first peak.

Likewise, thresholds 90 - 92 would have equal probabilities of exceedance because they are exceeded by all three peaks. It is only threshold 93, therefore, that would have a unique probability of exceedance because it's neighbouring thresholds are exceeded a different number of times. Of course, in reality each threshold would have a unique probability of exceedance, but it is only possible to determine this value accurately if enough peaks are simulated to distinguish between each threshold.

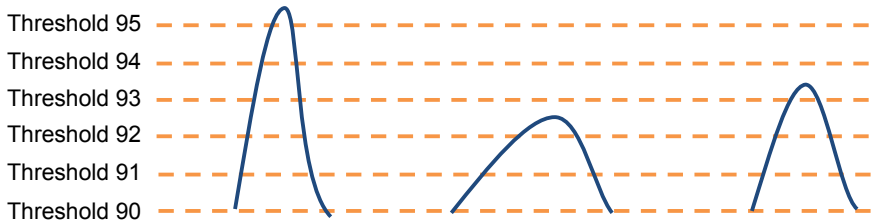

Figure 5.13: Examples of Threshold Upcrossings to Demonstrate Clustering of Points Due to Sampling Variability

5.2.3 Reliability Comparisons

In order to properly compare the reliability of the two methods, sampling variability 'envelopes' are plotted in figure 5.14 using the same approach as in section 5.1. The envelopes are made up of 500 response distributions plotted on top of one another, with 20 simulations in each group.

Again, the results are surprising, but much more promising than the 'enhanced' ETS method comparison. In both figures 5.14a and 5.14b, the ETU method performs at least as well as the ETS method, with a small improvement in reliability in the lower parts of the distributions. The difference in sampling variability is far less significant than was expected based on the argument in section 5.2.2. This may be because the number of simulations in the interim groups was not low enough to demonstrate the advantage. In theory, a distribution curve could be generated with no sample records in the interim groups using the ETU method, whereas this would not be possible with the ETS method. Also, the 'envelopes' in figure 5.14 do not allow the difference in reliability to be quantified because the envelopes would expand as the number of distributions plotted were increased. So if the number of distributions plotted were, say, 10,000 instead

of 500, which would be far too time-consuming to demonstrate, the ETU method might appear much more reliable, even though the number of simulations were identical. In other words, the important thing to note is that ETU method performs *at least* a little better than the ETS method, and thus, should be suitable for application to the aircraft gust loading problem discussed in chapter 2.

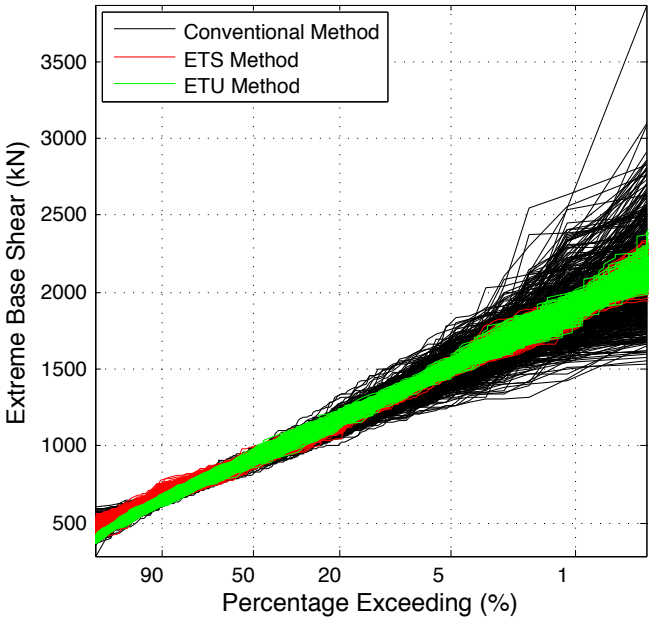

(a) Base Shear

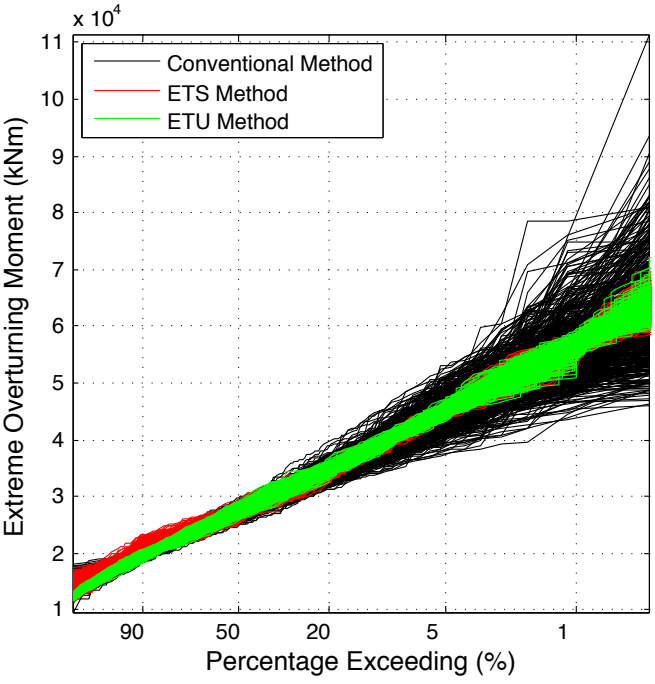

(b) Over-turning Moment

Figure 5.14: Sampling Variability 'Envelopes' for ETU and ETS Methods Using 20 Simulations in Each Group

Chapter 6

Mathematical Modelling of Gust Loading

6.1 Simulation of Continuous Turbulence

6.1.1 Reliable Gust Velocity Sample Records

As outlined in chapter 3, the velocity of the continuous turbulence that an aircraft is subjected to can be modelled as an ergodic random process, where the gust velocity w_g is made up of a large number of harmonics with random, uniformly distributed phase angles. A 'frozen field' hypothesis is assumed, which means that the aircraft is either considered to be at a single point in space while w_g varies with time, or moving through space within a 'snapshot' of turbulence from a single point in time, as shown in figure 6.1. This means that it is relatively simple to go back and forth between the spatial domain $w_g(x)$ and the time domain $w_g(t)$ where necessary, as long as the speed of the aircraft V is known. At a single point in space, from equation 3.6, the velocity of a continuous gust is defined as

$$w_g(t) = \sum_{n=1}^{N_h} a_n \cos(\omega_n t + \delta_n) \tag{6.1}$$

Time-domain sample records of gust velocity can be obtained using the spectral analysis procedure outlined in section 3.3, where the spectral density of the atmosphere

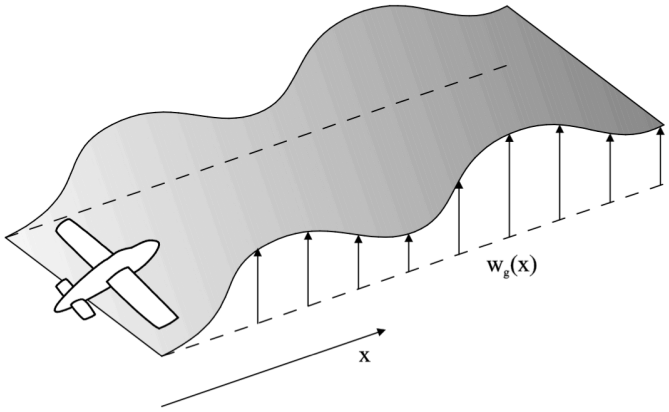

Figure 6.1: Aircraft Entering a Gust (Wright & Cooper 2007)

is described by the widely-accepted Von Karman spectrum (von Karman 1948) shown in figure 6.2, which is usually defined as a function of spatial frequency as

$$\Phi_w(\Omega) = {\sigma_w}^2 \frac{L}{\pi} \frac{1 + (8/3)(1.339\Omega L)^2}{\left[1 + (1.339\Omega L)^2\right]^{11/6}} \tag{6.2}$$

where L is the characteristic scale wavelength, which is taken to be 762 m.

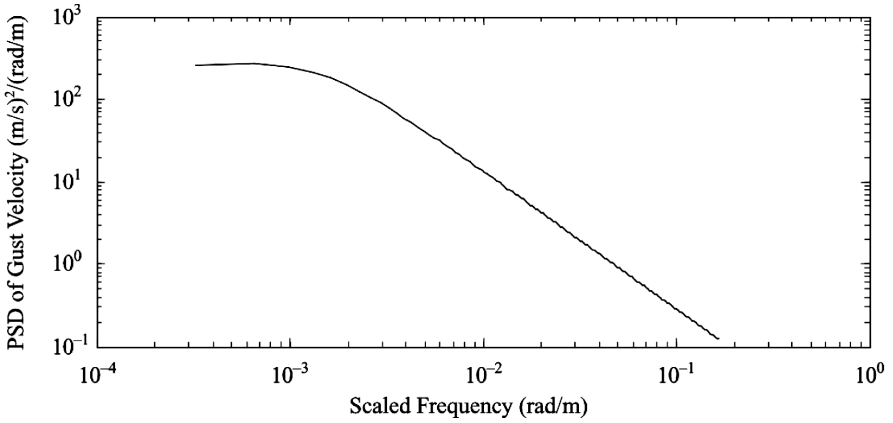

Figure 6.2: Von Karman Frequency Spectrum (Wright & Cooper 2007)

In current methods, the spectral amplitudes are only calculated deterministically using equation 3.14, but in this project, the amplitude of the n^{th} harmonic is modelled as a random process with a mean value of $a_{n_{\text{DSA}}}$. This is achieved using equation 3.14, which is a more robust approach (Morooka & Yokoo 1997, Tucker et al. 1984) because it means that shorter sample records are able to more accurately represent the frequency

spectrum from which they were generated.

This has been demonstrated in figure 6.3 by calculating CDFs of extreme gust velocity using both deterministic and non-deterministic spectral amplitudes. The empirical distributions were each derived from the 10,000 sample records, first with relatively long sample records of 10-minute duration, then with relatively short sample records of only 2-minute duration. Figure 6.3a clearly shows that the technique used has no effect on distributions that are derived from long sample records, but in figure 6.3b the sample records with non-deterministic spectral amplitudes are shown to produce a distribution that much more accurately fits the theoretical distribution. This is a significant finding because current continuous gust response models, such as the NLR model (Vink & de Jonge 1997) introduced in chapter 2, are limited to producing sample records using only the deterministic spectral amplitudes, which means they are likely to be underestimating the magnitude of the aircraft response if short sample records are used.

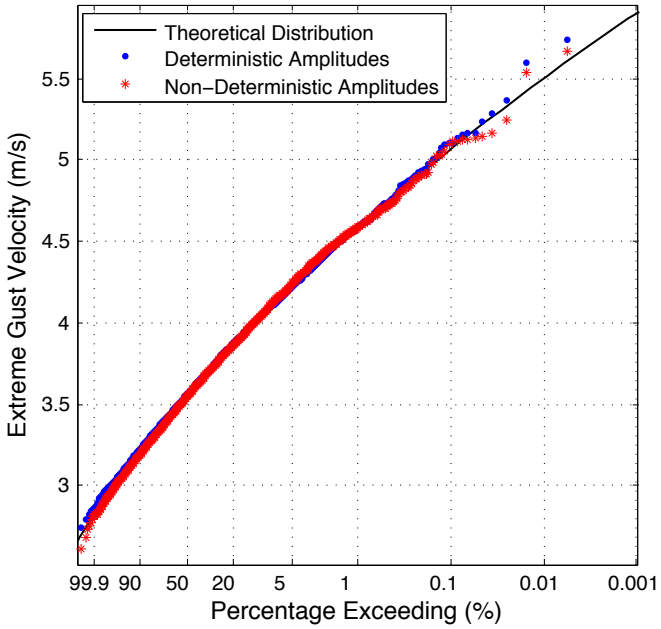

(a) Long Sample Records (10 minutes)

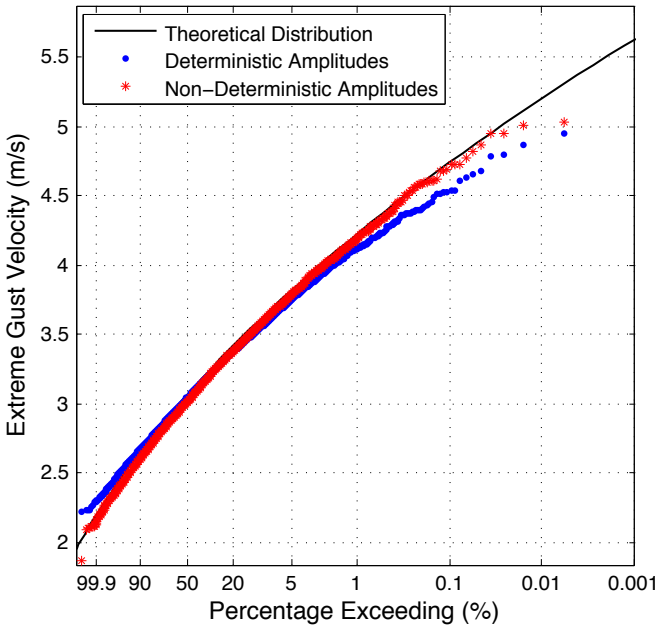

(b) Short Sample Records (2 minutes)

Figure 6.3: Effect of Using Deterministic and Non-Deterministic Spectral Amplitudes on Extreme Gust Velocity CDF. $V = 280$ m/s, $\sigma_w = 1.0$ m/s.

6.1.2 Exceedance Curves

So far in this thesis, cumulative probability distributions of extreme values have been used to describe the statistical behaviour of the random processes. However, when dealing with continuous turbulence and aircraft design loads it is conventional to deal with exceedance curves, which express the probability distribution as the expected number of peaks that will exceed a given threshold per unit time.[1] The frequency of exceedance of the threshold x is denoted as $\mathrm{N}(x)$ and an exceedance curve is made up of the values of $\mathrm{N}(x)$ that correspond to a range of values of x. Thus, the theoretical exceedance curve for vertical gust velocity is simply a slight variation on the combination of equations 3.4 and 5.5, and is defined as

$$\mathrm{N}(w_g) = N_0 \exp\left(-\frac{{w_g}^2}{2{\sigma_w}^2}\right) \tag{6.3}$$

where N_0 is the expected number of peaks per unit time, which is known as the characteristic frequency and is calculated by

$$N_0 = \frac{1}{2\pi}\sqrt{\frac{\int \omega^2 \Phi_w(\omega)\,\mathrm{d}\omega}{\int \Phi_w(\omega)\,\mathrm{d}\omega}} \tag{6.4}$$

Figure 6.4 shows that the method used in this project for simulating gust velocity sample records is capable of producing reliable exceedance curves, by comparing a simulated curve to the theoretical curve defined in equation 6.3. The simulated curve was derived from 10,000 gust velocity sample records, each with a duration of 3 minutes.

It is common practice to plot the frequencies of exceedance on a logarithmic scale against the *squares* of the threshold values because this produces a straight line for a stationary-Gaussian process.

[1] Not necessarily the sample record duration; usually one second or one hour.

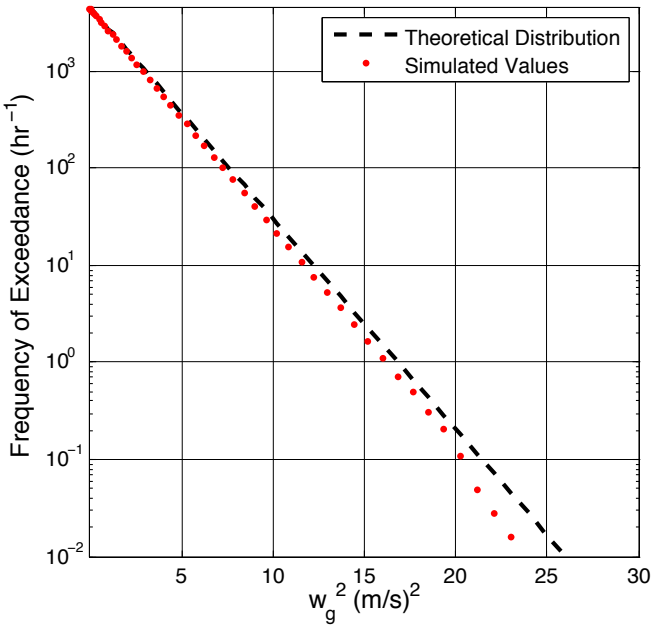

Figure 6.4: Gust Velocity Exceedance Curve Validation. $V = 280$ m/s, $\sigma_w = 1.0$ m/s.

6.1.3 Turbulence Severity States

So far, there has not been a model that takes into account the non-Gaussian nature of real turbulence using PSD methods, which is probably because this combination is assumed impossible. This assumption is true if the task is to generate a single stationary sample record that has the non-Gaussian attributes of real turbulence. However, as discussed in chapter 2, it *is* possible to simulate the non-Gaussian nature of turbulence by modelling it as a non-stationary process made up of a large number of *locally* Gaussian sample records; an idea that is backed up by Hoblit (1988). This can be done by calculating the *long-term* statistics of gust velocity, which means plotting an exceedance curve that takes into account all the possible conditions that the aircraft will encounter in its lifetime. In order to do this, the concept of a 'Turbulence Severity State' (TSS) must be introduced, which is essentially the aerospace equivalent of the sea state introduced in section 4.2.

A Turbulence Severity State is a period of time where the gust velocity can be assumed to be stationary (i.e. constant conditions) and each one is determined by the magnitude of the frequency spectrum, which varies depending only on the RMS value

σ_w. This means that a TSS is defined by a range of RMS values that is small enough to be adequately represented by its midpoint value of σ_w. Therefore, because each TSS has its own probability of occurrence, all the possible conditions to which an aircraft might be exposed can be accounted for by applying the probability distribution of a range of Turbulence Severity States. This is simpler than it is for an offshore structural analysis for two reasons. Firstly, long-term wave statistics are dependent on the joint probability distribution of H_s and T_z, whereas turbulence conditions are only defined by a single variable σ_w. Secondly, the *shape* of the frequency spectra that describe ocean waves varies depending on the particular part of the world that they are in, whereas the description of atmospheric turbulence is not dependent upon location.

The RMS gust velocity is itself a random variable with probability density function $\mathrm{p}(\sigma_w)$, which was first defined by Press et al. (1956) as

$$\mathrm{p}(\sigma_w) = P_1 \frac{1}{b_1}\sqrt{\frac{2}{\pi}} \exp\left(-\frac{{\sigma_w}^2}{2b_1}\right) + P_2 \frac{1}{b_2}\sqrt{\frac{2}{\pi}} \exp\left(-\frac{{\sigma_w}^2}{2b_2}\right) \tag{6.5}$$

Thus, only the short-term probability distribution of w_g is Gaussian, i.e. when the turbulence is only considered to have a single value of σ_w. The long-term statistics of gust velocity, and therefore aircraft response, can easily be calculated using the conditional probability distributions of w_g and the probability distribution of σ_w by

$$\mathrm{p}(w_g) = \int_0^\infty \mathrm{p}(w_g \mid \sigma_w)\, \mathrm{p}(\sigma_w)\, \mathrm{d}\sigma_w \tag{6.6}$$

Using a stationary-Gaussian model, it is possible to generate an exceedance curve of w_g, but the probabilities will be based on the condition that a particular TSS has already occurred (i.e. It doesn't account for fluctuations in σ_w). However, the use of long-term statistics enables the *total probability* of w_g to be determined on the basis of a discretised range of all possible Turbulence Severity States. In other words, it takes into account the fact that atmospheric turbulence is actually non-stationary, making it non-Gaussian, by applying the probability of occurrence of a large number of stationary processes (i.e. individual Turbulence Severity States). Implementing total probability theorem, long-term exceedance curves are determined by equation 6.7 given that the

discrete Turbulence Severity States are mutually exclusive and collectively exhaustive.

$$\mathrm{N}\left(w_g\right) = \sum_{j=1}^{N_\mathrm{T}} \mathrm{N}\left(w_g \mid \sigma_{wj}\right) \mathrm{P}\left(\sigma_{wj}\right) \tag{6.7}$$

Suppose that the sample space consists of only 3 possible Turbulence Severity States that have RMS values of 0.5, 1.0 and 2.0 m/s, and probabilities of occurrence of 0.6, 0.3 and 0.1, respectively. Instead of assuming a worst case and calculating the corresponding exceedance curve, the long-term case can be considered, which is the exceedance curve of w_g across the whole sample space, by generating a number of sample records for each σ_w value and applying equation 6.7, using the corresponding TSS's probability of occurrence $\mathrm{P}\left(\sigma_{wj}\right)$.

Figure 6.5 shows the long-term exceedance curve and compares it to the conditional exceedance curves for each TSS, each of which is based on 10,000 sample records of 3-minute duration.

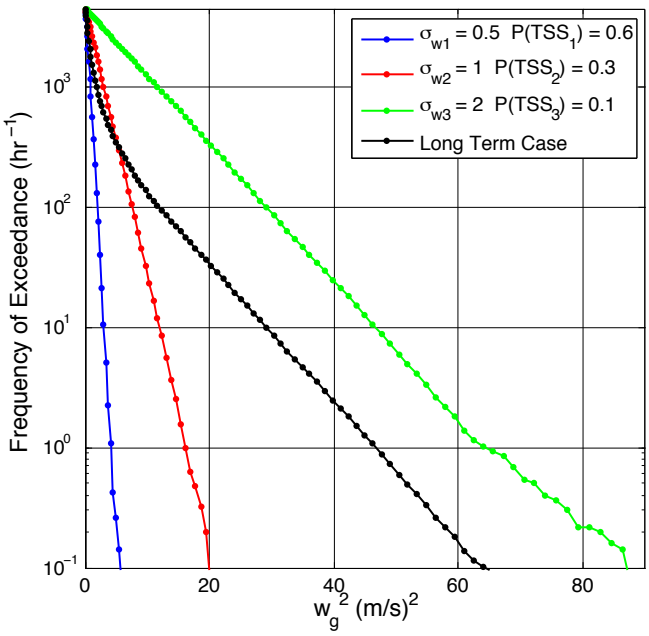

Figure 6.5: The Effect of Long-Term Statistics on Gust Velocity Exceedance Curves . $V = 280$ m/s.

It is clear from figure 6.5 that using the exceedance curve for the worst possible TSS would yield a higher gust velocity than the long-term case for a given probability

of exceedance. This would result in overestimated design loads, leading to unnecessary material costs and a heavier aircraft. This demonstrates the potential advantage of accounting for long-term statistics in that it gives more realistic exceedance probabilities but produces lower design gust velocities.

The RMS value of the long-term case can easily be calculated (as if it were a single stationary condition) as a combination of the three Turbulence Severity States:

$$\sigma_{w\mathrm{LT}} = \sqrt{(0.6)(0.5)^2 + (0.3)(0.1)^2 + (0.1)(2.0)^2} = 0.92\mathrm{m/s} \tag{6.8}$$

Figure 6.6 compares the long-term (non-stationary) case to a stationary exceedance curve with an equivalent RMS value $\sigma_{w\mathrm{EQ}} = \sigma_{w\mathrm{LT}}$, that was generated from the same number of sample records of equal duration.

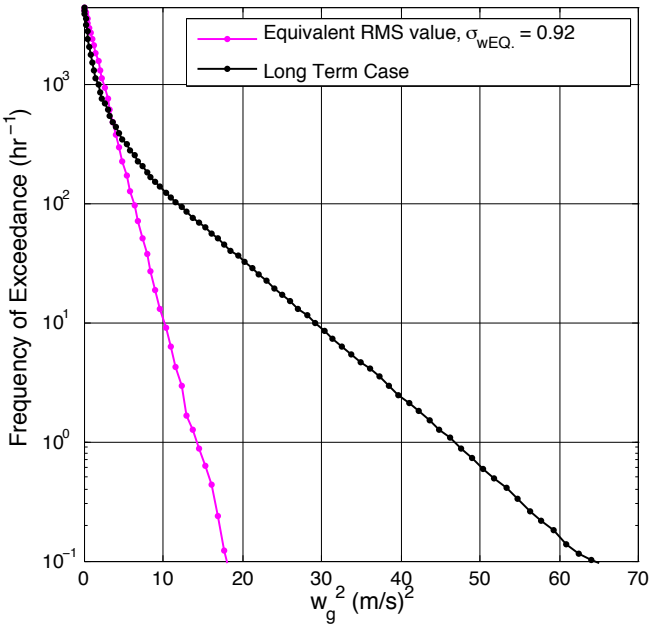

Figure 6.6: Comparison of Long-Term Case with an Equivalent RMS Value Exceedance Curve. $V = 280$ m/s.

Figure 6.6 shows that even with just three Turbulence Severity States, the long-term case predicts higher extreme values in the region from which design values are selected, than would be predicted by an equivalent stationary-Gaussian model. This verifies the claim that this model has the potential to take into account the more extreme fluctuations found in non-Gaussian turbulence by modelling it as a

non-stationary process. This being said, the literature (Jones 2009*b*) still suggests that there are some other underlying assumptions that cause PSD methods to underestimate the gust velocity in cases of very extreme turbulence. Jones et al. (1993) argues that this is due to the PSD method's failure to account for wavelet phase correlations that define the local structure of the turbulence. This is an important consideration but is beyond the scope of this thesis, although it may be considered in future work.

6.1.4 Altitude Considerations

In reality, the sample space consists of a great deal more than 3 turbulence severity states, so in order to account for the long-term case the probability distribution for the full range of σ_w must be known. The problem is that the probabilities of non-storm and storm turbulence P_1 and P_2, along with corresponding intensity scale parameters b_1 and b_2, are all dependent upon altitude, so $\mathrm{p}(\sigma_w)$ and hence the long-term exceedance curves are different for every altitude in the flight envelope.

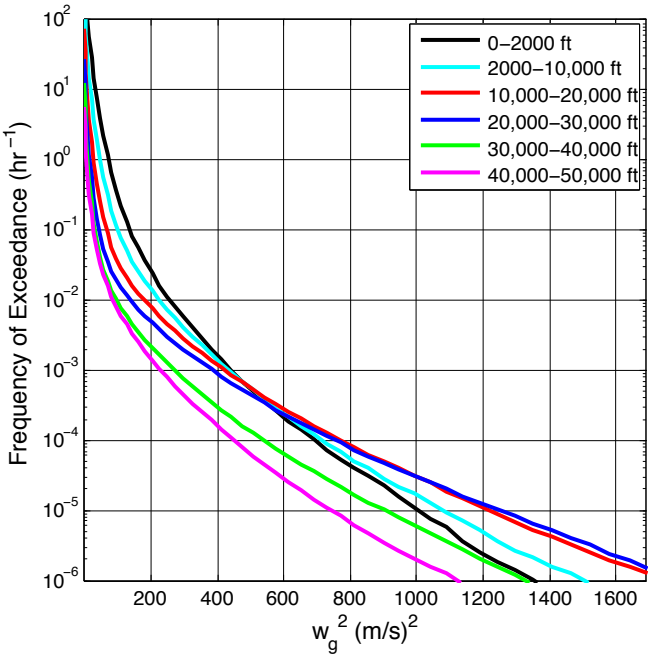

Figure 6.7: Effect of Altitude on Long-Term Gust Velocity Exceedance Curves. $V = 280$ m/s.

Figure 6.7 shows long-term exceedance curves that were obtained from the

simulation of 10,000 gust patches where a continuous range of possible altitudes has been divided into 6 altitude bands, accounting for each altitude band's different probability distribution of σ_w. The values of the non-storm and storm turbulence parameters for each altitude band are presented in table 6.1, and are based on data read from graphs in Hoblit (1988). Since $\mathrm{p}(\sigma_w)$ is dependent upon altitude, the frequency of exceedance curves are not truly long-term until they account for the amount of time an aircraft is likely to spend in each altitude band. However, this is only possible on a case-by-case basis and is part of the mission analysis design procedure, in which a single long-term exceedance curve for gust velocity can be obtained when the total probability distribution of σ_w is calculated by

$$\mathrm{p}(\sigma_w) = \sum_{n=1}^{N_\mathrm{A}} t_n \left[P_{1n} \frac{1}{b_{1n}} \sqrt{\frac{2}{\pi}} \exp\left(-\frac{{\sigma_w}^2}{2b_{1n}} \right) + P_{2n} \frac{1}{b_{2n}} \sqrt{\frac{2}{\pi}} \exp\left(-\frac{{\sigma_w}^2}{2b_{2n}} \right) \right] \tag{6.9}$$

where t_n is the proportion of flight that an aircraft is expected to spend in the n^{th} altitude band.

Table 6.1: Non-Storm & Storm Turbulence Parameters for 6 Altitude Bands (Data Extracted from Figures in Hoblit (1988))

Altitude Band	$\boldsymbol{P_1}$	$\boldsymbol{P_2}$	$\boldsymbol{b_1}$	$\boldsymbol{b_2}$
0 - 2,000 ft	0.63	0.004	1.1125	2.3316
2,000 - 10,000 ft	0.20	0.0012	1.0515	2.6516
10,000 - 20,000 ft	0.06	0.00027	1.0058	3.2002
20,000 - 30,000 ft	0.023	0.00011	0.9448	3.5355
30,000 - 40,000 ft	0.011	0.00010	0.8991	3.0174
40,000 - 50,000 ft	0.0046	0.00011	0.9753	2.7278

In the absence of information about a specific aircraft mission profile, the long-term exceedance curves used in this thesis will assume that the aircraft is always in the 0 - 2000 ft altitude band. However, in Dale et al. (2013), the long-term gust model outlined in this chapter, including altitude data, was used for a specific mission profile to explore the effect of continuous turbulence on a newly developed camber morphing concept.

6.2 Simulation of Linear Aircraft Structural Response

6.2.1 Frequency Domain Response

For the analysis presented in this thesis, an aircraft structural model has been created that enables the full range of possible conditions to be taken into account in a single analysis so that long-term response upcrossing rates can be calculated if required. This means that the model can be used to calculate design loads based on a mission analysis, provided the aircraft is considered to be linear. The assumption of aircraft linearity allows the structural response to be calculated in the frequency domain, where the frequency spectrum Φ_y of a response variable y is obtained by

$$\Phi_y(\omega) = \Phi_w(\omega) |H_y(\omega)|^2 \tag{6.10}$$

The generalised response $\boldsymbol{q}$ to an individual gust harmonic with amplitude a can be expressed as a frequency domain vector $\tilde{\boldsymbol{q}}$ that accounts for all the degrees of freedom in the model, such that

$$\boldsymbol{q}(t) = \tilde{\boldsymbol{q}} \mathrm{e}^{\mathrm{i}\omega t} \tag{6.11}$$

where the frequency domain vector can be found by

$$\tilde{\boldsymbol{q}} = \boldsymbol{H}_{qg}(\omega)\, a \tag{6.12}$$

in which $\boldsymbol{H}_{qg}$ is the vector of transfer functions relating the generalised response to the gust velocity (Wright & Cooper 2007) and is defined as

$$\boldsymbol{H}_{qg}(\omega) = \left[-\omega^2 \mathbf{M} + \mathrm{i}\omega \mathbf{C} + \mathbf{K}\right]^{-1} \left\{ \boldsymbol{R}_W + \boldsymbol{R}_T \exp\left(-\frac{\mathrm{i}\omega l}{V}\right) \right\} \phi\left(\frac{\omega c}{2V}\right) \tag{6.13}$$

where the mass matrix $\mathbf{M}$, the aerodynamic damping matrix $\mathbf{C}$, the stiffness matrix $\mathbf{K}$ and the gust-dependent aerodynamic vectors $\boldsymbol{R}_W$ and $\boldsymbol{R}_T$, are defined in appendix A.

The exponential term in equation 6.13 relating to the gust-dependent response at the tailplane, introduces a phase shift to account for the time delay that occurs between the wing and the tailplane encountering the gust. This phenomenon, which is demonstrated in figure 6.8, is known as the gust penetration effect.

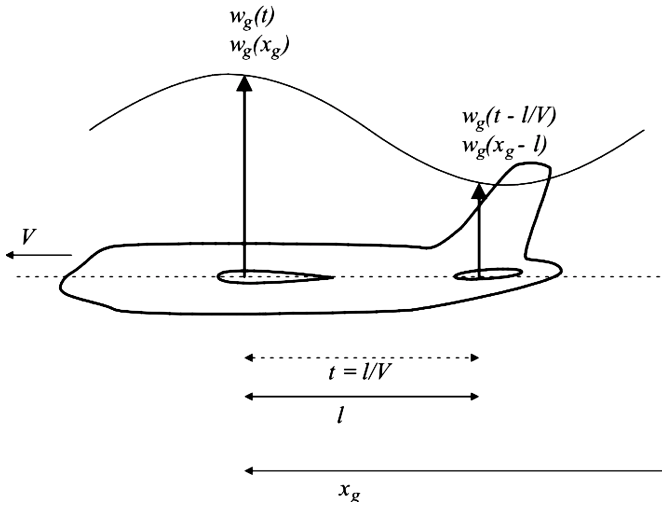

Figure 6.8: Gust Penetration Effect (Wright & Cooper 2007)

Furthermore, Theodorsen's function ϕ has been included in the linear analysis, which accounts for the fact the aircraft does not respond to the gust instantaneously, but the response takes a certain amount of time to build up, depending on the chord length c.

The physical response $\boldsymbol{z}$ at a particular point on the aircraft is also obtained in the frequency domain using a transformation matrix $\mathbf{T}_{zq}$ that relates the generalised response to the values of rigid body and flexible modal displacements. The aircraft displacements and their derivatives are calculated by

$$\tilde{\boldsymbol{z}} = \mathbf{T}_{zq}\tilde{\boldsymbol{q}} \tag{6.14a}$$

$$\dot{\tilde{\boldsymbol{z}}} = \mathrm{i}\omega\mathbf{T}_{zq}\tilde{\boldsymbol{q}} \tag{6.14b}$$

$$\ddot{\tilde{\boldsymbol{z}}} = -\omega^2\mathbf{T}_{zq}\tilde{\boldsymbol{q}} \tag{6.14c}$$

Time domain response sample records of each interesting quantity y, e.g. 'internal' loads such as wing root torsion moment, can then be obtained simply by taking the inverse Fourier transform of their frequency domain response $\tilde{y}$. Once $\tilde{\boldsymbol{q}}$ is known, the frequency

domain response to an individual gust harmonic with amplitude a is calculated by

$$\tilde{y} = \left[-\omega^2 \boldsymbol{A}_y + \mathrm{i}\omega \boldsymbol{B}_y + \boldsymbol{C}_y\right] \tilde{\boldsymbol{q}} + \boldsymbol{D}_y a \tag{6.15}$$

where $\boldsymbol{A}_y$, $\boldsymbol{B}_y$, $\boldsymbol{C}_y$ and $\boldsymbol{D}_y$ are all transformation vectors that relate the aircraft motion or the gust input to the interesting quantity y. Of course, these vectors will vary depending on the interesting quantity, so the transformation vectors for the main interesting quantities used in this thesis are defined in Appendix B.

6.2.2 Linear Response Exceedance Curves

In order to derive linear response exceedance curves, the aircraft transfer functions only need to be calculated once, then response time-histories to a large number of randomly generated gust patches can be obtained using equation 6.12 for all the harmonics in each gust patch. Again, the exceedance rates of a range of thresholds of each interesting quantity are calculated for all the gust patches by counting the number of threshold upcrossings and dividing by the total simulation time. This provides the statistical information required for an empirical exceedance curve. The simulated exceedance rates for the short-term case, i.e. assuming σ_w is constant, can be compared to the theoretical exceedance curve for linear response, which is described as

$$\mathrm{N}\left(y\right) = N_0 \exp\left[-\frac{\left(y/\bar{A}\right)^2}{2{\sigma_w}^2}\right] \tag{6.16}$$

where $\bar{A}$ is defined as

$$\bar{A} \equiv \frac{\sigma_y}{\sigma_w} \tag{6.17}$$

Thus, based on equation 3.12, it can be calculated by

$$\bar{A} = \frac{\sqrt{\int_0^\infty \Phi_y\left(\omega\right) \mathrm{d}\omega}}{\sqrt{\int_0^\infty \Phi_w\left(\omega\right) \mathrm{d}\omega}} \tag{6.18}$$

Therefore, given that the aircraft behaves linearly, both $\bar{A}$ and N_0 are constant

for each interesting quantity and ultimately depend upon the transfer functions, which means that it is a very simple matter to determine the theoretical exceedance curve for a particular linear response. In fact, one might argue that it is not necessary to simulate any results at all since response statistics are so easily available analytically. However, with the intention of later applying probabilistic analysis to nonlinear aircraft, for which there are no such analytical methods, the methodology must first be demonstrated upon a linear model. Furthermore, the linear model will later be used as part of the methodology for deriving nonlinear response statistics and therefore it must be validated.

6.2.3 Basic Aircraft Model

The above methodology for the derivation of *linear* aircraft response statistics is demonstrated using a simple aircraft mathematical model (Vink & de Jonge 1997) (see figure 6.9) with 5 degrees of freedom; 2 rigid body motions and 3 flexible modes.

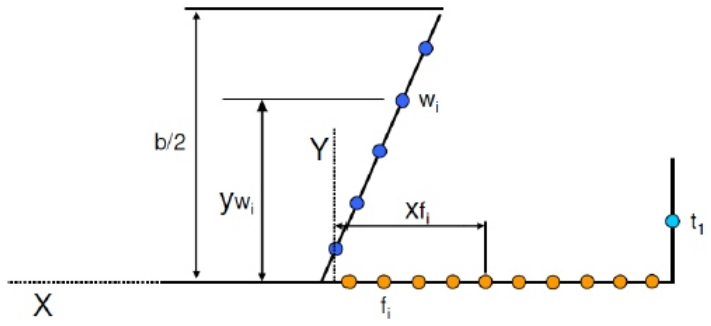

(a) Structural Elements

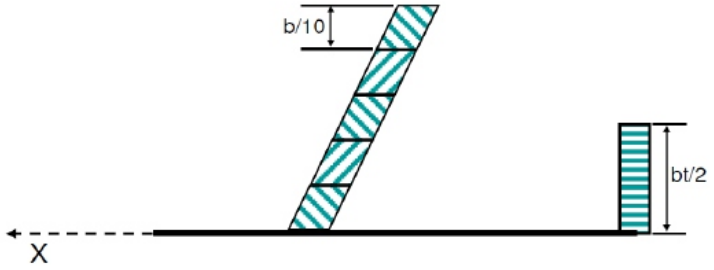

(b) Aerodynamic Elements

Figure 6.9: Schematic of the NLR Model (Vink & de Jonge 1997)

The model's default values for the aircraft geometry were used, thus, the aircraft

has a 24 m span, a chord of 3.83 m and a sweep angle of 17°. Unless stated otherwise, it is assumed that the true airspeed V of the aircraft is 280 m/s. The original NLR model enables the user to calculate a single 10-second time history of each interesting quantity, corresponding to a continuous gust patch of the same duration. The model has been modified so that the duration of the gust velocity sample records can be varied and non-deterministic spectral amplitudes are used.

Five interesting quantities can be determined by the gust response model: load factor n, wing shear force Z_w, wing bending moment M_{bw}, wing torsion moment M_{tw} and tailplane shear force Z_t. To avoid repetitive figures and for reasons that will later become apparent, the load factor, wing shear and wing torsion are the only results that will be presented from the linear analysis.

It is important to note that the modified NLR model described here was only used for the preliminary study presented in section 7.1 of the following chapter. The linear part of the analysis in section 7.2 was performed on a different aircraft structural model (see section 6.3.1) that could also be analysed in the time domain, as the NLR model does not have this capability. However, every linear analysis in the frequency domain was carried out according to the same procedure outlined in this section, regardless of the structural model that was used.

Figure 6.10 shows that the linear model can produce reliable empirical exceedance curves for short-term response. The simulated data was extracted from 10,000 gust patches along with their corresponding response time-histories. Evidently, it agrees very well with the analytical distribution up until the increase in sampling variability at the tail of the distribution. The fact that the curves are straight lines indicates that the model is linear, and that the gust inputs are both locally and globally Gaussian and stationary.

It is more useful however, to simulate the long-term exceedance curves for each interesting quantity so that design loads of for the life of the aircraft can be obtained. Usual practise when conducting a mission analysis is to define the design load as the load that is only exceeded once in every 50,000 hours of flight. This corresponds to a frequency of exceedance $\mathrm{N}(y) = 2 \times 10^{-5}$ hr^{-1}, for which the corresponding load can

be read directly from its long-term exceedance curve. The analytical description of the long-term response exceedance curve is obtained by combining equations 6.6 and 6.16 such that

$$\mathrm{N}(y) = N_0 \left[P_1 \exp\left(-\frac{y/\bar{A}}{b_1} \right) + P_2 \exp\left(-\frac{y/\bar{A}}{b_2} \right) \right] \tag{6.19}$$

Using the method outlined in section 6.1.3, long-term response exceedance curves that account a range of turbulence severity states, were simulated using 10,000 gust patches along with their corresponding response time-histories. Due to the absence of data for an actual mission profile, which may vary for every aircraft, it was assumed that the aircraft would only fly between 0 and 2000 ft. In other words, there was only one probability distribution of σ_w, for which the values of P_1, P_2, b_1 and b_2 were taken from table 6.1. Again, the results demonstrate that the linear model has the ability to accurately calculate empirical long-term response exceedance curves for the purpose of obtaining probabilistic design loads.

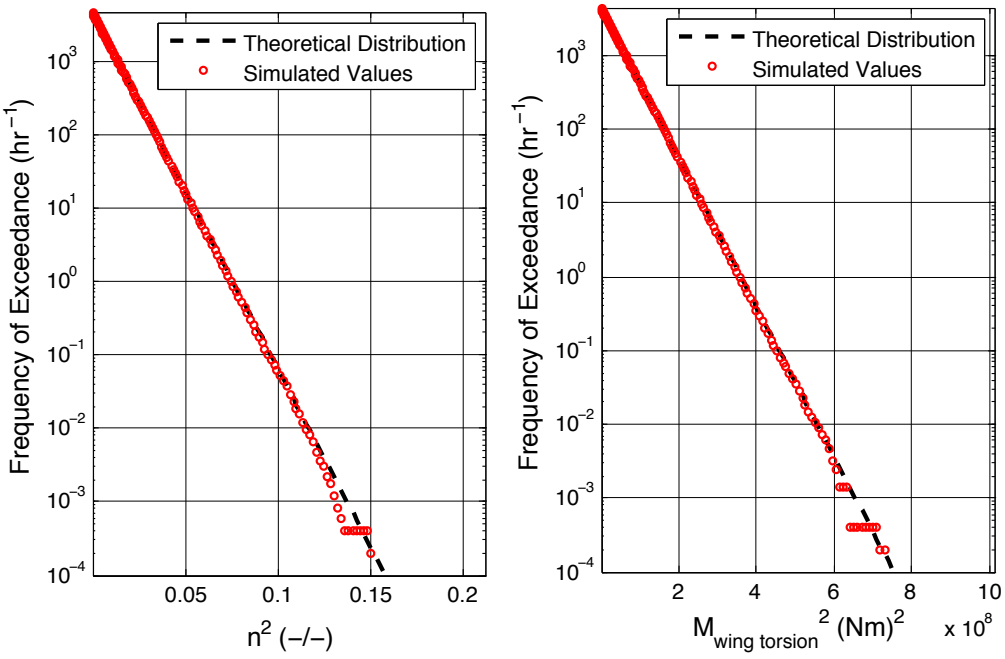

(a) Load Factor

(b) Wing Torsion

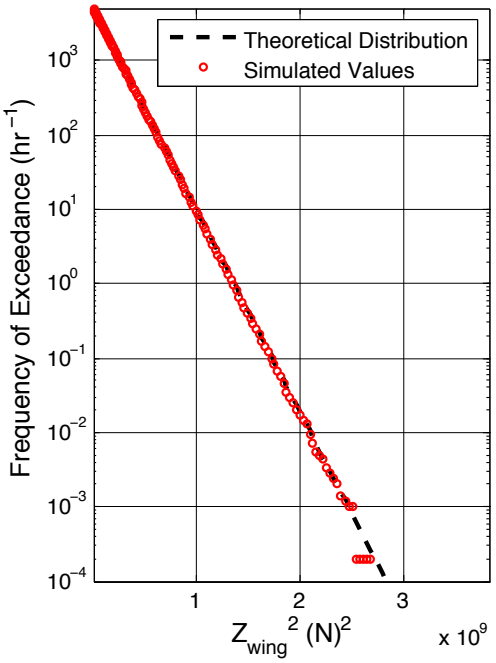

(c) Wing Shear

Figure 6.10: Validation of Simulated Short-Term Response Exceedance Curves. $V = 280$ m/s, $\sigma_w = 1.0$ m/s.

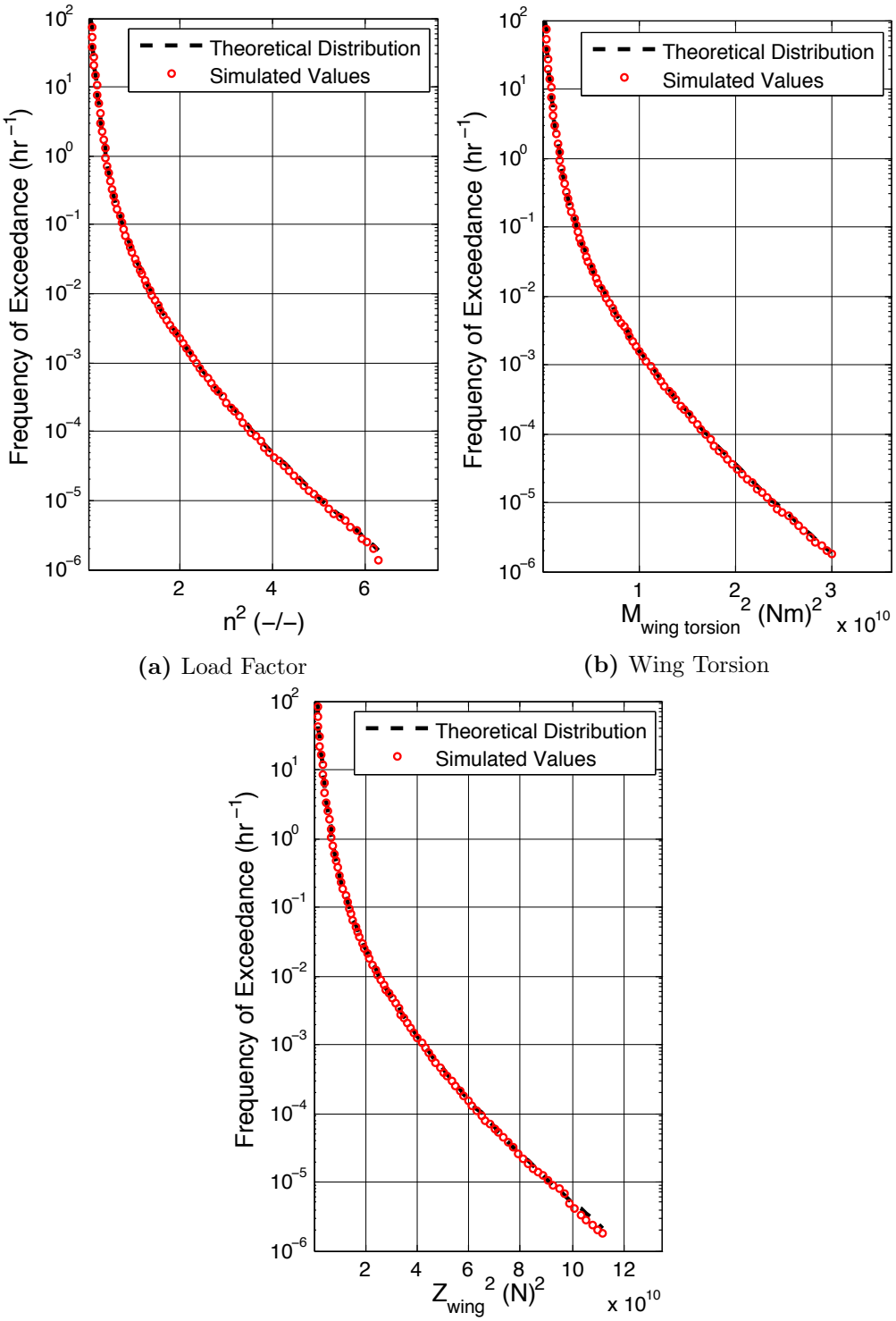

(a) Load Factor

(b) Wing Torsion

(c) Wing Shear

Figure 6.11: Validation of Simulated Long-Term Response Exceedance Curves for A = 0 - 2000 ft. V = 280 m/s.

6.3 Simulation of Nonlinear Aircraft Structural Response

6.3.1 Nonlinear Aircraft Model

A new aircraft model was developed in order to enable the gust response to be calculated in the time domain, which enables the introduction of structural nonlinearity. It is similar to the NLR model, but has been simplified so that the computational time is not excessive, yet not so much that the techniques developed in this thesis cannot be adequately demonstrated. The new model, shown in figure 6.12, does not allow the wing to be swept, so that each strip of the wing encounters the gust at the same time. Otherwise, for a time domain response, there would effectively be a different gust input for each strip, instead of just two inputs (one for the wing and one for the tailplane). Also, the model has a rigid fuselage and is limited to 3 degrees of freedom instead of 5; 2 rigid body modes (heave and pitch), and 1 flexible mode (wing bending).

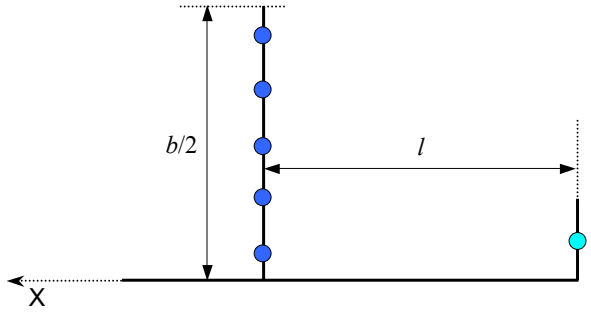

(a) Structural Elements

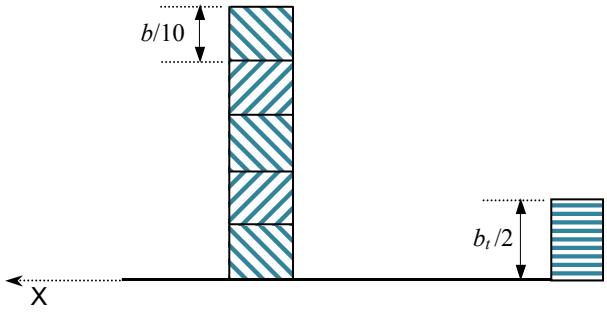

(b) Aerodynamic Elements

Figure 6.12: Schematic of the Model Used for Nonlinear Analysis

The gust inputs are generated as outlined in section 6.1, using non-deterministic spectral amplitudes based on the Von Karman frequency spectrum. Unless stated

otherwise, the true airspeed V and the air density ρ is assumed to be 280 m/s and 0.30 kg/m^3, respectively.

6.3.2 Time Domain Response and Validation

Linear Response in the Time Domain

When an aircraft exhibits nonlinear behaviour, and thus equation 6.10 is not a valid assumption, the response to a gust must be calculated in the time domain, which means that the response at each time step is calculated separately and combined to form a response sample record. The generalised response $\boldsymbol{q}$ to a gust input $w_g(t)$ can be determined from the aircraft equations of motion, which are expressed in the time domain as

$$\mathbf{M}\ddot{\boldsymbol{q}} + \mathbf{C}\dot{\boldsymbol{q}} + \mathbf{K}\boldsymbol{q} = \boldsymbol{R}_W w_g(t) + \boldsymbol{R}_T w_g\left(t - \frac{l}{V}\right) \tag{6.20}$$

where the response vector for the *linear* case $\boldsymbol{q}$ is defined as

$$\boldsymbol{q} = \begin{bmatrix} z_C \\ \theta \\ q_e \end{bmatrix} \tag{6.21}$$

where z_C, θ and q_e are the generalised displacements for each degree of freedom: heave, pitch and wing bending, respectively.

For the time domain solution, the differential equations were solved using the ode45 (Dormand-Prince) solver in MATLAB and SIMULINK, which is based on a Runge-Kutta integration scheme with a variable time-step. The second order differential equation (6.20) is re-written as two first order differential equations, where the initial conditions $\dot{q}(0)$ and $q(0)$ are taken to be zero.

Once the equations of motion have been solved and $\boldsymbol{q}$ is known, time domain response sample records of each interesting quantity y are calculated directly by

$$y(t) = \boldsymbol{A}_y \ddot{\boldsymbol{q}} + \boldsymbol{B}_y \dot{\boldsymbol{q}} + \boldsymbol{C}_y \boldsymbol{q} + \boldsymbol{D}_y w_g \tag{6.22}$$

It is important to note that the time domain model does not include unsteady effects, which would be represented by Wagner's and Kussner's functions, in order to the reduce computational cost of running a large number of simulations in the time domain. This actually reinforces the need for new techniques that require fewer simulations to derive reliable response statistics, because it demonstrates that if more efficient techniques are available, the models can increase in complexity without incurring an impractically high computational cost.

Before structural nonlinearity is included in the model, it is important to verify that the time domain model produces reliable response sample records by computing the linear response in the time domain and comparing it to the frequency domain response to the same gust input. In order to enable this comparison, a frequency domain model was developed for the new aircraft shown in figure 6.12, that uses the procedure outlined in section 6.2, except that unsteady effects are ignored, which means that Theodorsen's and Sears' functions are no longer included in the frequency domain analysis.

Figure 6.13 shows the heave response to a typical '1 - cosine' gust, along with its derivatives, demonstrating that both frequency and time domain solutions to the equations of motion yield almost identical results. The only discrepancy is that the time domain solution appears to produce slightly larger amplitude oscillations for acceleration than the frequency domain solution, but a difference that small should have an insignificant effect on the threshold exceedance curves.

As well as comparing the two MatLab models (frequency and time domain) to one another, it as also necessary to ensure that the loads on the aircraft are realistic to give a degree of confidence in the results presented in this thesis. In order to do this, a deterministic MSC NASTRAN gust response analysis (SOL 146) was carried out using the aircraft shown in figure 6.12, in order to compare response time histories with those from the MatLab model. The models were subjected to two typical '1 - cosine' gusts, with lengths of 80 m and 160 m, and a peak gust velocity of 6.25 m/s. Response time histories of wing root bending moment and wing root shear force are presented in

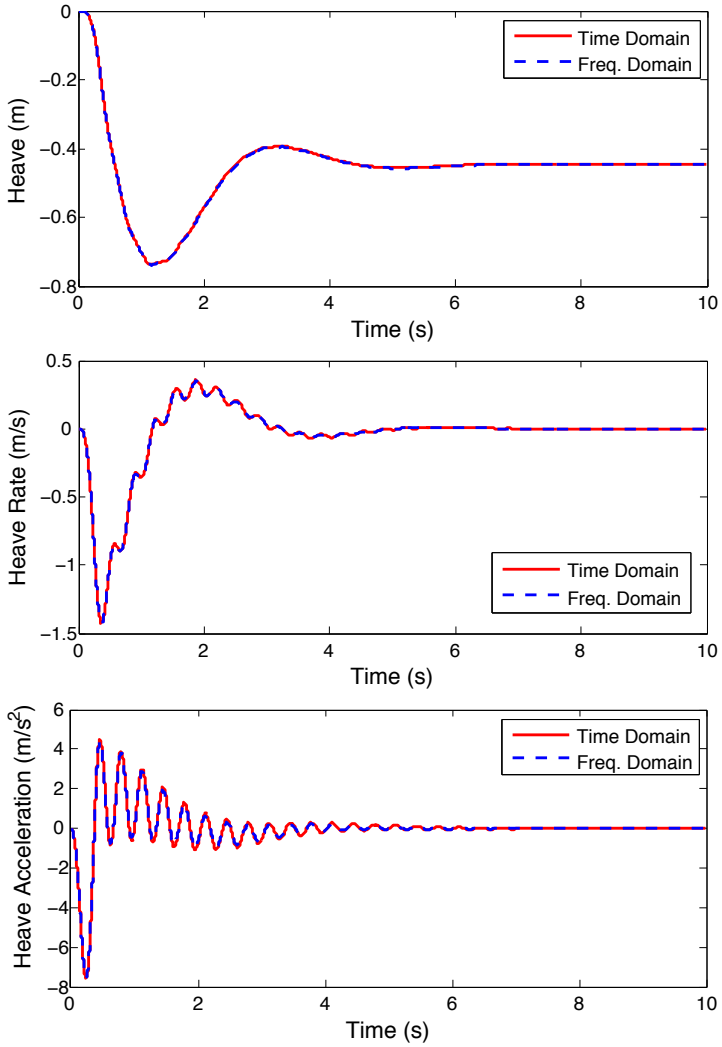

Figure 6.13: Time Domain and Frequency Domain Heave Response to a '1 - cosine' Gust. $V = 280$ m/s, $L_g = 80$ m, $w_{g0} = 6.25$ m/s.

figures 6.14 and 6.15. Some disparity in the results is to be expected since there are differences between the way the gust analysis is performed in NASTRAN compared to the MatLab model presented in this thesis. For example, the NASTRAN analysis uses the Doublet-Lattice Method to calculate the aerodynamic forces, and includes unsteady effects, whereas the MatLab model is limited to the use of Strip Theory and performs a quasi-steady analysis. This being said, the comparison is still beneficial because the fact that response time histories from both analyses show similar features is a source of assurance that the aircraft loads are somewhat realistic. The fact that MatLab model is not a perfect model of reality is not really an issue in this case, because it does not

prevent comparisons between conventional and efficient probabilistic methods *using the same model*, which is the main goal of this research.

In addition to the foregoing deterministic analysis, it must be ensured that the frequency and time domain solutions produce the same exceedance curves when the linear response to a large number of continuous gust patches is considered. The interesting quantities being considered in the nonlinear analysis are the wing root torsion moment M_{tw} and the wing root shear force Z_w. Exceedance curves for these interesting quantities were calculated using both solutions and are compared in figure 6.16, in which each curve is derived from 10,000 gust patches, assuming a constant RMS value of $\sigma_w = 1.0$ m/s. It is clear from this figure that the time domain model produces reliable response sample records, and that the statistical properties of the wing torsion and wing shear are almost identical to those of the frequency domain model. The simulated values for wing shear in figure 6.16b are very slightly higher in the time domain for a given frequency of exceedance, which is probably due to the small difference in acceleration amplitudes shown in figure 6.13.

Long-term exceedance curves using both frequency and time domain models are also compared in figure 6.17b, which shows very good agreement between the two solutions. The long-term case assumes that the aircraft only flies in the 30,000 - 40,000 ft altitude band, with a range of gust RMS values of 0 m/s $\leq \sigma_w \leq$ 15 m/s. Given that long-term exceedance curves are also derived from 10,000 gust patches, it may appear odd that the curves have relatively low sampling variability in the region of very low frequencies of exceedance, especially compared to the short term curves, for which data does not even exist in that region. This is because the long-term curves are influenced by the probability distribution of σ_w (see equation 6.5), and that distribution accounts for the probability that the aircraft will not encounter turbulence. In other words, $P_1 + P_2 < 1$, which means that the expected number of threshold upcrossings per hour is significantly reduced. Nonetheless, especially for aircraft models that are particularly complex, the computational cost for deriving long-term response exceedance curves in the time domain is still very high.

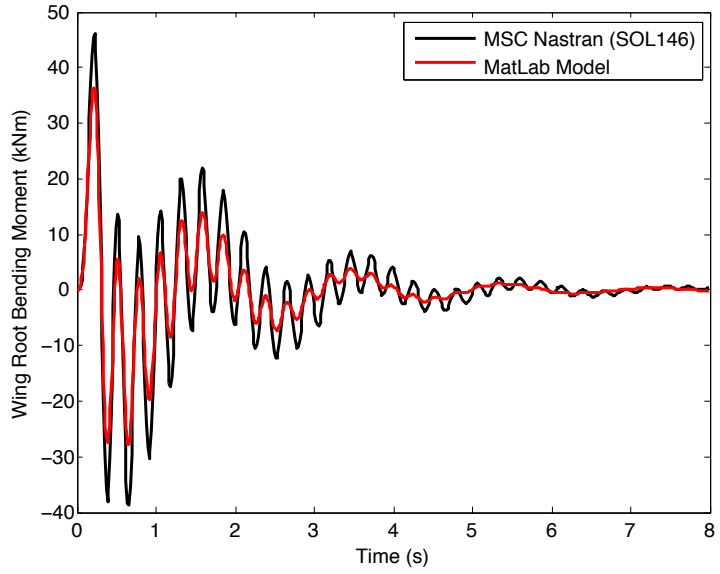

(a) $L_g = 80$ m

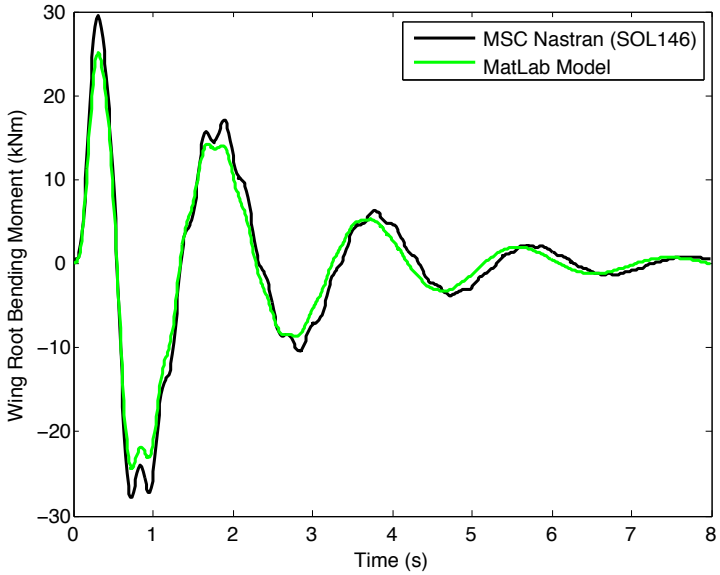

(b) $L_g = 160$ m

Figure 6.14: Comparison of MatLab and NASTRAN Response Time Histories for Change in Wing Root Bending Moment due to a '1 - cosine' Gust. $V = 220$ m/s, $w_{g0} = 6.25$ m/s.

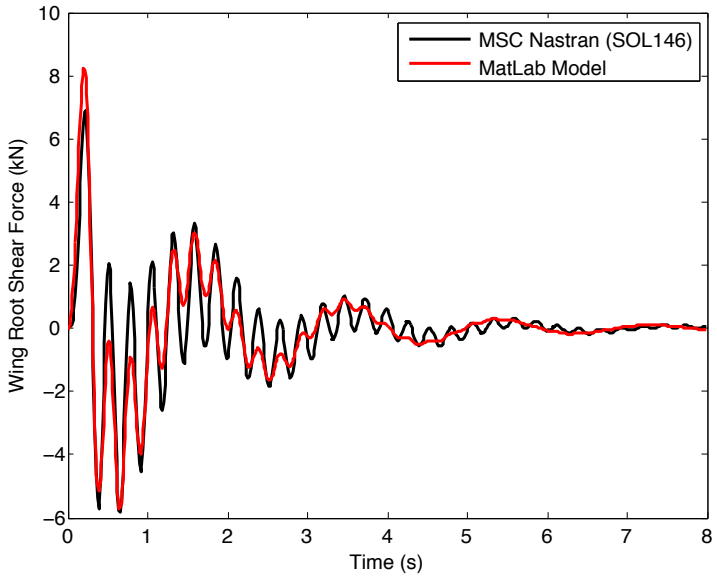

(a) $L_g = 80$ m

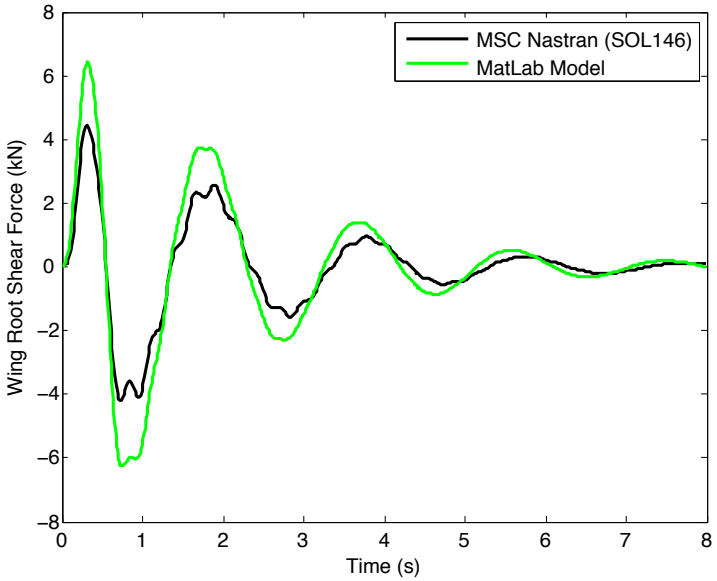

(b) $L_g = 160$ m

Figure 6.15: Comparison of MatLab and NASTRAN Response Time Histories for Change in Wing Root Shear Force due to a '1 - cosine' Gust. $V = 220$ m/s, $w_{g0} = 6.25$ m/s.

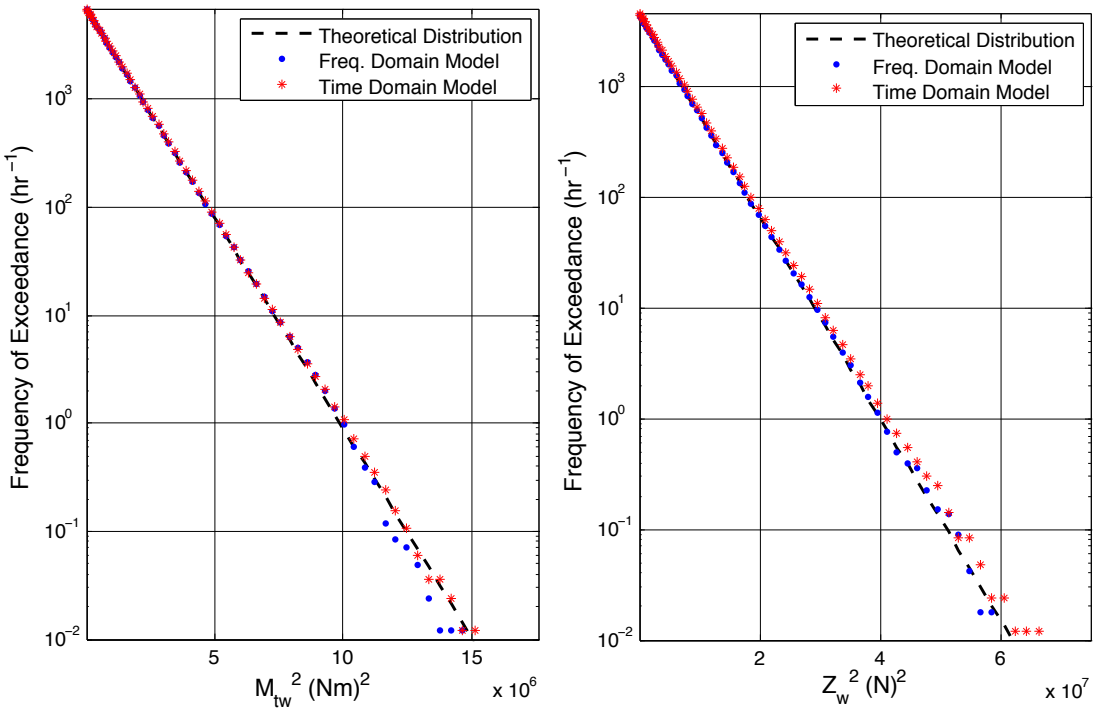

(a) Wing Torsion **(b)** Wing Shear

Figure 6.16: Comparison of Short-Term Time Domain and Frequency Domain Exceedance Curves for Linear Response. $V = 280$ m/s, $\sigma_w = 1.0$ m/s.

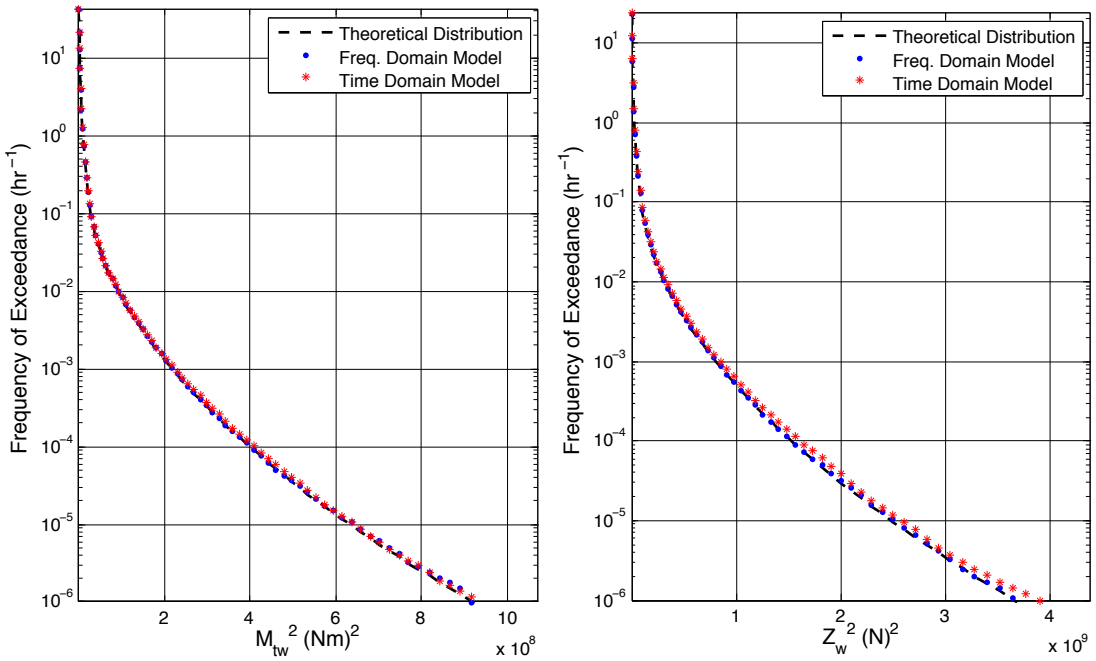

(a) Wing Torsion **(b)** Wing Shear

Figure 6.17: Comparison of Long-Term Time Domain and Frequency Domain Exceedance Curves for Linear Response. $V = 280$ m/s.

Introduction of Structural Nonlinearity

Given that the time domain model has been shown to produce reliable results, nonlinear characteristics can be introduced into the structural model. In this case, the nonlinearity is introduced into the flexible mode in the form of an additional cubic stiffening term, such that the restoring force F_e due to the wing bending stiffness is defined as

$$F_e = k_e q_e + \gamma_e k_e {q_e}^3 \tag{6.23}$$

where k_e is the original linear modal stiffness and γ_e is the hardening coefficient, which determines the proportion that the linear and nonlinear terms contribute to the total restoring force. Thus, the stiffness term for the flexible mode in the matrix $\mathbf{K}$ is expressed as $k_e \left(1 + \gamma_e {q_e}^2\right)$.

A hardening coefficient of $\gamma_e = 5$ was used for the work presented in this thesis, which ensured linear behaviour for small deflections (tip rotations of magnitude $0° < \theta_e < 5°$ in this case), but sufficient nonlinearity to observe the difference for the larger deflections that come from the more extreme gust cases; this is demonstrated in figure 6.18.

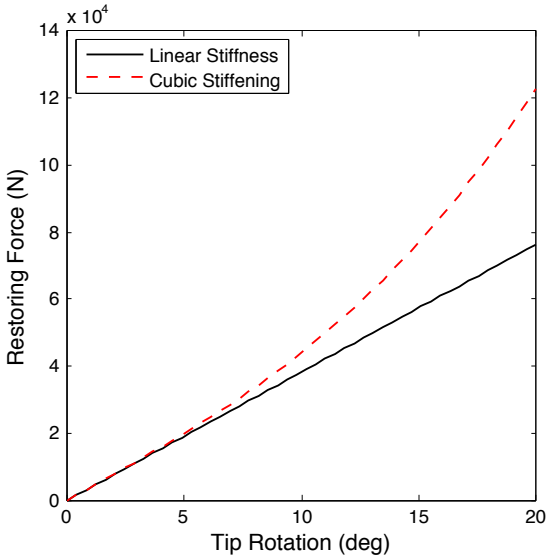

Figure 6.18: Effect of Cubic Stiffening Nonlinearity. $\gamma_e = 5$.

Figure 6.19 shows the fluctuation of the wing root torsion moment during a '1 - cosine' gust encounter, comparing the linear frequency domain and linear time domain

solutions along with that of the nonlinear time domain model.

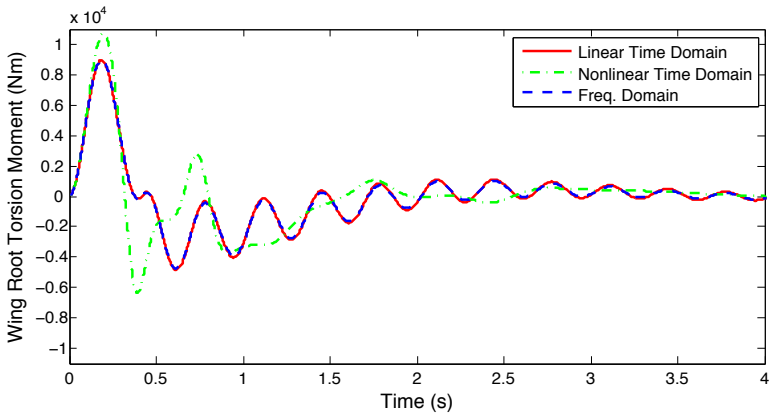

Figure 6.19: Linear and Nonlinear Wing Torsion Response to a '1 - cosine' Gust. $V = 280$ m/s, $L_g = 80$ m, $w_{g0} = 6.25$ m/s.

6.3.3 Nonlinear Response Exceedance Curves

Nonlinear response exceedance curves derived in the conventional manner are required in order to validate the alternative method demonstrated in the following chapter. The short-term and long-term exceedance curves that were used in this project are presented in figures 6.20 and 6.21, respectively, along with the corresponding linear response exceedance curves for comparison. Each curve was derived from 10,000 sample records and, again, the long-term case assumes that the aircraft only flies in the 30,000 - 40,000 ft altitude band, with a range of gust RMS values of 0 m/s $\leq \sigma_w \leq$ 15 m/s. The short-term case assumes a constant RMS value of $\sigma_w = 1.0$ m/s.

The nonlinear results cannot be validated by comparison to an analytical equation, which is the very reason that the simulations are necessary, so it must be assumed that the reliability of the linear time domain exceedance curve is synonymous with the validity of the nonlinear results, since the equations of motion are solved in the same way.

It can be observed that the cubic stiffening has very little effect on the short-term or long-term statistics of the wing root torsion moment, but has a substantial effect on those of the wing root shear force. One might argue that it is not necessary to speed up the derivation of the wing torsion exceedance curve, because the frequency domain

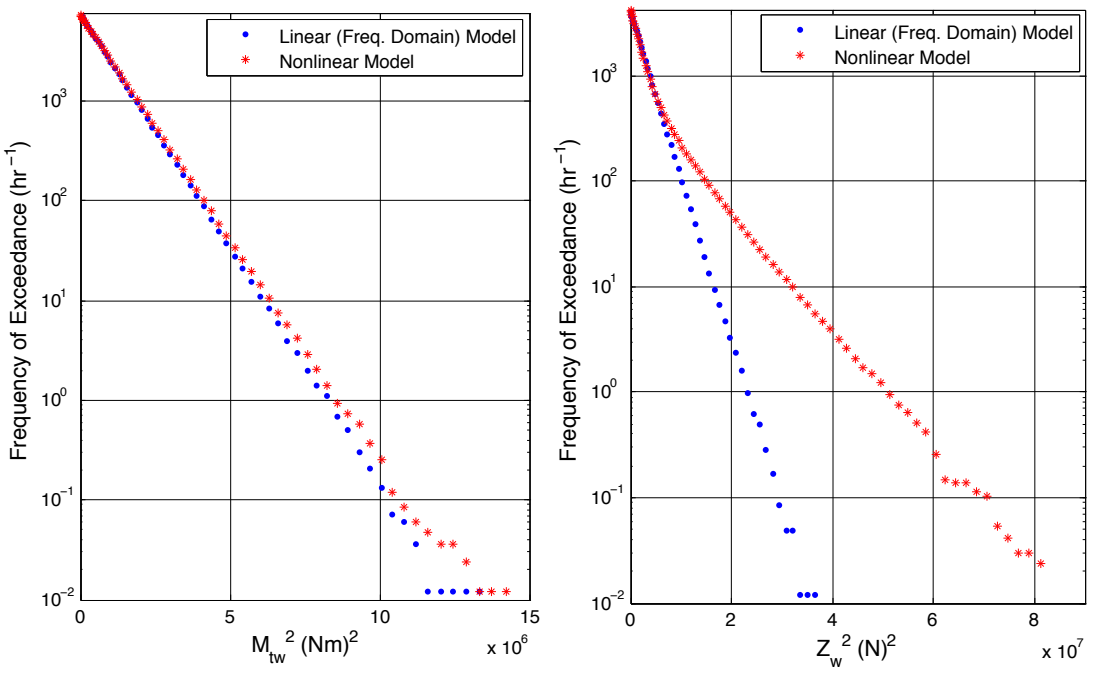

(a) Wing Torsion **(b)** Wing Shear

Figure 6.20: Comparison of Short-Term Linear and Nonlinear Response Exceedance Curves. $V = 280$ m/s, $\sigma_w = 1.0$ m/s.

model is sufficient in this case. This is true, but in this thesis the nonlinear model will still be used for both interesting quantities because it will enable the investigation of the effect of the extent of the nonlinear behaviour on the performance of the alternative method.

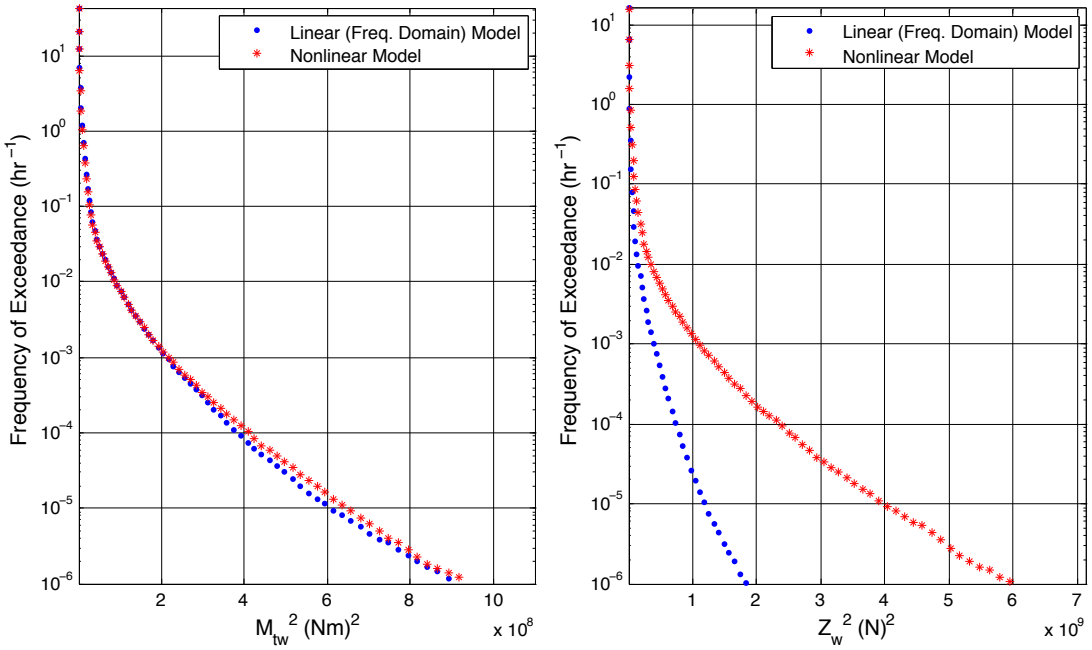

(a) Wing Torsion **(b)** Wing Shear

Figure 6.21: Comparison of Long-Term Linear and Nonlinear Response Exceedance Curves. $V = 280$ m/s.

Chapter 7

Application of the ETU Method to Gust Response

In chapter 5, the Efficient Threshold Upcrossing method was developed in the context of its original application to nonlinear offshore structural response. This chapter seeks to apply the method to the efficient derivation of both short-term and long-term aircraft response exceedance curves. The method was first demonstrated using only a short-term linear aircraft model in the preliminary study presented in section 7.1, which was published in 2013 (Lambert, Najafian & Cooper 2013). It has since been extended to account for cubic stiffening nonlinearity and long-term statistics, for which the findings are presented in sections 7.2 and 7.3.

7.1 A Preliminary Study: Linear Aircraft Response

The ETU method works by exploiting the strong correlation between maximum surface elevation values and maximum response, as demonstrated in figure 5.2. This correlation means that surface elevation sample records with high extreme values are likely to produce response sample records that also have high extreme values. Conversely, low surface elevation extreme values can be expected to bring about low response extreme values. The ETU method can then be applied if the theoretical probability distribution of extreme surface elevation (in the offshore case) is known.

Initially, it was expected that a similar correlation would exist between extreme values of gust velocity and the corresponding aircraft response extreme values, and that since the theoretical distribution of extreme gust velocity is known, the ETU method could be applied to calculate aircraft response to continuous turbulence. However, figure 7.1, which is based on data from 20,000 simulations, shows that there is in fact no such correlation. This means that the largest gusts do not produce the highest structural response values.

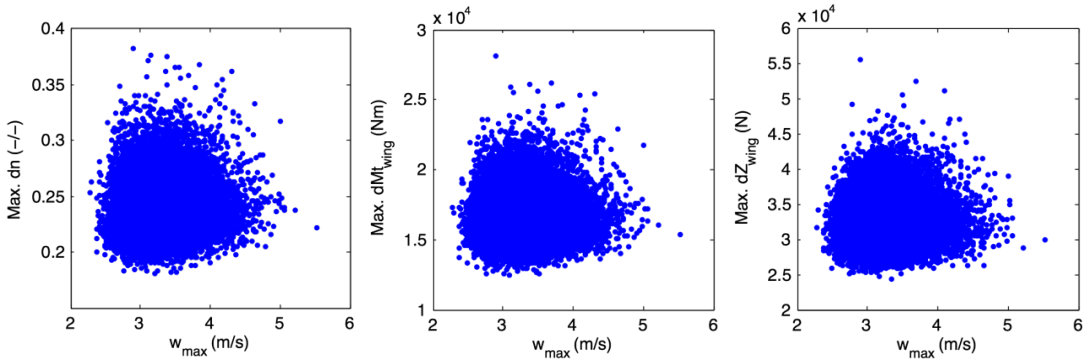

(a) Load Factor **(b)** Wing Torsion **(c)** Wing Shear

Figure 7.1: Correlation of Extreme Gust Velocity with Corresponding Maximum Response

Furthermore, the same type of analysis was conducted to check for correlations of maximum response with both maximum gust height (from peak to trough) and maximum gust steepness (taken from both positive and negative slopes). These were also found to be uncorrelated, as shown in figures 7.2 and 7.3, which also means that the steepest gusts also do not necessarily produce the highest responses.

One possible explanation for the absence of correlation demonstrated by figures 7.1-7.3 can be deduced from the frequency spectra shown in figure 7.4. The frequency spectra of load factor and wing torsion show peak spectral densities at around 5 rad/s, whereas the peak spectral density of gust velocity peaks at a much lower frequency of around 0.2 rad/s and is close to zero at 5 rad/s. This means that the frequencies that produce the highest aircraft response are not the ones associated with the highest gust velocities and, therefore it is actually unlikely that the sample records with the largest gusts will produce response sample records with the highest extreme values.

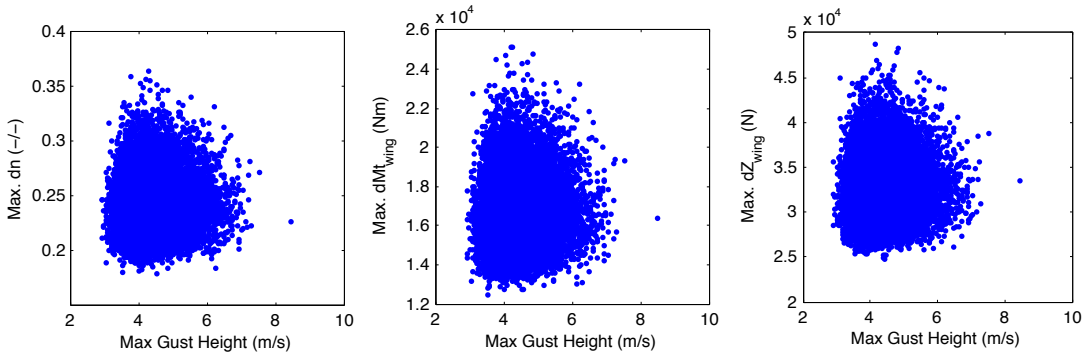

(a) Load Factor **(b)** Wing Torsion **(c)** Wing Shear

Figure 7.2: Correlation of Maximum Gust Height with Corresponding Maximum Response

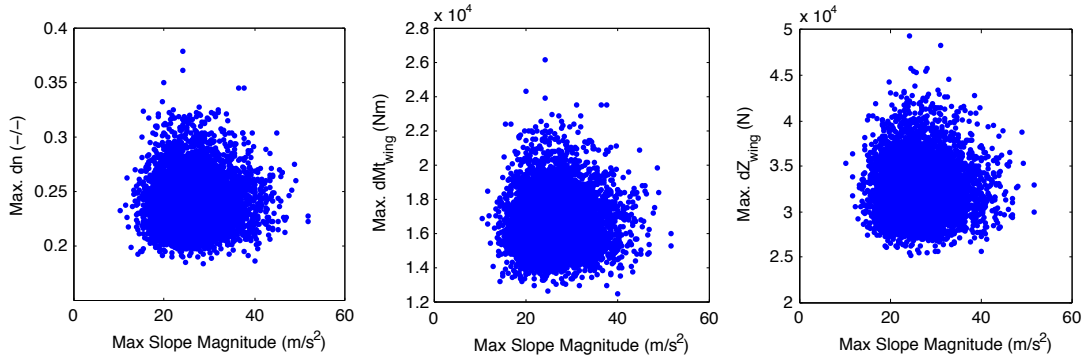

(a) Load Factor **(b)** Wing Torsion **(c)** Wing Shear

Figure 7.3: Correlation of Steepest Gust with Corresponding Maximum Response

Fortunately, the foregoing argument does not rule out the application of the ETU method to gust loading. This is because in order for the method to work, it is only necessary to find a strong correlation between the maximum response and any other variable provided that (i) the theoretical cumulative probability distribution of its extreme values is known, and (ii) the time taken to calculate its corresponding sample record is small compared to that of the response. For the sake of clarity, the variable that satisfies conditions (i) and (ii) will be known as the 'low-demand' variable, and the variable that it is correlated with, but has a relatively high computational cost (e.g. non-linear response), will be known as the 'high-demand' variable.

From figure 7.4 it is clear that there is a much better chance of correlation between extreme load factor and extreme wing torsion, because their spectra both peak at the

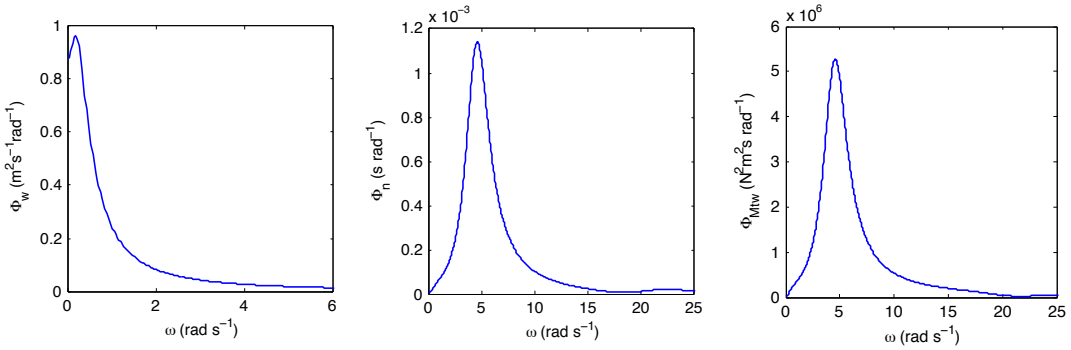

(a) Gust Velocity **(b)** Load Factor **(c)** Wing Torsion

Figure 7.4: Frequency Spectra of Gust Velocity and 2 IQs

same frequencies. Therefore, it is possible that the load factor may be considered as the low-demand variable while treating the other four interesting quantities as the high-demand variables. Clearly, since they are also linear responses, their computational cost is not very high, but in the absence of a non-linear model at the time of the preliminary study, they were suitable for the purpose of demonstrating the methodology and validity of the ETU method.

Correlation coefficients for maximum load factor and the extreme values of the other four IQs were calculated based on 20,000 simulations, two of which are shown in figure 7.5. Table 7.1 shows that wing torsion and wing shear had the highest correlations coefficients, with very strong (0.95) and moderate (0.68) correlations, respectively, which is why they have been selected to represent the so-called high-demand variables in this study. The difference in correlation strength will also provide some insight into the extent to which the ETU method is limited by correlation.

Table 7.1: Correlation Coefficients of 4 IQs with Extreme Load Factor Based on 20,000 Simulations

Wing Shear	Wing Bending	Wing Torsion	Tail Shear
0.68	0.55	0.95	0.51

Now that a suitable low-demand variable has been established, the ETU method can be applied. The correlation between the low and high-demand variables is exploited by dividing the theoretical CDF of the low-demand variable (load factor) into several groups such that the probability that a given low-demand extreme value h will fall into

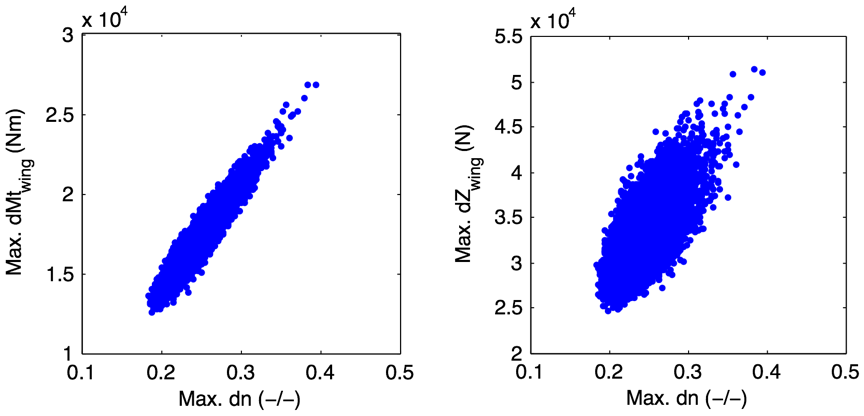

(a) Wing Torsion **(b)** Wing Shear

Figure 7.5: Correlation of Maximum Load Factor with Corresponding Maximum Response

a certain group can be easily calculated. The theoretical distribution for extreme load factor is given by

$$\mathrm{P}\left(n_{\max} \leq h\right) = \exp\left\{-N_{0_n} T \exp\left[-\frac{\left(h/\bar{A}_n\right)^2}{2{\sigma_w}^2}\right]\right\} \tag{7.1}$$

For the application to aircraft gust response, eight groups will be used for the ETU analysis, instead of seven groups, which were used for the original application to offshore structures. Hence, there are now nine boundaries, for which the chosen cumulative probability values are $P_{\text{lim.}}$= [0, 0.1, 0.5, 0.8, 0.95, 0.99, 0.995, 0.999, 1].

Again, let S be the set of all the simulated response extreme values such that $S = \{S_1, S_2, \ldots, S_{\mathrm{G}}\}$ where $S_i \subset S$. The values in S are divided into these subsets based on the extreme values of their corresponding load factor sample records, using the boundaries of $n_{\max}$ that are calculated using equation 7.1. The probability P_i that a sample record belongs to the i^{th} subset of S is given by equation 5.1.

Given that the conditions for low and high-demand variables are satisfied, it is simply a matter of implementing the procedure outlined in figure 5.7. When the number of threshold upcrossings of the response thresholds are counted from each high-demand sample record, the expected frequency of exceedance values are those based on the condition that the sample record belongs to a particular subset, i.e $\mathrm{E}\left[\mathrm{N}\left(y\right) \mid h \in S_i\right]$.

Thus, total probability theorem must be applied for each response threshold to calculate the expected number of upcrossings:

$$\mathrm{E}\left[\mathrm{N}\left(y\right)\right] = \sum_{i=1}^{\mathrm{G}} \mathrm{E}\left[\mathrm{N}\left(y\right) \mid h \in S_i\right] P_i \tag{7.2}$$

It was explained in chapter 5 that one of the advantages of the ETU method is that each subset does not need to contain the same number of high-demand sample records, allowing the distribution to be 'tailored' to minimise unnecessary computational cost. It was also shown that a more accurate 'tail' can be obtained from the same number of simulations by allowing more simulations in the extreme group and fewer in the interim groups. Therefore, since the tail of the exceedance curve is the area of greatest interest when it comes to design loads, two cases were considered in the preliminary study, which vary the number of simulations in the extreme group along with the total number of simulations, as defined in table 7.2.

Table 7.2: Number of Simulations in Each Group in the ETU Analysis for Each Case

	Total No. of Simulations	Interim Groups (1-7)	Extreme Group (8)	Computational Cost Reduction
Case 1	800	100	100	99.2%
Case 2	200	10	130	99.8%

For the sake of simplicity, the exceedance curves in each case are based on short-term statistics, where $\sigma_w = 1.0$, and the probability that an aircraft will encounter turbulence was not taken into account in the initial study.

It can be seen from figure 7.6 that the wing torsion exceedance curve from the ETU method agrees extremely well with that of the Monte-Carlo method, even though in this case it is derived from 125 times fewer simulations. For the wing shear, however, it clear that the weaker correlation has an adverse impact on the accuracy of the curve. On the other hand, the ETU method still produced a very accurate curve for the more frequently exceeded thresholds. Nevertheless, this still demonstrates that for the ETU method to be effective, a very strong correlation is required between the low and high-demand variables.

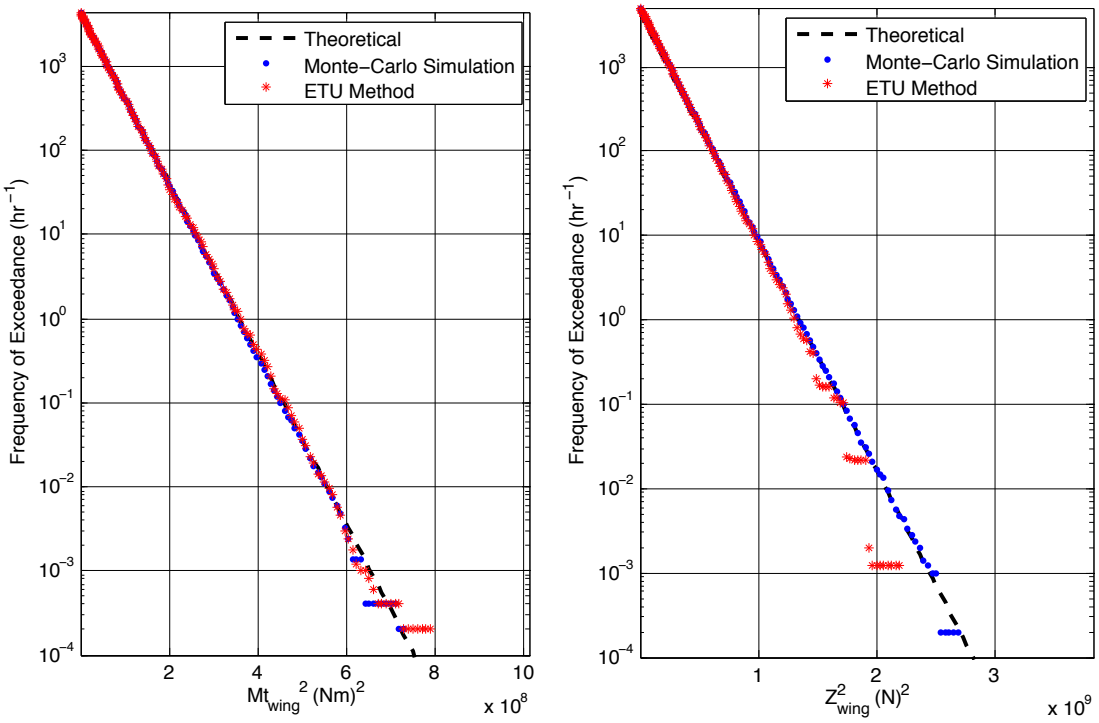

(a) Wing Torsion **(b)** Wing Shear

Figure 7.6: Short-Term Exceedance Curves using the ETU Method for Case 1: $\sim$ 125 Times Faster. $V = 280$ m/s, $\sigma_w = 1.0$ m/s.

Figure 7.7 shows that, even with 500 times fewer simulations, the ETU method produces a very reliable exceedance curve for wing torsion. In fact, despite the drastically lower computational cost, the tail of the ETU curve is smoother and more reliable than that of the Monte-Carlo curve. This is because, in the ETU method, the sampling variability is effectively 'shared out' and distributed to the areas of the curve that are of lower interest when it comes to obtaining design loads. Interestingly, the wing shear curve shows very little difference from that of case 1 in that it still produces an accurate curve for the first half of the distribution, with the results becoming meaningless for the least frequently exceeded half of the thresholds.

In the foregoing analysis, the linear responses were used to represent the high-demand variables when, in reality, they incur a very low computational cost. Also, given that analytical solutions for linear response exceedance curves are available, neither the Monte-Carlo simulation approach nor the ETU method offer any real benefit in this case. However, the objective of this study was to provide a

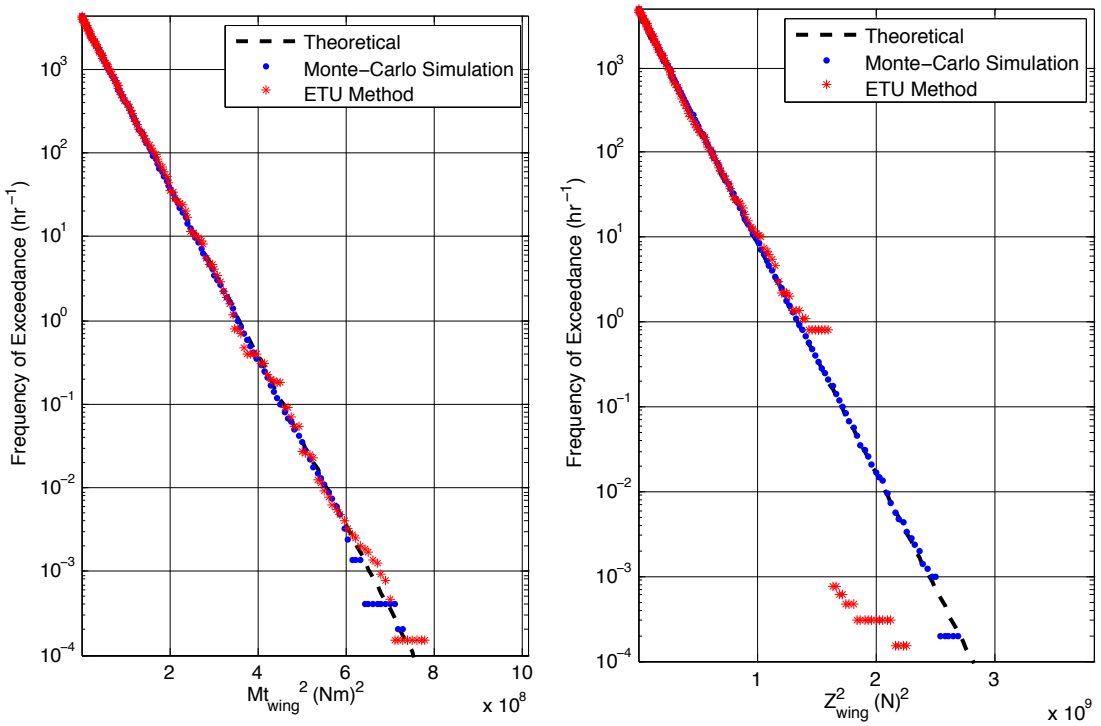

(a) Wing Torsion **(b)** Wing Shear

Figure 7.7: Short-Term Exceedance Curves using the ETU Method for Case 2: ~ 500 Times Faster. $V = 280$ m/s, $\sigma_w = 1.0$ m/s.

demonstration of the ETU method in order to show that it *would* be beneficial if applied to a nonlinear aircraft model. For the nonlinear case, it is expected that a strong correlation could be found between the maximum values of linear and nonlinear response, a hypothesis that is investigated in the following section (7.2). Provided such a correlation exists, the linear response may be used as the low-demand variable so that the statistics of the nonlinear response, which is the high-demand variable, can be derived with great efficiency.

7.2 Efficient Nonlinear Aircraft Response

As previously mentioned, it is much more convenient to compute response exceedance curves using equation 6.16 rather than carrying out a large number of simulations that produce the same results. However, Monte-Carlo simulation techniques become much more beneficial when there is no analytical description of the response statistics, which is certainly the case when considering nonlinear aircraft.

For nonlinear cases, equation 6.10 is not valid, which means that the aircraft response must be calculated in the time domain. This induces a much higher computational cost than the simple PSD analysis, making it impractical to include nonlinear response statistics as part of the design requirements. This means that so far, nonlinear aircraft models only account for so-called 'worst case' gusts and not for continuous turbulence. Nevertheless, there is no reason why response sample records cannot be generated by computing the nonlinear response to each continuous gust patch in the time domain. The statistical information such as the number of threshold upcrossings can then be extracted from each of the nonlinear response sample records. The only problem is that it would take an unacceptably long time to generate the number of sample records required to sufficiently reduce sampling variability such that accurate design loads could be obtained.

This section seeks to apply the Efficient Threshold Upcrossing method to the derivation of nonlinear response exceedance curves so that, for the first time, aircraft with nonlinear characteristics can be designed probabilistically and hence, it is hoped, more economically and efficiently.

The first step is to establish the so-called low-demand and high-demand variables for use in the analysis. The high-demand variables in this case are the desired interesting quantities that are calculated based on the nonlinear structural response; namely, the wing torsion moment M_{tw} and the wing root shear force Z_w. According to the conditions outlined in the previous section, the linear structural response may be a suitable low-demand variable, as the analytical probability distribution of its extreme values is known, but it is first necessary to assess whether a strong correlation exists between linear and nonlinear response. In order to determine the correlation, 20,000 gust patches

were simulated, and the corresponding linear and nonlinear response time-histories were calculated for each gust patch. Then the maximum values of both linear and nonlinear response were taken and plotted against one another so that the correlation coefficients for each interesting quantity could be calculated.

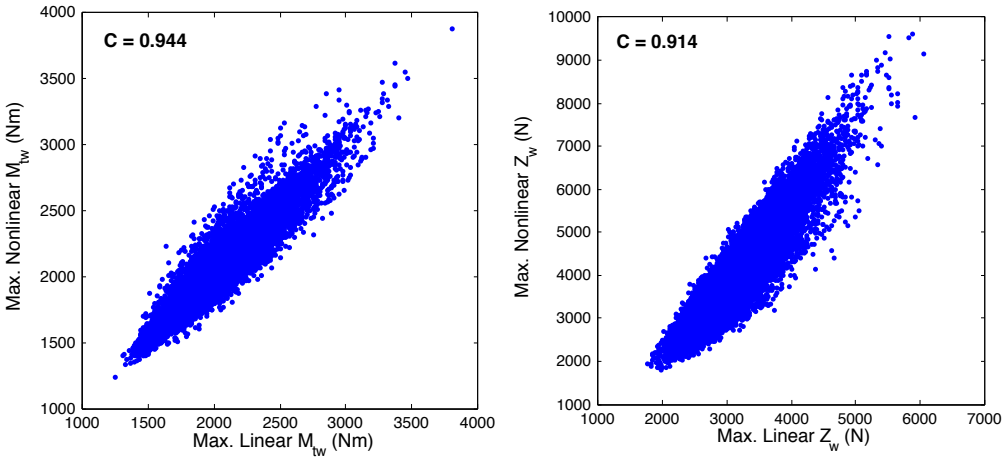

(a) Wing Torsion **(b)** Wing Shear

Figure 7.8: Correlation of Maximum Linear Response with Corresponding Maximum Nonlinear Response

Figure 7.8 shows that a strong correlation *does* exist between the extreme values of linear and nonlinear response for both of the interesting quantities considered. The correlation coefficients for wing root torsion moment and wing root shear force were found to be 0.944 and 0.914, respectively. Based on the previous study, it is reasonable to assume that the correlation is sufficiently strong so as to qualify the linear response as the low-demand variable. The question remains, however, of how strong the correlation needs to be to ensure that the ETU method is effective. As explained earlier, the ETU method works based on the assumption that high-demand variables belong to the same subsets as their corresponding low-demand variables. This would only truly be the case if the correlation coefficient between the two variables was equal to 1. In other words, if the value of a low-demand variable increases, the value of the corresponding high-demand variable will *always* be increased, and vice versa. It follows then, that as the correlation coefficient gets lower, the probability that the two variables will *actually* belong to the same subset will reduce, even though it is still assumed to be the case in

the ETU method.

The effect of using a weakly correlated low-demand variable on the response exceedance curve was observed in figures 7.6b and 7.7b, where the correlation coefficient was only 0.68. It seems that too many of the simulations in that case violated the assumption of equal probability to produce any meaningful data. However, since a correlation does exist, weak though it is, it would be reasonable to expect the reliability of the exceedance curve to improve if the number of simulations in each group was increased, because there would be a higher chance that sample records would occur that complied with the assumption of equal probability. Of course, as the correlations became weaker, there would come a point where the number of sample records in a group would need to be so high that it would not be worth using the ETU method at all. Thus, any computational cost savings cannot be considered independently from the strength of the corresponding correlations.

There is not enough information based on the current work to give a specific value for a correlation coefficient above which the ETU method remains effective, but it is fair to say that the computational cost reductions presented in this thesis can be achieved for systems which have low- and high-demand variables with correlation coefficients above at least 0.91. This is backed up by the following analysis, in which there was no noticeable effect of the small reduction in correlation coefficient in comparison to the previous study.

The procedure that is used to apply the ETU method to nonlinear aircraft response, using the corresponding linear response as the low-demand variable, is outlined in the flow chart shown in figure 7.9.

The cases that describe the number of simulations in each group for the nonlinear analysis are defined in table 7.3. Eight groups are used for the nonlinear ETU analysis, but more cases are defined in comparison to the preliminary study in section 7.1. This enables the capability of the ETU method to be explored further by including the option to vary the number of simulations in group 7 *as well as* group 8. The reason for this is that in previous studies, when the majority of the simulations have been concentrated into the extreme group, a large difference in accuracy suddenly occurs at the point in the

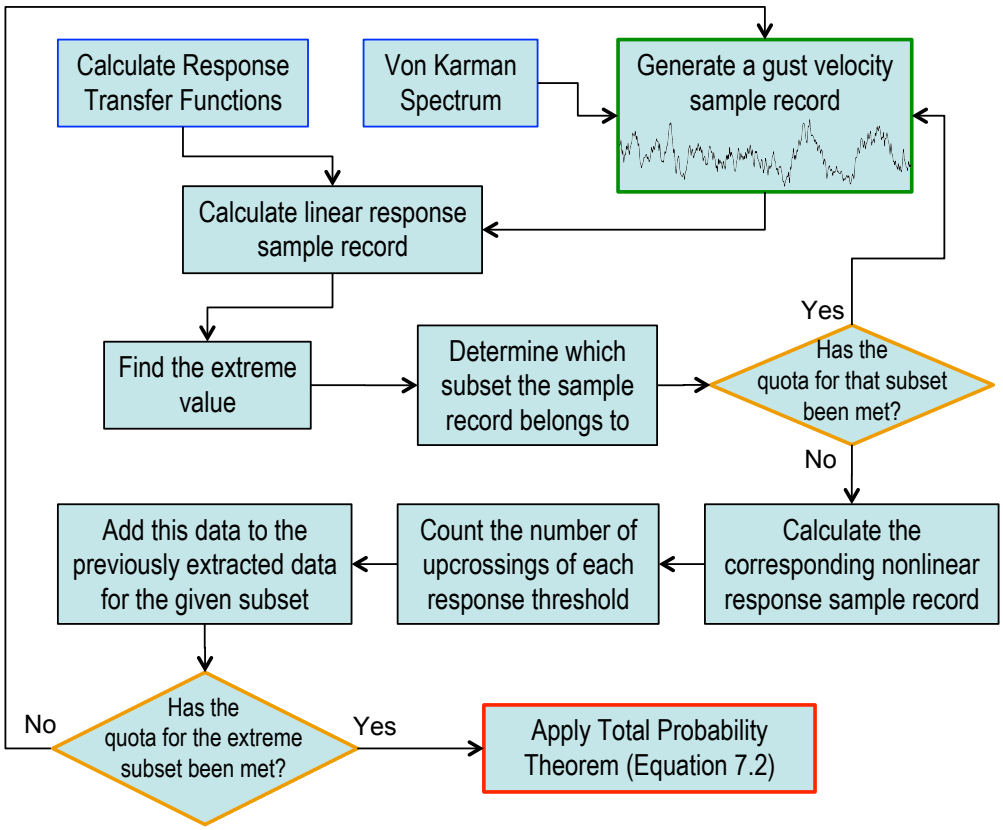

Figure 7.9: Procedure for the Derivation of Nonlinear Response Exceedance Curves Using the ETU Method

curve that corresponds to the lower boundary of the extreme group. This phenomenon can be most clearly observed in figure 5.11 from the ETU analysis for efficient offshore structural response. In an effort to reduce this effect and produce a more accurate curve, some of the cases (Cases 3, 6 and 9) focus more of the simulation time in the highest of the interim groups (group 7), at the expense of the lower interim groups along with the extreme group. As in the previous studies, the other cases either distribute the simulation time approximately equally between all the groups (Cases 1, 4 and 7), or focus most of the simulation time towards sample records in the extreme group (Cases 2, 5 and 8).

It is worth noting that, although the computational cost reductions shown in table 7.3 are an order of magnitude lower than the previous studies, it is because the results of the ETU analyses are compared to the conventional exceedance curves in figure 6.20, which are derived 10,000 sample records instead of 100,000 in order to save time. The

Table 7.3: Number of Simulations in Each Group in the Nonlinear ETU Analysis for Each Case

	Total No. of Simulations	Lower Interim Groups (1-6)	Highest Interim Group (7)	Extreme Group (8)	Computational Cost Reduction
Case 1		125	125	125	
Case 2	1000	40	40	720	90%
Case 3		30	220	600	
Case 4		50	50	50	
Case 5	400	20	20	260	96%
Case 6		15	110	200	
Case 7		12	14	14	
Case 8	100	4	4	72	99%
Case 9		3	22	60	

boundaries for the probability distribution of extreme linear response that define each subset have been lowered accordingly so that the conventional and ETU exceedance curves can be compared. The nine probability boundaries used to define the eight groups for the nonlinear ETU analysis in this section are $P_{\text{lim.}} = [0, 0.10, 0.50, 0.65, 0.80, 0.90, 0.95, 0.99, 1]$.

It is clear from the earlier studies shown in this thesis that the computational cost reduction provided by the ETU method is not actually proportional to the number of simulations required by the conventional simulation, which means that it becomes more effective as the number of simulations required by the conventional analysis increases. This is because the probability boundaries that define the groups used in the ETU analysis can be adjusted if information about less frequently exceeded thresholds is needed, which would not necessarily require any more simulations in the ETU method, but may require many orders of magnitude more simulations in a conventional analysis.

The short-term exceedance curves for nonlinear response that were derived using the ETU analysis, along with comparisons to the conventionally derived exceedance curves from section 6.3, for the cases defined in table 7.3, are presented in figures 7.10 - 7.18.

The first thing to notice from the exceedance curves in cases 1 - 3 (figures 7.10 - 7.12), which were derived from 100 times fewer simulations than the reference curves (i.e. the ones based on the conventional method), is that there is some systematic deviation from the reference curve for the wing root shear. This is most likely due to the higher degree

of nonlinearity in the wing shear compared to the wing torsion, which agrees almost perfectly with the reference distribution. The difference in accuracy between the two IQs is not surprising given that the nonlinear wing torsion has a stronger correlation with its corresponding linear extreme values than the wing shear does. Despite this discrepancy, the simulated values from the ETU method for the wing shear are still within 2% of the reference values around the tail of the exceedance curves in cases 1 - 3. The error is only magnified in its presentation because the frequencies of exceedance are plotted against the *square* of the response thresholds, rather than simply the threshold values.

Secondly, for a given total number of simulations, the ETU method always produces a more reliable curve when the majority of the simulation time is concentrated into the extreme groups. This is demonstrated by the fact that exceedance curves in cases 1, 4 and 7 (figures 7.10, 7.13 and 7.16), in which the simulations are spread out more evenly between the groups, are clearly more affected by sampling variability around the tail than any of the other cases that are derived from the same number simulations. This again highlights one of the major benefits of the ETU method: that the effect of sampling variability can moved away from the tail of the distribution by changing the number of simulations in each group. It is especially advantageous because the earlier studies in this thesis showed that reducing the number of simulations does not have as significant an effect in the lower groups, which is due to the fact that the more extreme sample records still provide upcrossing data for the lower thresholds.

Furthermore, the inclusion of the option to vary the number of simulations in the highest interim group (group 7) proved to be worthwhile. Cases 3, 6 and 9 (figures 7.12, 7.15 and 7.18) consistently produced exceedance that were less affected by sampling variability around the than the respective curves in cases 2, 5 and 8 (figures 7.11, 7.14 and 7.17). This went some way towards solving the problem of the occurrence of a sudden difference in accuracy that results in a large step in the exceedance curve corresponding to the boundary of the extreme group. In other words, it shows that the ETU method is generally more effective when the difference in the number of simulations varies more gradually between groups, instead of focussing a

large amount the extreme group. Therefore, it may be expected that there is some optimum distribution of simulation time between then groups that produces a curve that is minimally affected by sampling variability, which could be investigated in future work.

Finally, it can be observed from figure 7.18 that, with as little as 1% of the computational cost of the conventional method, the ETU method has the ability to produce short-term exceedance curves that are in good agreement with the reference curves, even where there is a high degree of nonlinearity in the response. One issue that has not been solved regarding the reduction in computational cost, however, is that in order to perform an ETU analysis it is first necessary to establish a low-demand variable that is strongly correlated with the nonlinear response. This means that a certain number of sample records of the high-demand variable must be simulated to verify that such a correlation exists, which incurs further computational cost. In this thesis, for example, 20,000 simulations were used in each case to evaluate the correlations, but it is uncertain how many simulations are actually sufficient. It may be much fewer than 20,000 but might vary depending upon the degree of nonlinearity in the model. There is also the question of whether it could be assumed that the linear response will *always* be strongly correlated with the nonlinear response for each interesting quantity, so that the additional simulations were no longer required, but so far there has not been enough research on this issue to justify such an assumption. Nevertheless, the ETU method remains promising when it comes to the derivation of short-term aircraft response statistics with cubic stiffening nonlinearity and will be extended to the long-term case in following section.

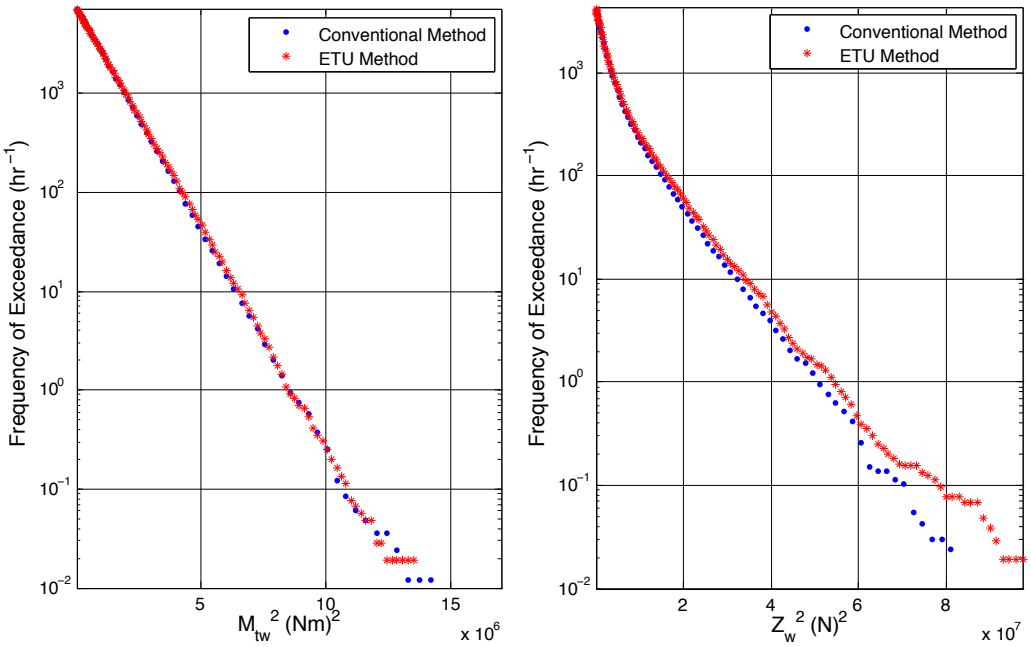

(a) Wing Torsion **(b)** Wing Shear

Figure 7.10: Short-Term Exceedance Curves for Nonlinear Response using the ETU Method for **Case 1**: $\sim$ 10 Times Faster. $V = 280$ m/s, $\sigma_w = 1.0$ m/s.

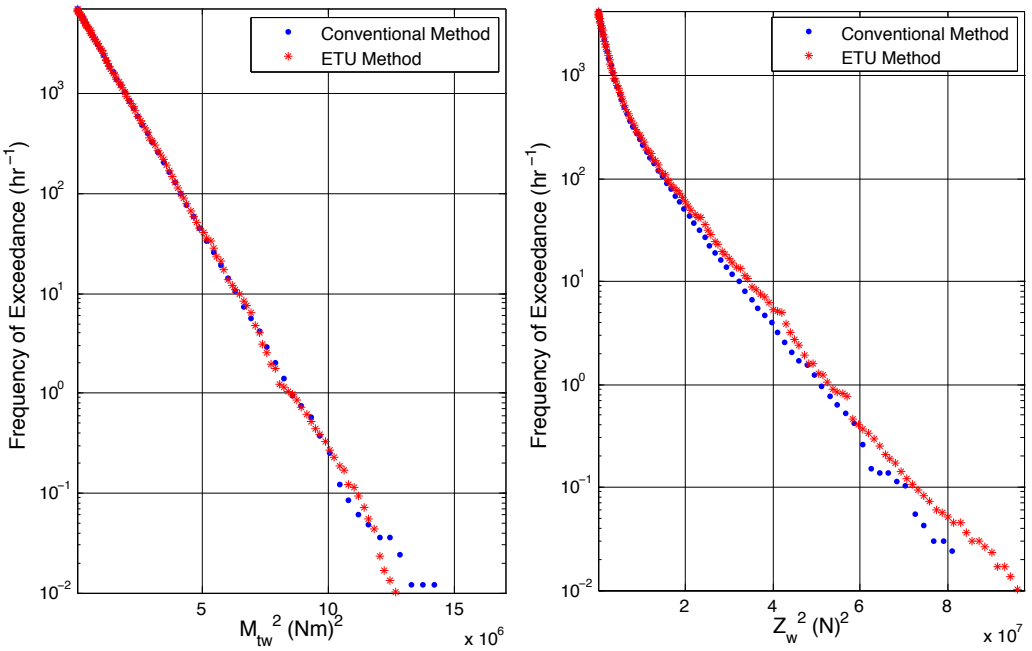

(a) Wing Torsion **(b)** Wing Shear

Figure 7.11: Short-Term Exceedance Curves for Nonlinear Response using the ETU Method for **Case 2**: $\sim$ 10 Times Faster. $V = 280$ m/s, $\sigma_w = 1.0$ m/s.

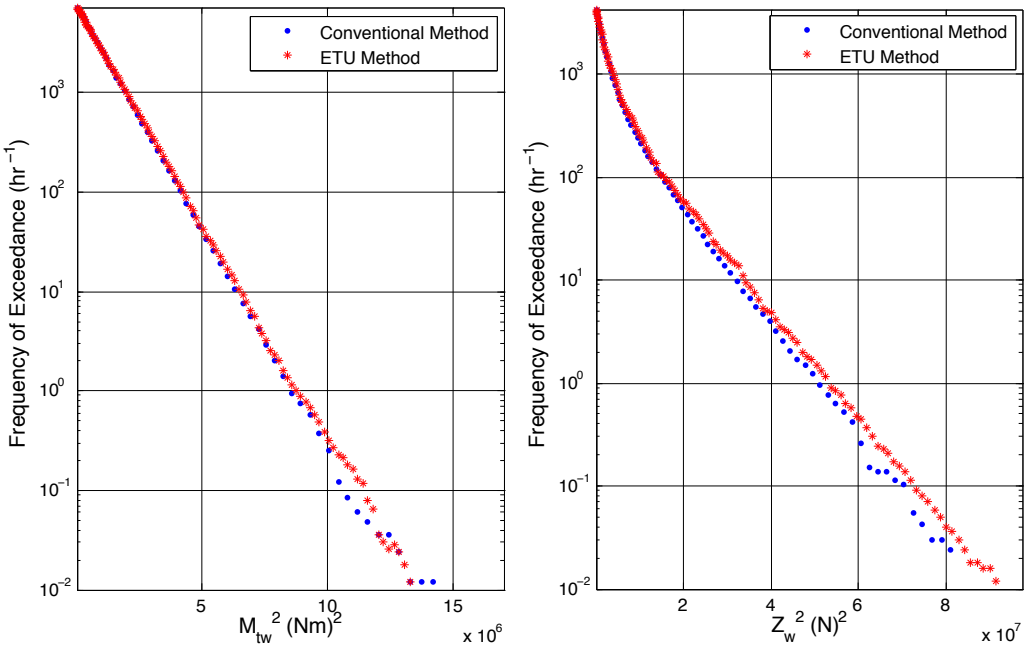

(a) Wing Torsion **(b)** Wing Shear

Figure 7.12: Short-Term Exceedance Curves for Nonlinear Response using the ETU Method for **Case 3**: $\sim$ 10 Times Faster. $V = 280$ m/s, $\sigma_w = 1.0$ m/s.

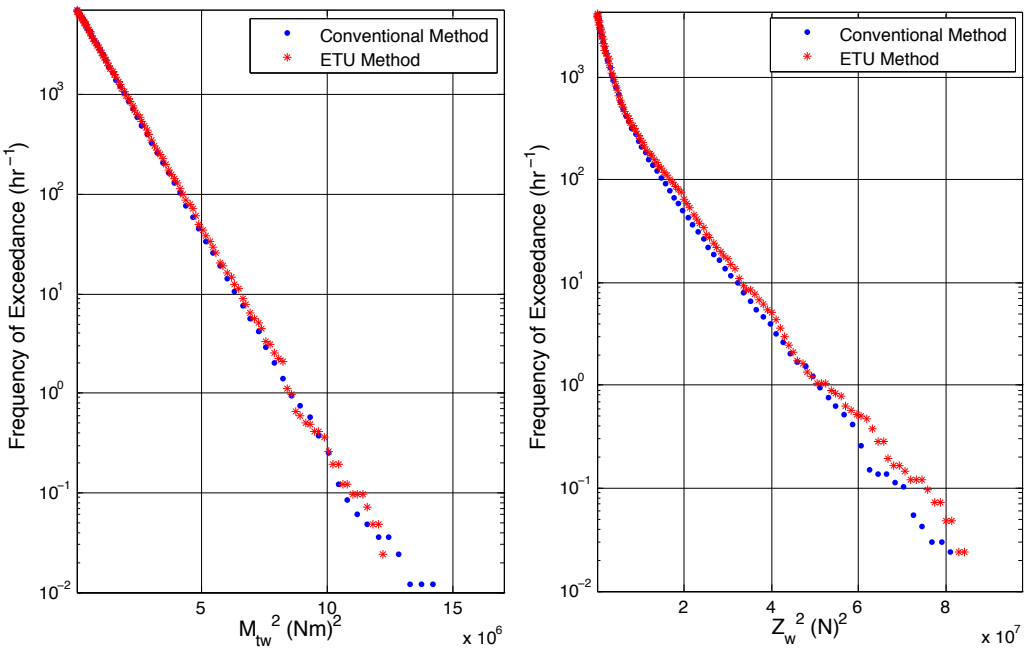

(a) Wing Torsion **(b)** Wing Shear

Figure 7.13: Short-Term Exceedance Curves for Nonlinear Response using the ETU Method for **Case 4**: $\sim$ 25 Times Faster. $V = 280$ m/s, $\sigma_w = 1.0$ m/s.

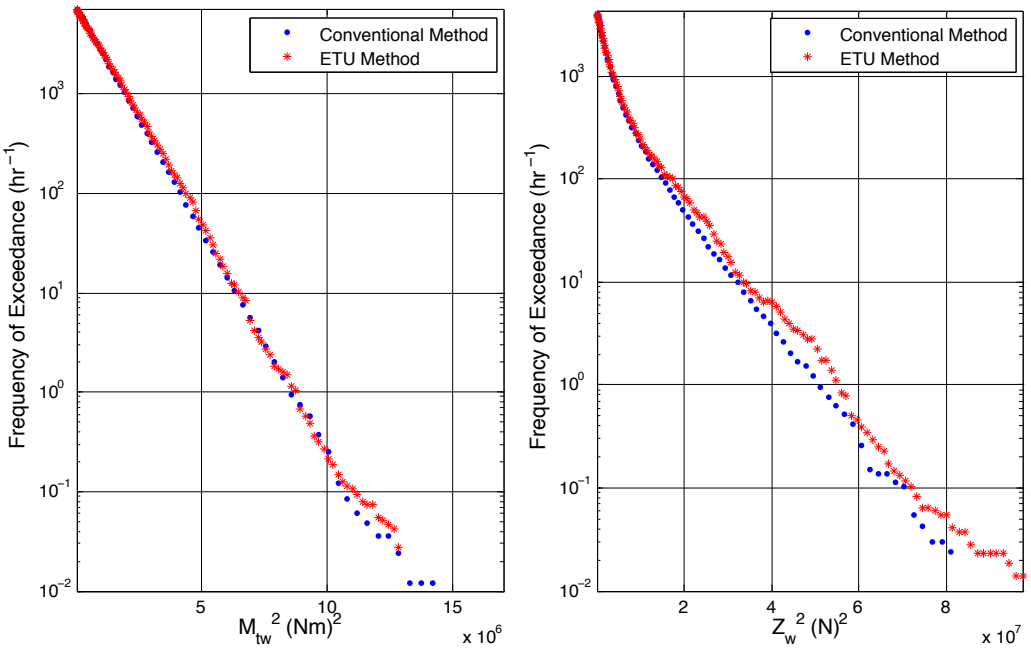

(a) Wing Torsion **(b)** Wing Shear

Figure 7.14: Short-Term Exceedance Curves for Nonlinear Response using the ETU Method for **Case 5**: $\sim$ 25 Times Faster. $V = 280$ m/s, $\sigma_w = 1.0$ m/s.

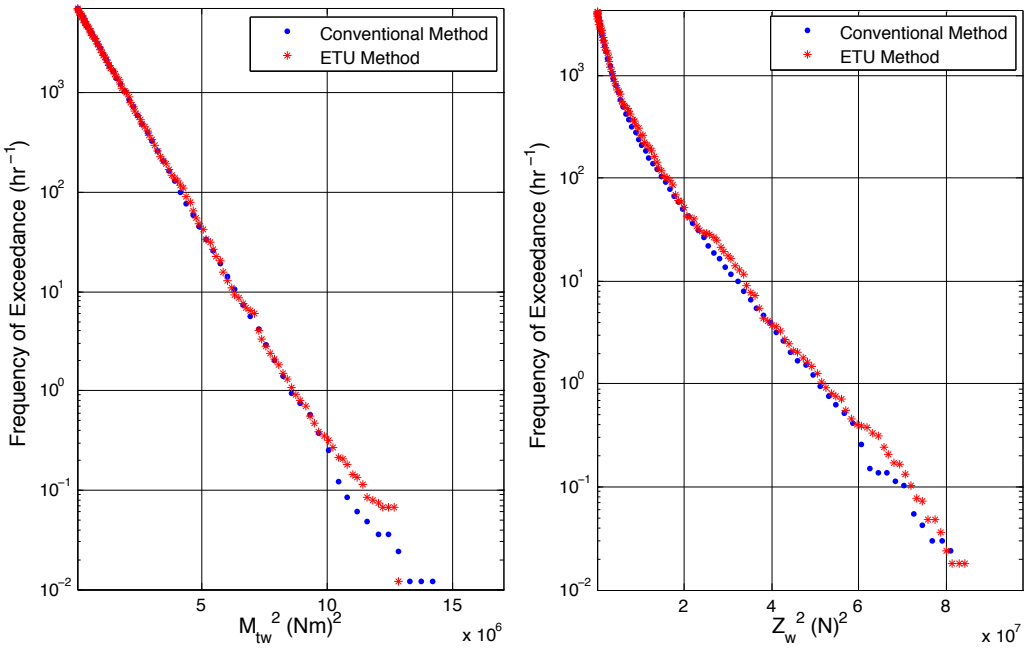

(a) Wing Torsion **(b)** Wing Shear

Figure 7.15: Short-Term Exceedance Curves for Nonlinear Response using the ETU Method for **Case 6**: $\sim$ 25 Times Faster. $V = 280$ m/s, $\sigma_w = 1.0$ m/s.

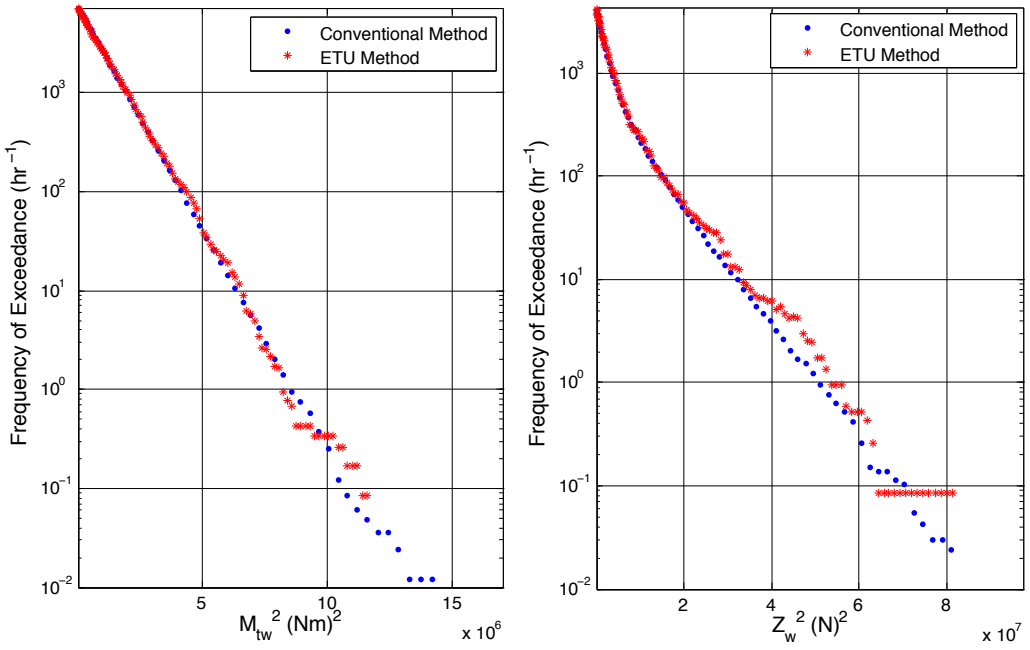

(a) Wing Torsion **(b)** Wing Shear

Figure 7.16: Short-Term Exceedance Curves for Nonlinear Response using the ETU Method for **Case 7**: $\sim$ 100 Times Faster. $V = 280$ m/s, $\sigma_w = 1.0$ m/s.

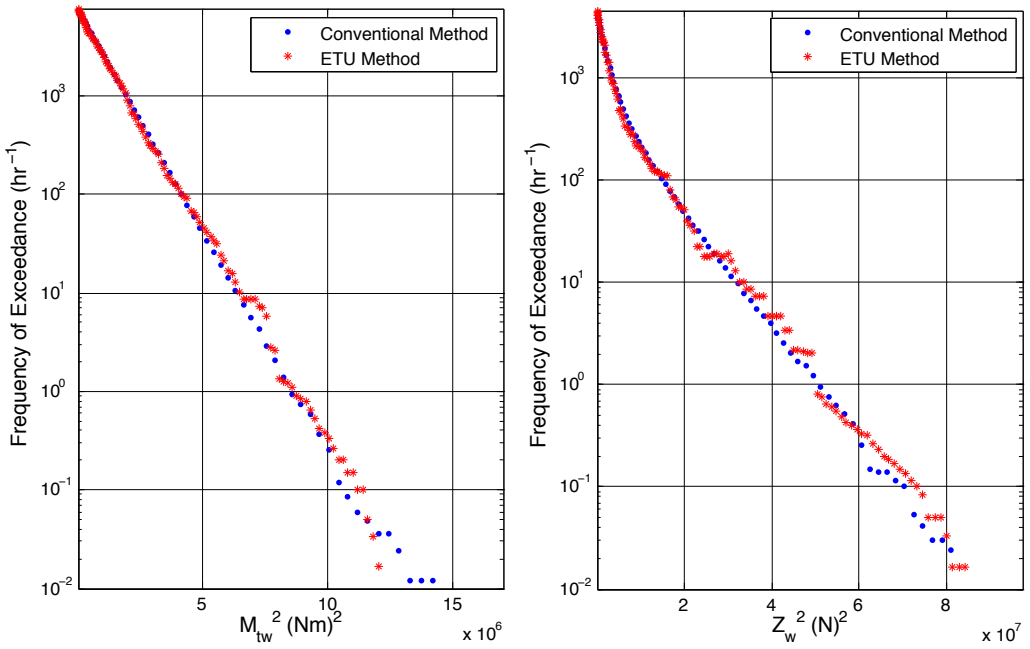

(a) Wing Torsion **(b)** Wing Shear

Figure 7.17: Short-Term Exceedance Curves for Nonlinear Response using the ETU Method for **Case 8**: $\sim$ 100 Times Faster. $V = 280$ m/s, $\sigma_w = 1.0$ m/s.

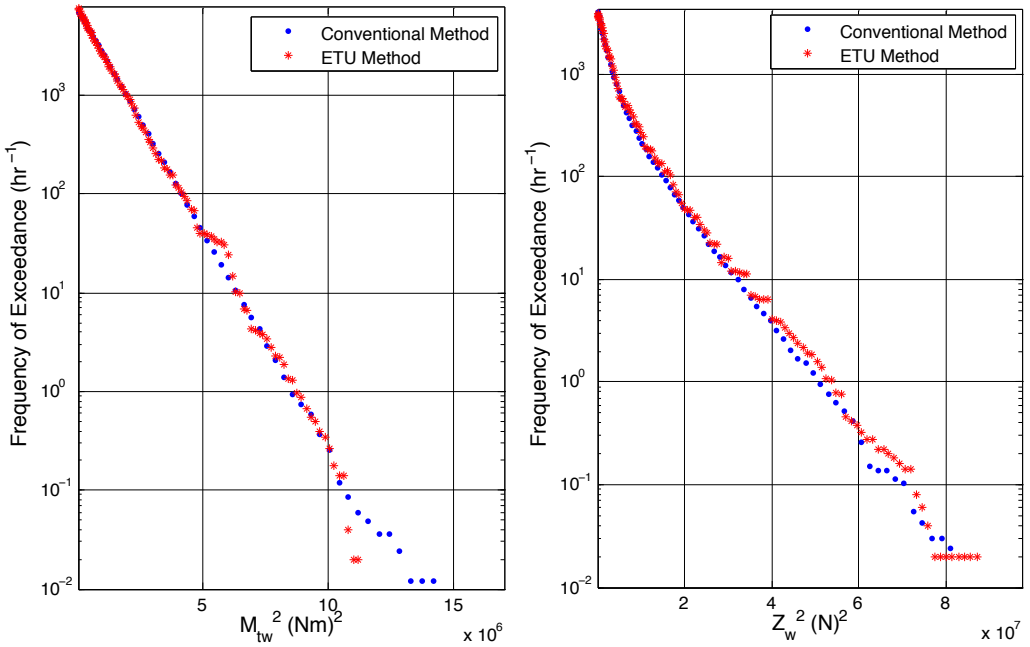

(a) Wing Torsion **(b)** Wing Shear

Figure 7.18: Short-Term Exceedance Curves for Nonlinear Response using the ETU Method for **Case 9**: $\sim$ 100 Times Faster. $V = 280$ m/s, $\sigma_w = 1.0$ m/s.

7.3 Extension to Long-Term Statistics

This section seeks to extend the capability of the ETU method to account for the long-term statistics of *nonlinear* aircraft gust response. As previously discussed, in order to obtain reliable aircraft design loads probabilistically, the entire range of conditions that the aircraft may encounter in its lifetime must be accounted for. These conditions can be defined by so-called turbulence severity states, which are discrete ranges of RMS gust velocities that are adequately represented by their midpoint. For the long-term analysis presented in this section, ten turbulence severity states are applied and it is assumed that $0 < \sigma_w < 15$ m/s, which are sufficient conditions to produce realistic exceedance curves in the area of interest for design loads (see figure 6.17). Evidently, the fact that there is a range of values for σ_w means that the analytical extreme value distribution for the linear response is not constant when it is based on equation 6.16. It may be possible to use the distribution given by equation 6.19 to define the boundaries of each subset, but difficulties would arise because it would take a very long time for simulations with low values of σ_w to produce response sample records that fall in to the extreme groups. For this reason, a slightly different procedure is used in this section, which is outlined as follows:

(1) The total number of simulations to be used in the analysis is divided equally by the number of turbulence severity states, ten in this case.

(2) Using the procedure shown in figure 7.9, a separate short-term ETU analysis is carried out for each value of σ_w, using the fraction of the total number of simulations defined in step (1). This means that each analysis has a separate extreme value distribution for the low-demand variable that is based on equation 6.16

(3) Total probability theorem is applied to the short-term threshold exceedance rates using the equation

$$\mathrm{E}\left[\mathrm{N}\left(y\right)\right] = \sum_{j=1}^{N_\mathrm{T}} \mathrm{E}\left[\mathrm{N}\left(y\right) \mid \sigma_{wj}\right] \mathrm{P}\left(\sigma_{wj}\right) \tag{7.3}$$

which gives the long-term frequencies of exceedance of the given range of thresholds.

(4) The results are compared to the long-term exceedance curves in figure 6.21, which was generated from 10,000 simulations using the method outlined in section 6.1.3.

The cases[1] that describe the number of simulations in each group in the long-term nonlinear ETU analysis, for each value of σ_w, are defined in table 7.4. The total number of simulations is the sum of the number of simulations in each group multiplied by the number of turbulence severity states, e.g. For case 10, total No. of simulations = $[(3 \times 6) + 22 + 60] \times 10 = 1000$. The number of simulations in each subset have been distributed in a similar manner to cases 3, 6 and 9 in the previous section because these were the cases that produced the most reliable curves relative to the other respective cases that had the same total number of simulations.

Table 7.4: Number of Simulations in Each Group in the Nonlinear ETU Analysis for Each Long-Term Case

	Total No. of Simulations	Lower Interim Groups (1-6)	Highest Interim Group (7)	Extreme Group (8)	Computational Cost Reduction
Case 10	1000	3	22	60	90%
Case 11	400	2	10	18	96%
Case 12	100	1	2	2	99%

The nine probability boundaries used to define the eight groups for the ETU analysis are $P_{\text{lim.}} = [0,\ 0.10,\ 0.50,\ 0.80,\ 0.90,\ 0.95,\ 0.99,\ 0.999,\ 1]$. Also, in the absence of information about a specific aircraft mission profile, it has again been assumed that the aircraft only flies in the 30,000 - 40,000ft altitude band. The results of the long-term ETU analysis based on the foregoing procedure for the cases defined in table 7.4 are shown in figures 7.19 - 7.21.

It can be observed form figures 7.19 and 7.20 that there is very little difference between the reliability of the exceedance curves from cases 10 and 11. Both cases produce exceedance curves that agree very well with the reference curves, and the high degree of nonlinearity in the wing root shear force does not appear to have any effect on the results of the nonlinear ETU analysis.

[1] Although there are only three cases in this section, the first case is labelled as case 10 in order to avoid confusion with the cases in section 7.2.

Figure 7.21, which presents the results form case 12, shows that although there is a fairly good agreement with the reference curves for each of the interesting quantities, it would be somewhat difficult to obtain reliable design values in the region where $\mathrm{N}(y) = 2 \times 10^{-5}$, due to the increased sampling variability. Nevertheless, it is surprising that separate ETU analyses that have such a low number of simulations in each group are able to produce reliable exceedance curves when they are combined using total probability theorem.

Although it may be concluded that case 12 has too few simulations to produce exceedance curves with adequately low sampling variability, the exceedance curves from case 11 would certainly be suitable for obtaining design values in the region of interest. This means that reliable long-term exceedance curves for aircraft with cubic stiffening nonlinearity can be obtained by at least as little as 4% of the computational cost of the conventional method, which is a significant outcome given that it is these curves that are used to determine the aircraft design loads in a mission analysis.

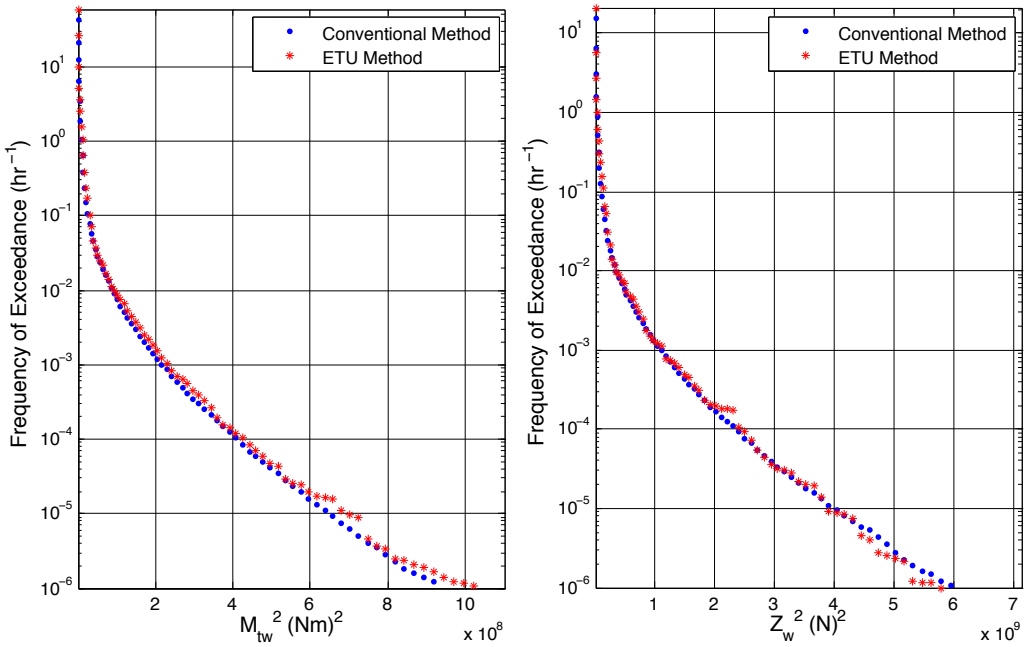

(a) Wing Torsion **(b)** Wing Shear

Figure 7.19: Long-Term Exceedance Curves for Nonlinear Response using the ETU Method for **Case 10**: $\sim$ 10 Times Faster. $V = 280$ m/s.

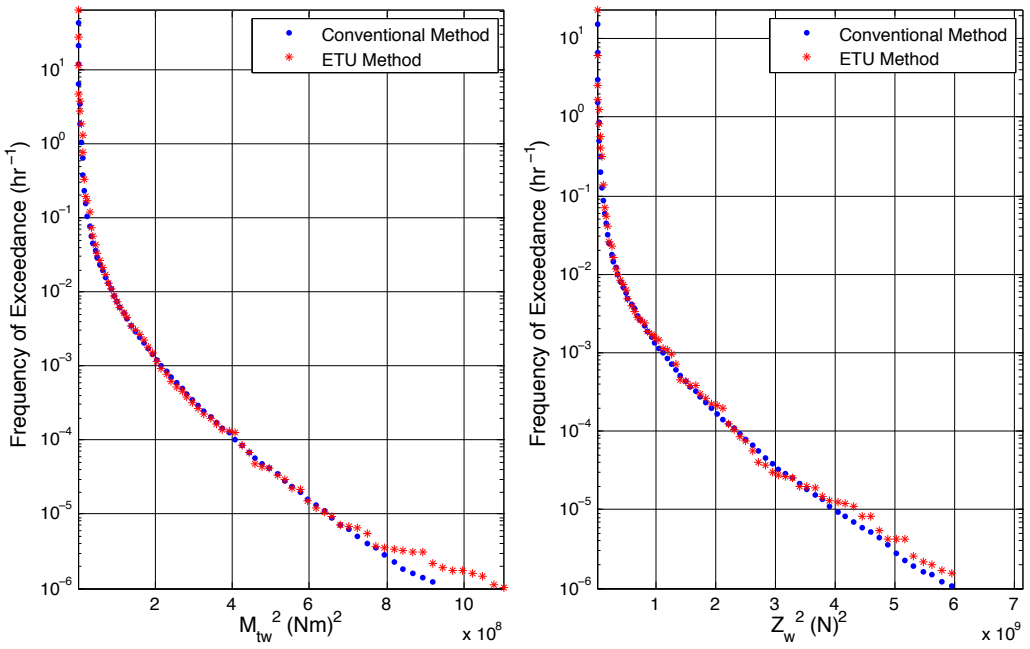

(a) Wing Torsion **(b)** Wing Shear

Figure 7.20: Long-Term Exceedance Curves for Nonlinear Response using the ETU Method for **Case 11**: $\sim$ 25 Times Faster. $V = 280$ m/s.

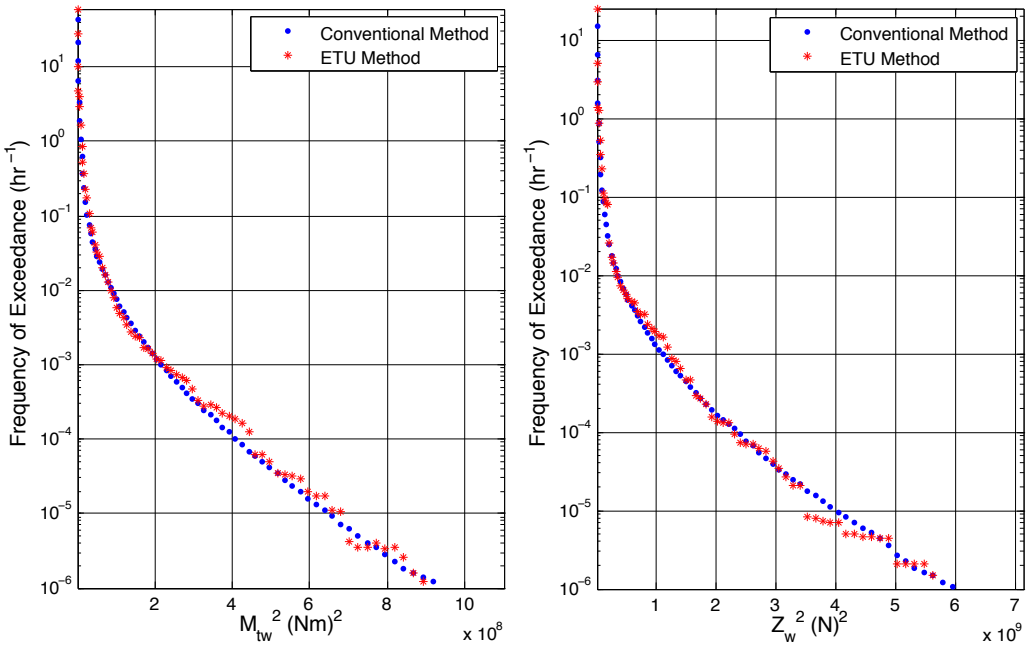

(a) Wing Torsion **(b)** Wing Shear

Figure 7.21: Long-Term Exceedance Curves for Nonlinear Response using the ETU Method for **Case 12**: $\sim$ 100 Times Faster. $V = 280$ m/s.

Concluding Remarks

The studies presented in this chapter demonstrate that the ETU method has successfully enabled the probabilistic response of *nonlinear* aircraft to continuous turbulence to be calculated at a practically feasible computational cost, where it was previously limited to the deterministic '1 - cosine' gust. It is important to note that conclusions about the capability of the ETU method can only be limited to the specific type of nonlinearity addressed in this thesis, namely, cubic stiffening of the wing, and even that area has not been covered in great detail. For example, it is necessary to explore how the effectiveness of the ETU method would be impacted by changes in the hardening coefficient γ_e, which essentially defines how much the nonlinear term contributes to the overall stiffness of the wing (see equation 6.23). The hardening coefficient was always taken to equal 5 in this work, but it cannot be assumed that if this value were to be increased, that the strong correlations shown in figure 7.8 would still exist between the linear and nonlinear responses.

Nevertheless, some progress has been made towards a unified model for aircraft design gust loads, in which the current design criteria would be replaced with a single criteria that did not rely on the safety record of older aeroplanes, and was able to account for the infinite number of possible shapes of gust profile that an aircraft might encounter. There are still some obstacles that need to be overcome, however, before such a model exists; for example, the aforementioned issue of the correlated phase differences that result in gust velocity profiles that cannot be adequately represented by a Gaussian turbulence model, even when non-stationarity is accounted for.

Chapter 8

Conclusions and Future Work

This chapter seeks to summarise the findings from each of the studies presented in this thesis and outline areas where further research might be beneficial. Although, there has been plenty of overlap, the conclusions from each engineering discipline are presented separately for the purpose of clarity.

8.1 Offshore Wave Loading

8.1.1 Conclusions

The main aims of this project, with respect to offshore engineering uncertainty, were to explore techniques that speed up the derivation of offshore structural response statistics and find ways to improve existing techniques as well as develop new ones, so that offshore structures may be designed more efficiently. To this end, a study that sought to enhance the Efficient Time Simulation method was carried out and in a separate study, a new method was developed, which was called the Efficient Threshold Upcrossing Method. Regarding these studies, the following conclusions have been drawn:

- Although Conventional (Monte Carlo) Time Simulation is a favourable technique when deriving offshore structural response probability distributions, it requires the simulation of an excessively large number of response sample records to achieve acceptably low sampling variability. This renders the method impractical for design use due to the resultant high computational cost.

- An existing method, known as the Efficient Time Simulation (ETS) method, has been presented as a solution to this problem because it allows response probability distributions to be derived from a relatively small number of simulations, without sacrificing the versatility of the conventional method.

- The ETS method works by exploiting the strong correlation between surface elevation extreme values and corresponding response extreme values. Surface elevation sample records are divided into subsets according to their extreme values, which allows a limit to be placed upon the number of response sample records that are calculated from within each subset.

- An attempt was made to enhance the capability of ETS method by fitting the data from each subset to a generalised extreme value distribution before apply total probability theorem. which produced response probability distributions that appeared 'smoother,' but were actually slightly less reliable than those derived from the original ETS method.

- In an effort to improve the reliability and efficiency of the response probability distributions, the Efficient Threshold Upcrossing (ETU) method was developed. The ETU method works in a similar way to the ETS method, but extracts more data from the response sample records by utilising information about the average threshold upcrossing rates instead of simply the extreme values, increasing the accuracy of the distributions.

- The ETU method has been validated against the conventional method by comparing the probability distributions of extreme quasi-static base shear force and extreme quasi-static overturning moment and it was shown that even a very small number of simulations exhibit a good agreement. The ETU method is shown to be up to 3 orders of magnitude more efficient than the conventional method.

- Both ETU and ETS methods were also compared and it was shown that probability distributions derived from the ETU method were slightly more reliable than those

of the ETS method, especially in the lower part of the distributions. They also appeared to become increasingly more stable in comparison as the number of simulations was reduced.

8.1.2 Recommendations for Future Work

Based on the findings presented in this thesis, in the field of offshore wave loading, the following recommendations are made for future work that may prove beneficial:

- The offshore structural analysis in this project was limited to the quasi-static response, where current and load intermittency in the splash zone were assumed to have a negligible effect. It is recommended that the ETU method should be applied to an dynamic analysis that takes these factors into account.

- The offshore model itself was as simple as it could possibly be, so that the methodology could be demonstrated at minimal computational cost. It is recommended that a more complex structure should be included the ETU analysis, and it may be worthwhile to integrate a high fidelity offshore structural response software package such as SESAM into the procedure. This would enable different types of structures, such as floating structures, to be analysed probabilistically at a potentially low computational cost.

- Because the ETU method depends on a correlation between high- and low-demand variables, it is impossible to say how widely it can be applied to more realistic structures, due to the simplicity of the offshore model used in this work. It may be that the correlation exists only because of the simplicity of the model. This, an investigation into the correlations for a wide range of different structural models must be carried out in order to determine the effect of model complexity on the validity of this critical assumption.

8.2 Aircraft Gust Loading

8.2.1 Conclusions

The main aims of this project, with respect to aerospace engineering uncertainty, were to produce a stochastic model for nonlinear aircraft response to continuous turbulence and to make it practically feasible for obtaining aircraft design loads by significantly reducing the simulation time. To this end, such a model has been developed in MATLAB/SIMULINK that also employs a robust technique for simulating patches of continuous turbulence, and these aims were achieved by applying a new technique for speeding up probabilistic response calculations to the aircraft gust model. Studies were carried out using both linear and nonlinear aircraft models, and the following conclusions have been drawn:

- Models that calculate both linear and non-linear aircraft response statistics have been developed and it is shown that for both models, long-term exceedance curves for design loads can be accurately derived by Monte-Carlo simulation. The models use non-deterministic spectral amplitudes, which were shown to produce much more reliable gust velocity sample records than the conventional deterministic spectral amplitudes. However, the difference becomes smaller as the duration of each sample record approaches infinity.

- The Efficient Threshold Upcrossing method was applied to aircraft gust loading and it was shown that it can be used to accurately calculate short-term nonlinear response statistics while reducing computational cost by at least 2 orders of magnitude in comparison to Monte-Carlo simulation. This technique, however, is dependent on a strong correlation between so-called 'low-demand' and 'high-demand' variables.

- It was found that such a correlation does *not* exist between extreme gust velocity and extreme linear response, nor does it exist for extreme gust slope. The ETU method was therefore demonstrated by exploiting the strong correlations that were found between extreme linear response and extreme nonlinear response for each

of the interesting quantities, namely, wing root shear force and wing root torsion moment.

- It was explained that, practically, the ETU method is only beneficial when applied to a response with high computational demand and for which the analytical solution of the exceedance curve is not known. This means that it is best applied to nonlinear response but is of little value in the linear case.

- One major problem was pointed out that is yet to be solved, which concerns the correlation requirements between high- and low-demand variables, namely, linear and nonlinear response. It may be that a correlation only existed in this case because the type of nonlinearity, cubic stiffening, does not produce vastly different results from the linear case for most sample records. Therefore, no wider conclusions can be drawn about other types of nonlinearity because they were not investigated in this work.

- The effect of varying the number of simulations in each subset in an ETU analysis was investigated and it was shown that the ETU method is more effective when the majority of the simulation time is concentrated towards the extreme groups, so that the effect of sampling variability is moved away from the 'tail' of the exceedance curves (where the most infrequently exceeded thresholds are). However, it was also found that more reliable exceedance curves were generally produced when the difference in the number of simulations varies more gradually between the groups. This indicated that there may be some optimum solution for the distribution of simulation time between the groups that produces a curve that is minimally affected by sampling variability.

- The ETU method was successfully extended to take into account long-term statistics and it was shown that reliable long-term exceedance curves for the response of aircraft with structural nonlinearity can be obtained by at least as little as 4% of the computational cost of the conventional method, which means that nonlinear aircraft design loads based a mission analysis can be obtained very efficiently.

- It should be noted that all of the simulations in this work were perform on a single desktop computer, but running 100,000 simulations took approximately 9 days using the conventional method, which was reduced to a matter of a few hours using the ETU method. The model was kept as simple as possible, however, and it is common for industrial finite element models to contain thousands of degrees of freedom. This means that, even with access to high-performance computers, the conventional method would probably still incur an impractically high computational cost. It is hard to say with certainty whether the ETU method would lead to sufficiently practical simulation times, but based on the author's discussion with industrial loads engineers, a cost reduction of 2-3 orders of magnitude would be very beneficial.

- Finally, it is widely understood that the calculation of design loads for nonlinear aircraft are limited to discrete, '1 - cosine' gust encounters and that continuous turbulence models are only applicable to linear aircraft response. However, the most important conclusion that can be drawn from this thesis is that *this is no longer the case*, because the ETU method provides a way to calculate structurally nonlinear response statistics in the time domain at a significantly lower computational cost.

8.2.2 Recommendations for Future Work

Based on the findings presented in this thesis, in the field of aircraft gust loading, the following recommendations are made for future work that may prove beneficial:

- The gust response model used for the nonlinear ETU analysis did not fully account for unsteady effects, because Kussner's and Wagner's functions were not included in the equations of motion. Although it would be very time consuming to derive the exceedance curves using the conventional method, which would be required for validation, it is recommended that the model should be extended so that the ETU method can take these effects into account.

- It was stated earlier that there may be an optimum solution for the distribution of

simulation time between the groups in an ETU analysis. Future work to investigate this further may significantly improve the reliability of exceedance curves that are derived from the ETU method.

- An investigation into the effects of different types of nonlinearity on the correlations between high- and low-demand variables is necessary, in order to establish the scope of the ETU method's application.

- It would also prove beneficial to gain a more specific understanding of the computational reductions that are actually required by industry in order to make a nonlinear probabilistic gust analysis possible.

- Lastly, although progress towards a unified certification model for gust loads has been made in this project, one of the obstacles that still remains is the inability of non-stationary Gaussian turbulence to account for the apparent phase correlations that lead to higher gust velocities in some extreme cases. Until this issue is successfully tackled, there will always be a need for both discrete and continuous turbulence models in the design process. It is hoped that future research will be carried out in this area so that the aerospace industry can benefit from simplified certification criteria for gust response that results in more economical but reliable aircraft designs.

Appendix A: Definitions of Aerodynamic Derivatives

The matrices of aerodynamic derivatives used in the aircraft equations of motion, given in equations 6.13 and 6.20 are defined as

$$\mathbf{M} = \left[\begin{array}{cc|c} m & 0 & 0 \\ 0 & I_y & 0 \\ \hline 0 & 0 & m_e \end{array}\right] \tag{A.1}$$

$$\mathbf{C} = \left[\begin{array}{cc|c} -Z_{\dot{z}} & -Z_q & -Z_{\dot{e}} \\ -M_{\dot{z}} & -M_q & -M_{\dot{e}} \\ \hline -Q_{\dot{z}} & -Q_q & c_e - Q_{\dot{e}} \end{array}\right] \tag{A.2}$$

$$\mathbf{K} = \left[\begin{array}{cc|c} 0 & -Z_\alpha & -Z_e \\ 0 & -M_\alpha & -M_e \\ \hline 0 & -Q_\alpha & k_e - Q_e \end{array}\right] \tag{A.3}$$

The vectors of gust-related derivatives are defined as

$$\boldsymbol{R}_W = \left[\begin{array}{c} Z_{g\mathrm{W}} \\ M_{g\mathrm{W}} \\ \hline Q_{g\mathrm{W}} \end{array}\right] \quad \text{and} \quad \boldsymbol{R}_T = \left[\begin{array}{c} Z_{g\mathrm{T}} \\ M_{g\mathrm{T}} \\ \hline Q_{g\mathrm{T}} \end{array}\right] \tag{A.4}$$

The definitions of all the aerodynamic derivatives, which are taken from Wright & Cooper (2007), are shown in table A.1.

Table A.1: Definitions of Aerodynamic and Gust-Related Derivatives

Derivative	Mathematical Definition
Z_α	$-\frac{1}{2}\rho V^2[S_\mathrm{W}a_\mathrm{W} + S_\mathrm{T}a_\mathrm{T}(1-k_\varepsilon)]$
$Z_{\dot{z}}$	$-\frac{1}{2}\rho V[S_\mathrm{W}a_\mathrm{W} + S_\mathrm{T}a_\mathrm{T}(1-k_\varepsilon)]$
Z_q	$-\frac{1}{2}\rho V S_\mathrm{T}a_\mathrm{T}l_\mathrm{T}$
Z_e	$\frac{1}{2}\rho V^2[-S_\mathrm{W}a_\mathrm{W}J_1 - S_\mathrm{T}a_\mathrm{T}\gamma_{e\mathrm{T}}]$
$Z_{\dot{e}}$	$-\frac{1}{2}\rho V S_\mathrm{T}a_\mathrm{T}\kappa_{e\mathrm{T}}$
$Z_{g\mathrm{W}}$	$-\frac{1}{2}\rho V S_\mathrm{W}a_\mathrm{W}$
$Z_{g\mathrm{T}}$	$-\frac{1}{2}\rho V S_\mathrm{T}a_\mathrm{T}(1-k_\varepsilon)$
M_α	$\frac{1}{2}\rho V^2[S_\mathrm{W}a_\mathrm{W}l_\mathrm{W} - S_\mathrm{T}a_\mathrm{T}(1-k_\varepsilon)l_\mathrm{T}]$
$M_{\dot{z}}$	$\frac{1}{2}\rho V[S_\mathrm{W}a_\mathrm{W}l_\mathrm{W} - S_\mathrm{T}a_\mathrm{T}(1-k_\varepsilon)l_\mathrm{T}]$
M_q	$-\frac{1}{2}\rho V S_\mathrm{T}a_\mathrm{T}l_\mathrm{T}^2$
M_e	$\frac{1}{2}\rho V^2[S_\mathrm{W}a_\mathrm{W}l_\mathrm{W}J_1 - S_\mathrm{T}a_\mathrm{T}l_\mathrm{T}\gamma_{e\mathrm{T}}]$
$M_{\dot{e}}$	$-\frac{1}{2}\rho V S_\mathrm{T}a_\mathrm{T}l_\mathrm{T}\kappa_{e\mathrm{T}}$
$M_{g\mathrm{W}}$	$\frac{1}{2}\rho V S_\mathrm{W}a_\mathrm{W}l_\mathrm{W}$
$M_{g\mathrm{T}}$	$-\frac{1}{2}\rho V S_\mathrm{T}a_\mathrm{T}l_\mathrm{T}(1-k_\varepsilon)$
Q_α	$\frac{1}{2}\rho V^2[S_\mathrm{W}a_\mathrm{W}J_2 - S_\mathrm{T}a_\mathrm{T}(1-k_\varepsilon)\kappa_{e\mathrm{T}}]$
$Q_{\dot{z}}$	$\frac{1}{2}\rho V[S_\mathrm{W}a_\mathrm{W}J_2 - S_\mathrm{T}a_\mathrm{T}(1-k_\varepsilon)\kappa_{e\mathrm{T}}]$
Q_q	$-\frac{1}{2}\rho V S_\mathrm{T}a_\mathrm{T}l_\mathrm{T}\kappa_{e\mathrm{T}}$
Q_e	$\frac{1}{2}\rho V^2[-S_\mathrm{W}a_\mathrm{W}J_3 - S_\mathrm{T}a_\mathrm{T}\gamma_{e\mathrm{T}}\kappa_{e\mathrm{T}}]$
$Q_{\dot{e}}$	$-\frac{1}{2}\rho V S_\mathrm{T}a_\mathrm{T}\kappa_{e\mathrm{T}}^2$
$Q_{g\mathrm{W}}$	$-\frac{1}{2}\rho V S_\mathrm{W}a_\mathrm{W}J_2$
$Q_{g\mathrm{T}}$	$-\frac{1}{2}\rho V S_\mathrm{T}a_\mathrm{T}(1-k_\varepsilon)\kappa_{e\mathrm{T}}$

Note that

$$J_1 = \frac{1}{s}\int_{y=0}^{s} \gamma_e \mathrm{d}y \tag{A.5}$$

$$J_2 = \frac{1}{s}\int_{y=0}^{s} (\kappa_e - l_A\gamma_e)\,\mathrm{d}y \tag{A.6}$$

$$J_3 = \frac{1}{s}\int_{y=0}^{s} (\kappa_e - l_A\gamma_e)\,\gamma_e \mathrm{d}y \tag{A.7}$$

where $\gamma_e = \gamma_e(y), \kappa_e = \kappa_e(y)$ are functions that describe the flexible mode shape.[1]

[1] In this instance, y denotes the spanwise coordinate of the aircraft, rather than the generic response variable that it signifies in the rest of this thesis.

Appendix B: Aircraft Internal Load Transformation Vectors

The internal load transformation vectors that are used in equations 6.15 and 6.22, are defined for wing root shear force (denoted by subscript Z) and wing root torsion moment (denoted by subscript T) as

$$\boldsymbol{A}_Z = \begin{bmatrix} A_{1Z} \\ A_{2Z} \\ A_{3Z} \end{bmatrix} = \begin{bmatrix} \mu s \\ -\mu s l_{\mathrm{WM}} \\ \mu s \left[\kappa_{e0} \left(1 + \frac{A}{3}\right) + l_{\mathrm{E}} \gamma_{e0} \left(1 + \frac{B}{2}\right) \right] \end{bmatrix} \tag{B.8}$$

$$\boldsymbol{B}_Z = \begin{bmatrix} B_{1Z} \\ B_{2Z} \\ B_{3Z} \end{bmatrix} = \begin{bmatrix} \frac{1}{4}\rho V a_{\mathrm{W}} S_{\mathrm{W}} \\ -\frac{1}{4}\rho V a_{\mathrm{W}} S_{\mathrm{W}} l_{\mathrm{W}} \\ \frac{1}{4}\rho V a_{\mathrm{W}} S_{\mathrm{W}} \left[\kappa_{e0} \left(1 + \frac{A}{3}\right) + l_{\mathrm{A}} \gamma_{e0} \left(1 + \frac{B}{2}\right) \right] \end{bmatrix} \tag{B.9}$$

$$\boldsymbol{C}_Z = \begin{bmatrix} C_{1Z} \\ C_{2Z} \\ C_{3Z} \end{bmatrix} = \begin{bmatrix} 0 \\ \frac{1}{4}\rho V^2 a_{\mathrm{W}} S_{\mathrm{W}} \\ \frac{1}{4}\rho V^2 a_{\mathrm{W}} S_{\mathrm{W}} \gamma_{e0} \left(1 + \frac{B}{2}\right) \end{bmatrix} \tag{B.10}$$

$$\boldsymbol{D}_Z = \frac{1}{4}\rho V a_{\mathrm{W}} S_{\mathrm{W}} \tag{B.11}$$

$$\boldsymbol{A}_T = \begin{bmatrix} A_{1T} \\ A_{2T} \\ A_{3T} \end{bmatrix} = \begin{bmatrix} -A_{1Z} l_{\mathrm{E}} \\ -A_{2Z} l_{\mathrm{E}} \\ -A_{3Z} l_{\mathrm{E}} \end{bmatrix} \tag{B.12}$$

$$\boldsymbol{B}_T = \begin{bmatrix} B_{1T} \\ B_{2T} \\ B_{3T} \end{bmatrix} = \begin{bmatrix} B_{1Z} l_{\mathrm{A}} \\ B_{2Z} l_{\mathrm{A}} \\ B_{3Z} l_{\mathrm{A}} \end{bmatrix} \tag{B.13}$$

$$\boldsymbol{C}_T = \begin{bmatrix} C_{1T} \\ C_{2T} \\ C_{3T} \end{bmatrix} = \begin{bmatrix} 0 \\ C_{2Z} l_{\mathrm{A}} \\ C_{3Z} l_{\mathrm{A}} \end{bmatrix} \tag{B.14}$$

$$\boldsymbol{D}_T = \boldsymbol{D}_Z l_{\mathrm{A}} \tag{B.15}$$

where

$$A = -3\frac{m}{m_{\mathrm{W}}}\left[1 + \frac{l_{\mathrm{WM}}\left(l_{\mathrm{E}} + l_{\mathrm{WM}}\right)}{{l_y}^2}\right] \tag{B.16}$$

and $B = 0$ for the case where wing bending is dominant, which has been assumed in this instance.

References

Abdulwahab, E. N. & Hongquan, C. (2008), 'Aircraft Gust Load Estimation due to Atmospheric Turbulence Under Different Flight Conditions', *Aeronautical journal* **112**(1132), 345 – 352.

Abu Husain, M., Mohd Zaki, N. I., Lambert, L. A., Wang, Y. & Najafian, G. (2013), Long-Term Probability Distribution of Extreme Offshore Structural Response Via an Efficient Time Simulation Method, *in* 'ASME 32nd International Conference on Ocean, Offshore and Arctic Engineering', Nantes, France.

Abu Husain, M. & Najafian, G. (2010), An Efficient Monte Carlo Simulation Technique for Derivation of the Probability Distribution of the Extreme Values of Offshore Structural Response, *in* 'ASME 29th International Conference on Ocean, Offshore and Arctic Engineering: Volume 2', ASME, Shanghai, China, pp. 369–375.

Abu Husain, M. & Najafian, G. (2011), Efficient Derivation of the Probability Distribution of the Extreme Values of Offshore Structural Response Taking Advantage of Its Correlation With Extreme Values of Linear Response, *in* 'ASME 30th International Conference on Ocean, Offshore and Arctic Engineering', ASME, Rotterdam, The Netherlands, pp. 335–346.

Airy, G. B. (1841), 'Tides and Waves', *Encyclopaedia Metropolitana (eds. Rose, H.J. et al.) Mixed Sciences* **3**, 1817–1845.

Bendat, J. S. & Piersol, A. G. (1971), *Random Data: Analysis and Measurement Procedures*, Wiley, New York.

Benson, C., Joyce, M. J., Winsby, A. & Silvie, J. (2002), 'Monte-Carlo Calculation of

the Response Functions for Two Prototype Cosmic Neutron Metrology Instruments', *Journal of Nuclear Science and Technology* **39**(2), 1361–1364.

Boyle, P. P. (1977), 'Options: A Monte Carlo Approach', *Journal of Financial Economics* **4**(3), 323–338.

Chen, R. P. (1995), 'Statistical Discrete Gust - Power Spectral Density Methods Overlap - Holistic Proof and Beyond', *Journal of Aircraft* **32**(3), 570–576.

Chen, W.-Y. (1972), 'Application of Rice's Exceedance Statistics to Atmospheric Turbulence', *AIAA Journal* **10**(8), 1103–1105.

Crooks, W. M., Hoblit, F. M. & Mitchell, F. A. (1968), Project HICAT High Altitude Clear Air Turbulence Measurements and Meteorological Correlations, Air Force Flight Dynamics Laboratory TR-68-127, Vol. I, Technical Report May.

Dale, A. S., Lambert, L. A., Cooper, J. E. & Mosquera, A. (2013), Aerodynamic Study of Adaptive Camber-Morphing Wing Using 0- Honeycomb, *in* 'Int. Forum on Aeroelasticity and Structural Dynamics', Bristol, UK.

Dean, R. G. & Dalrymple, R. A. (1991), *Water Wave Mechanics for Engineers and Scientists*, World Scientific.

Etkin, B. (1981), 'Turbulent Wind and Its Effect on Flight', *Journal of Aircraft* **18**(5), 327–345.

Etkin, B. (1992), 'Comment on 'NASA Investigation of a Claimed 'Overlap' Between Two Gust Response Analysis Methods'', *Journal of aircraft* **29**(4), 741–742.

Federal Aviation Regulations (1996), 'Part 25: Airworthiness Standards: Transport Category Airplanes'.

Flomenhoft, H. I. (1994), 'Brief History of Gust Models for Aircraft Design', *Journal of aircraft* **31**(5), 1225 – 1227.

Forristall, G. Z. (1984), 'The Distribution of Measured and Simulated Wave Heights as a Function of Spectral Shape', *Journal of Geophysical Research* **89**(6), 547–552.

Goda, Y. (2010), *Random Seas and Design of Maritime Structures*, 3 edn, World Scientific, New York.

Gringorten, I. I. (1963), 'A Plotting Rule for Extreme Probability Paper', *Journal of Geophysical Research* **68**(3), 813–814.

Hoblit, F. M. (1988), *Gust Loads on Aircraft: Concepts and Applications*, AIAA, Washington DC.

Hoffman, D. & Karst, O. J. (1975), 'The Theory of the Rayleigh Distribution and Some of Its Applications', *Journal of Ship Research* **19**(3), 172–191.

Inglis, R., Pijfers, J. & Vugts, J. (1985), A Unified Probabilistic Approach to Predicting the Response of Offshore Structures, Including the Extreme Response, *in* '4th International Conference on the Behaviour of Offshore Structures', pp. 95–109.

Joint Airworthiness Requirements (2007), 'JAR-25: Large Aeroplanes'.

Jones, J. G. (1968), A Theory for Extreme Gust Loads on an Aircraft Based on the Representation of the Atmosphere as a Self-similar Intermittent Random Process, Royal Aircraft Establishment TR 68030, Technical report, Royal Aircraft Establishment.

Jones, J. G. (1980), The Application of a Worst-Case Analysis to Aircraft Gust Response Assessment, a statistical discrete gust theory progress note, Royal Aircraft Establishment TM FS 309, Technical report, Royal Aircraft Establishment.

Jones, J. G. (1989), 'Statistical-Discrete-Dust Method for Predicting Aircraft Loads and Dynamic Response', *Journal of Aircraft* **26**(4), 382–392.

Jones, J. G. (2007), 'Measured Statistics of Multicomponent Gust Patterns in Atmospheric Turbulence', *Journal of Aircraft* **44**(5), 1559–1567.

Jones, J. G. (2009*a*), 'Nonlinear Aircraft Loads in Severe Atmospheric Turbulence', *Journal of Aircraft* **46**(5), 1627–1633.

Jones, J. G. (2009*b*), 'Statistics of Atmospheric Gust Patterns Expressed in Terms of Energy and Entropy', *Journal of Aircraft* **46**(4), 1430–1437.

Jones, J. G., Earwicker, P. G. & Foster, G. W. (1993), 'Wavelet Analysis of Gust Structure in Measured Atmospheric Turbulence Data', *Journal of Aircraft* **30**(1), 94–99.

Jones, J. G., Foster, G. W. & Haynes, A. (1988), 'Fractal Properties of Inertial-range Turbulence with Implications for Aircraft Response', *Aeronautical Journal* **92**, 301–308.

Jones, J. G., Foster, G. W. & Watson, G. H. (2004), 'Non-Gaussian Statistics of Atmospheric Turbulence and Related Effects on Aircraft Loads', *AIAA Journal* **42**(12), 2438–2447.

Jones, J. W. (1964), High Intensity Gust Investigation (WFT 1217 R3), Boeing Report D-13273-333A, Technical report, Boeing, Wichita.

Kolmogorov, A. (1941), 'The Local Structure of Turbulence in Incompressible Viscous Fluid for Very Large Reynolds' Numbers', *Akademiia Nauk SSSR Doklady* **30**, 301–305.

Lambert, L. A., Najafian, G. & Cooper, J. E. (2013), Probabilistic Modelling of Aircraft Response to Non-Gaussian Continuous Turbulence, *in* '54th AIAA/ASME/ASCE/AHS/ASC Structures, Structural Dynamics, and Materials Conference', Boston, Massachusetts.

Lambert, L. A., Najafian, G., Cooper, J. E., Abu Husain, M. & Mohd Zaki, N. I. (2013), Efficient Estimation of Offshore Structural Response Based on Threshold Upcrossing Rates, *in* 'ASME 32nd International Conference on Ocean, Offshore and Arctic Engineering', Nantes, France.

Liaw, C. Y. & Zheng, X. Y. (2003), 'Polynomial Approximations of Wave Loading and Superharmonic Responses of Fixed Structures', *Journal of Offshore Mechanics and Arctic Engineering* **125**(3), 161–167.

Liepmann, H. (1952), 'On the Application of Statistical Concepts to the Buffeting Problem', *Journal of Aeronautical Sciences* **19**(12), 793–800.

Mandelbrot, B. (1982), *The Fractal Geometry of Nature*, Freeman, San Francisco.

McLeish, D. (2005), *Monte Carlo Simluation and Finance*, Wiley, Hoboken, N.J.

Montgomery, D. C. & Runger, G. C. (2002), *Applied Statistics and Probability for Engineers - 3rd Edition*, Wiley, U.S.

Morison, J., O'Brien, M., Johnson, J. & Schaaf, S. (1950), 'The Force Exerted by Surface Waves on Pile', *ASME, Petroleum Transactions* **189**, 149–154.

Morooka, C. K. & Yokoo, I. H. (1997), 'Numerical Simulation And Spectral Analysis of Irregular Sea Waves', *Journal of Offshore and Polar Engineering* **7**(3), 189–196.

Naess, A., Gaidai, O. & Haver, S. (2007), 'Efficient Estimation of Extreme Response of Drag-dominated Offshore Structures by Monte Carlo Simulation', *Ocean Engineering* **34**(16), 2188–2197.

Noback, R. (1986), 'Comparison of Discrete and Continuous Gust Methods for Airplane Design Loads Determination', *Journal of Aircraft* **23**(3), 226–231.

North, D. O. (1943), Analysis of Factors which Determine Signal/Noise Discrimination in Radar, RCA Lab. Technical Report PTR-6C, Technical report, RCA Laboratory, Princeton.

Papoulis, A. (1970), 'Maximum Response with Input Energy Constraints and the Matched Filter Principle', *IEEE Transactions on Circuit Theory* **CT-17**(2), 175–182.

Perry, B. i., Pototzky, A. S. & Woods, J. a. (1990), 'NASA Investigation of a Claimed 'Overlap' Between Two Gust Response Analysis Methods', *Journal of Aircraft* **27**(7), 605–611.

Pierson, W. J. & Moskowitz, L. (1964), 'A Proposed Spectral Form for Fully Developed Wind Seas Based on the Similarity Theory of S. A. Kitaigorodskii', *Journal of Geophysical Research* **69**(24), 5181–5190.

Pototzky, A. S., Perry, B. i. & Zeiler, T. a. (1991), 'Calculating Time-correlated Gust Loads Using Matched Filter and Random Process Theories', *Journal of Aircraft* **28**(5), 346–352.

Pratt, K. G. (1953), A Revised Formula for the Calculation of Gust Loads, NACA TN 2964, Technical report.

Press, H. & Mazelsky, B. (1954), A Study of the Application of Power-Spectral Methods of Generalized Harmonic Analysis to Gust Loads on Airplanes, NACA TR 1172, Technical report.

Press, H., Meadows, M. T. & Hadlock, I. (1956), A Reeavulation of Data on Atmospheric Turbulence and Airplane Gust Loads for Application in Spectral Calculations, NACA TR 1272, Technical report.

Rhode, R. V. (1937), 'Gust Loads on Airplanes', *Journal of the Society of Automotive Engineers* **40**(3), 81–88.

Rhode, R. V. & Lundquist, E. E. (1931), Preliminary Study of Applied Load Factors in Bumpy Air, NACA TN 374, Technical report.

Rice, S. O. (1944), 'Mathematical Analysis of Random Noise', *Bell System Technical Journal* **23**(3), 282–332.

Sarpkaya, T. & Isaacson, M. (1981), *Mechanics of Wave Forces on Offshore Structures*, Van Nostrand Reinhold, London.

Scott, R. C., Perry, B. i. & Pototzky, A. S. (1993), 'Computation of Maximized Gust Loads for Nonlinear Aircraft Using Matched-Filter-Based Schemes', *Journal of Aircraft* **30**(5), 763–768.

Scott, R. C., Pototzky, A. S. & Perry, B. i. (1995), 'Matched-Filter and Stochastic-Simulation-Based Methods of Gust Loads Prediction', *Journal of Aircraft* **32**(5), 1047–1055.

Scraube, H., Mares, V., Roesler, S. & Heinrich, W. (1999), 'Experimental Verification and Calculation of Aviation Route Doses', *Radiation Protection Dosimetry* **86**(4), 309.

Seco, J. & Verhaegen, F. (2013), *Monte Carlo Techniques in Radiation Therapy*, Taylor & Francis, Boca Raton.

Steiner, R. & Pratt, K. G. (1967), 'Some Applications of Power Spectra to Airplane Turbulence Problems', *Journal of aircraft* **4**(4), 360–365.

Stokes, G. G. (1847), 'On the Theory of Oscillatory Waves', *Transactions of the Cambridge Philosophical Society* **8**, 441–445.

Strom, A. J. & Weatherman, T. G. (1963), NB-66-B High Altitude Survey: Vol. I, Technical Analysis, and Vol. III, Time Series, USAF ASD-TR-63-145, Technical report, USAF.

Tayfun, M. A. (1980), 'Narrow-Band Nonlinear Sea Waves', *Journal of Geophysical Research* **85**(9), 1548–1552.

Tayfun, M. A. (1981), 'Distribution of Crest-to-Trough Wave Heights', *Journal of the Waterway Port Coastal and Ocean Division* **107**(3), 149–158.

Tickell, R. (1977), 'Continuous Random Wave Loading on Structural Members', *The Structural Engineer* **55**(5), 209–222.

Tucker, M. J., Challenor, P. G. & Carter, D. J. T. (1984), 'Numerical Simulation of a Random Sea: A Common Error and Its Effect Upon Wave Group Statistics', *Applied Ocean Research* **6**(2), 118–122.

Tung, C. C. (1995), 'Effects of Free Surface Fluctuations on Total Wave Force on Cylinder', *Journal of Engineering Mechanics* **121**(2), 274–280.

Vink, W. J. & de Jonge, J. (1997), A MATLAB Program to Study Gust Loading on a Simple Aircraft Model, NLR TP 97379, Technical report, National Aerospace Laboratory NLR.

von Karman, T. (1948), Progress in the Statistical Theory of Turbulence, *in* 'Proceedings of the National Academy of Sciences of the United States of America', pp. 530–539.

Wright, J. R. & Cooper, J. E. (2007), *Introduction to Aircraft Aeroelasticity and Loads*, Wiley, Chichester.

Zeiler, T. a. (1997), 'Matched Filter Concept and Maximum Gust Loads', *Journal of Aircraft* **34**(1), 101–108.